Small-Signal Modeling and Stability Analysis of Grid-Converter Interactions

2019-06-03, IEEE PEDG 2019, Xi’an, China

Xiongfei Wang, Professor, Department of Energy Technology
Research Program Leader for Electronic Power Grid (www.egrid.et.aau.dk)

AALBORG UNIVERSITY
DENMARK

Instructor Bio

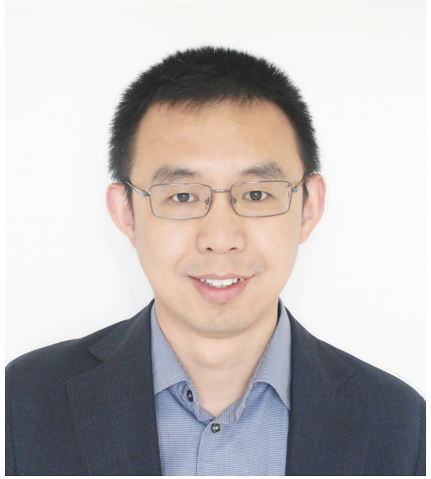

Xiongfei Wang is a Professor and Research Program Leader on Electronic Power Grid (eGrid) with the Department of Energy Technology, Aalborg University, Denmark. His research interests include modeling and control of grid-interactive converters, stability and power quality of power-electronic-based power systems, harmonic analysis and mitigation.

In 2016, he was selected into Aalborg University Strategic Talent Management Program, which aims at developing next-generation research leaders for Aalborg University. He received six Prize Paper Awards in IEEE Transactions and conferences, the 2017 Outstanding Reviewer Award for the IEEE Transactions on Power Electronics, the 2018 IEEE PELS Richard M. Bass Outstanding Young Power Electronics Engineer Award, and the 2019 IEEE PELS Sustainable Energy Systems Technical Achievement Award. He serves as an Associate Editor for the IEEE Transactions on Power Electronics, the IEEE Transactions on Industry Applications, and the IEEE Journal of Emerging and Selected Topics in Power Electronics.

CONTENT

- INTRODUCTION
- SMALL-SIGNAL MODELING
- IMPEDANCE-BASED STABILITY ANALYSIS
- PROSPECTS AND CHALLENGES

INTRODUCTION

- Grid-converter interactions
- Grid-forming/-following converters

Grid-Converter Interactions

Less physical properties, more control dependency

Traditional Generator
- Prime Mover — 0.1Hz
- Excitation Control — 1Hz

Large Wind Generator
- Turbine P & ω Control — 0.1Hz
- Grid Q &V Control
  DC-Link V Control — 10Hz
- Grid Synchronization — 100Hz
- Current Control — 500Hz
- IGBT Switching — 2500Hz

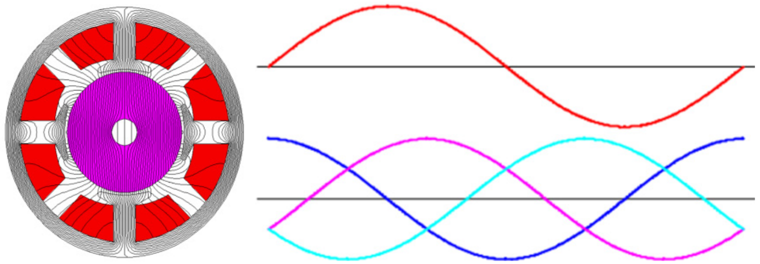

Traditional Generator Output Voltage

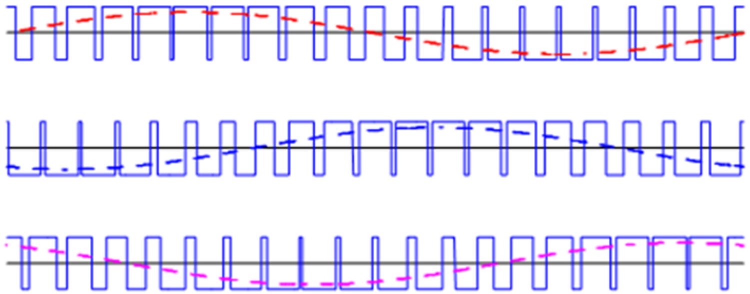

Wind Generator Output Voltage

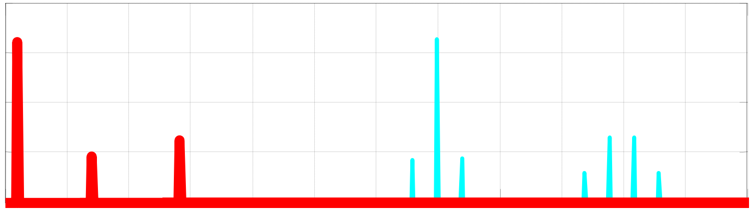

Harmonic Spectrum

Grid-Converter Interactions

Negative damping induced by converter controllers

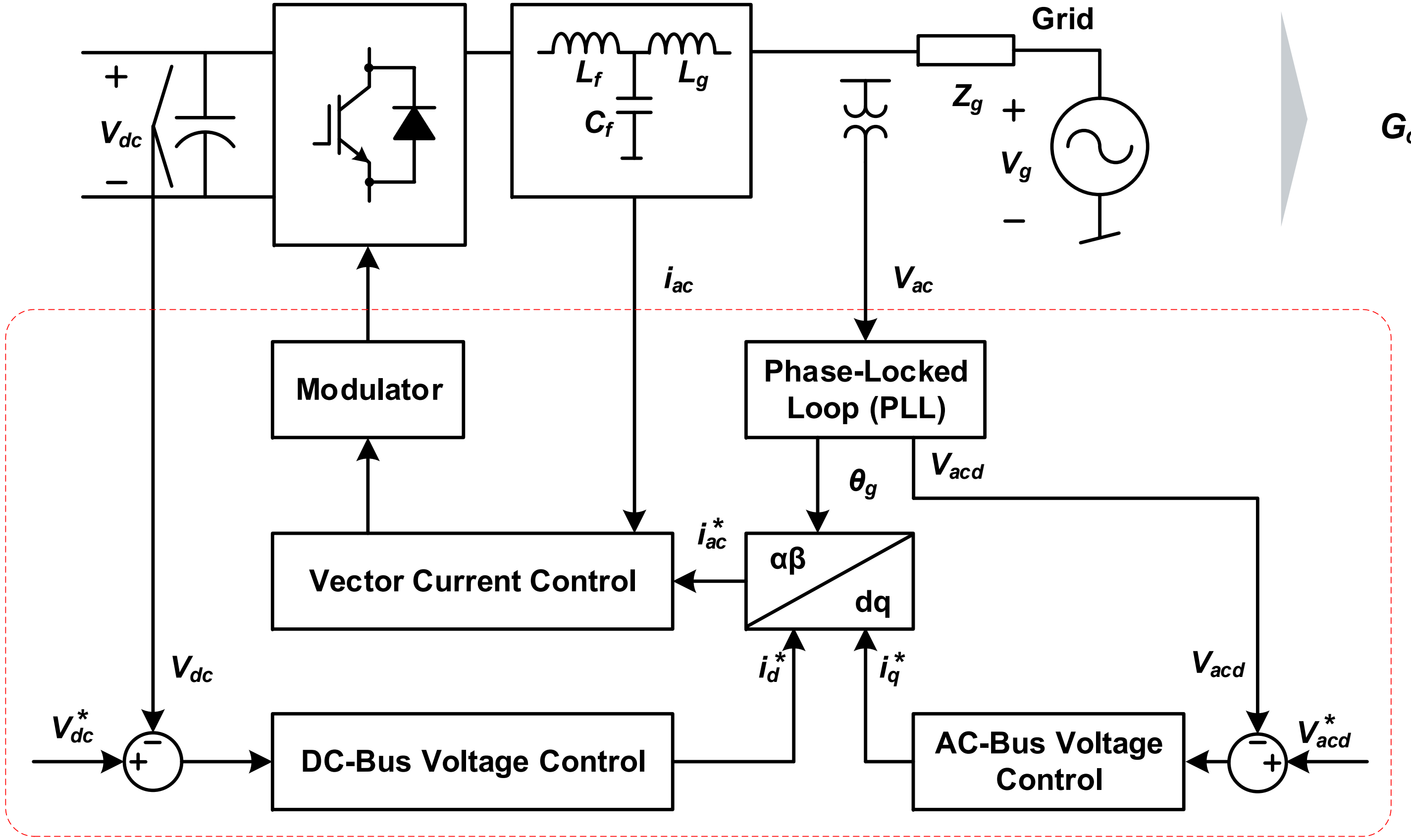

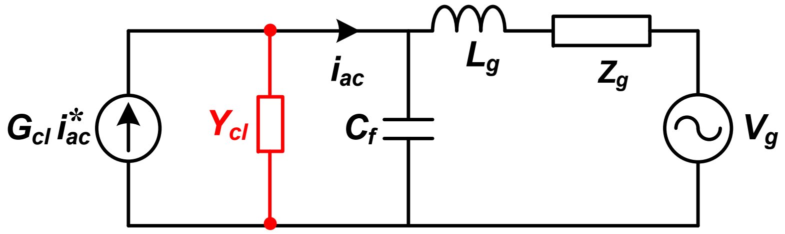

- Re{Y_{cl}}>0: stable, yet under-damped
- Re{Y_{cl}}=0: resonant, zero damping
- Re{Y_{cl}}<0: unstable, negative damping

Grid-Converter Interactions

Mapping from control loops to instability phenomena

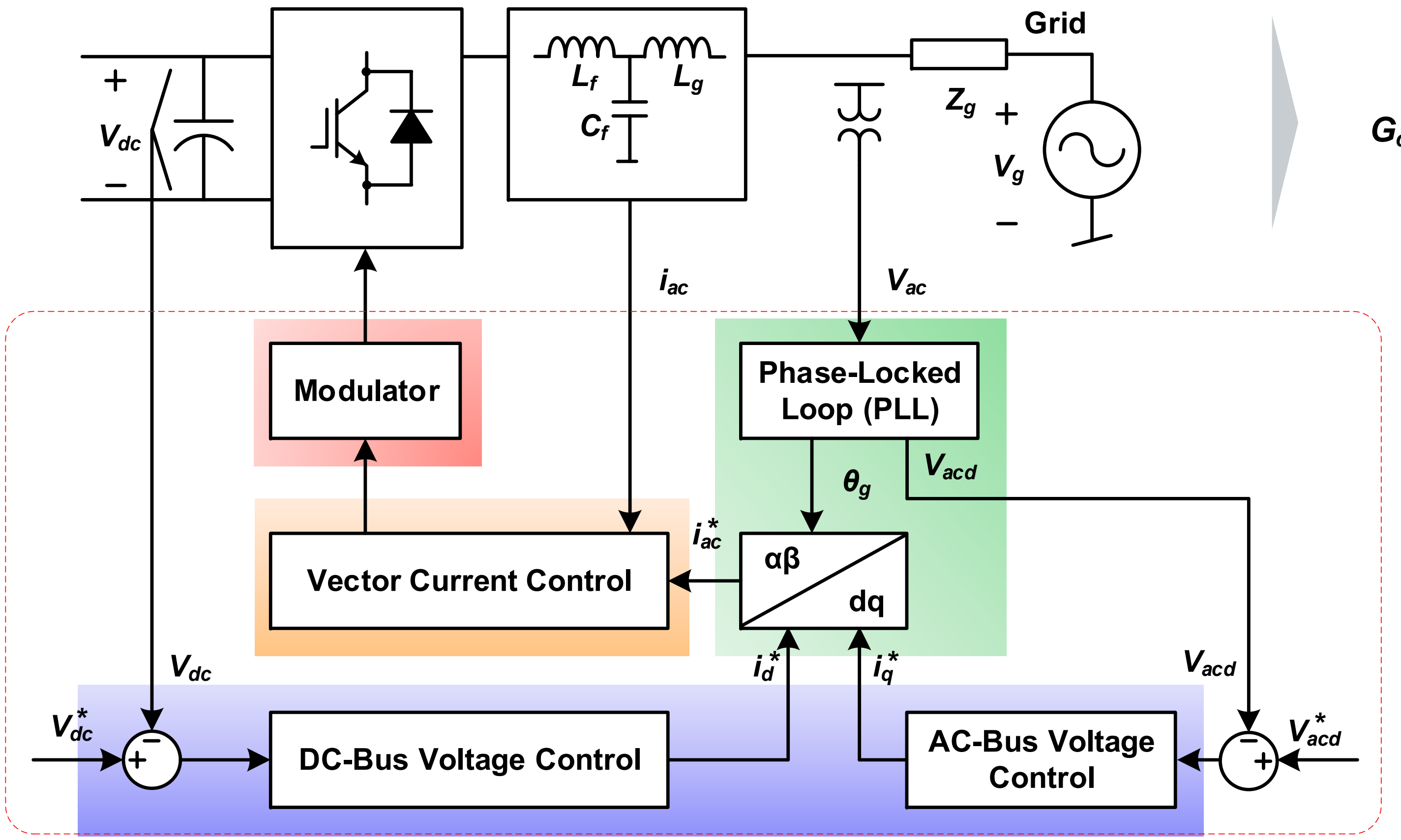

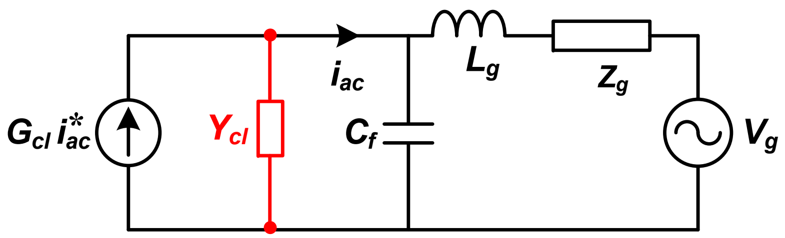

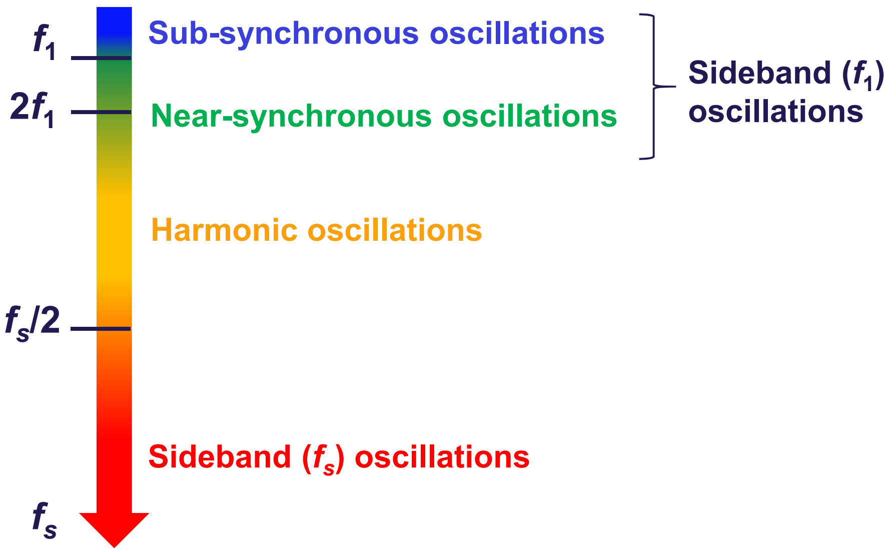

f_1: Grid fundamental frequency, f_s: Switching frequency

Grid-Converter Interactions
Weak grid with multiple resonance frequencies

- Short-Circuit Ratio (SCR) and inertia
- AC interconnect: low SCR, low-frequency parallel/series LC resonances
- DC interconnect: control interactions with HVDC converter station

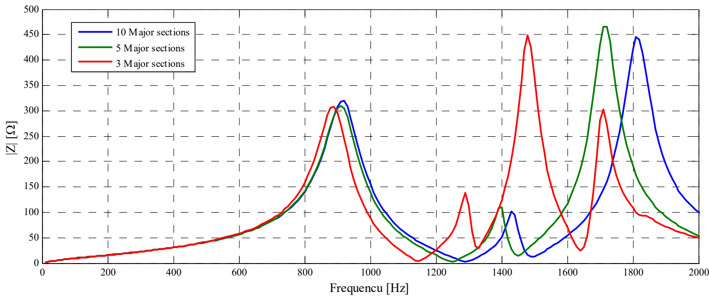

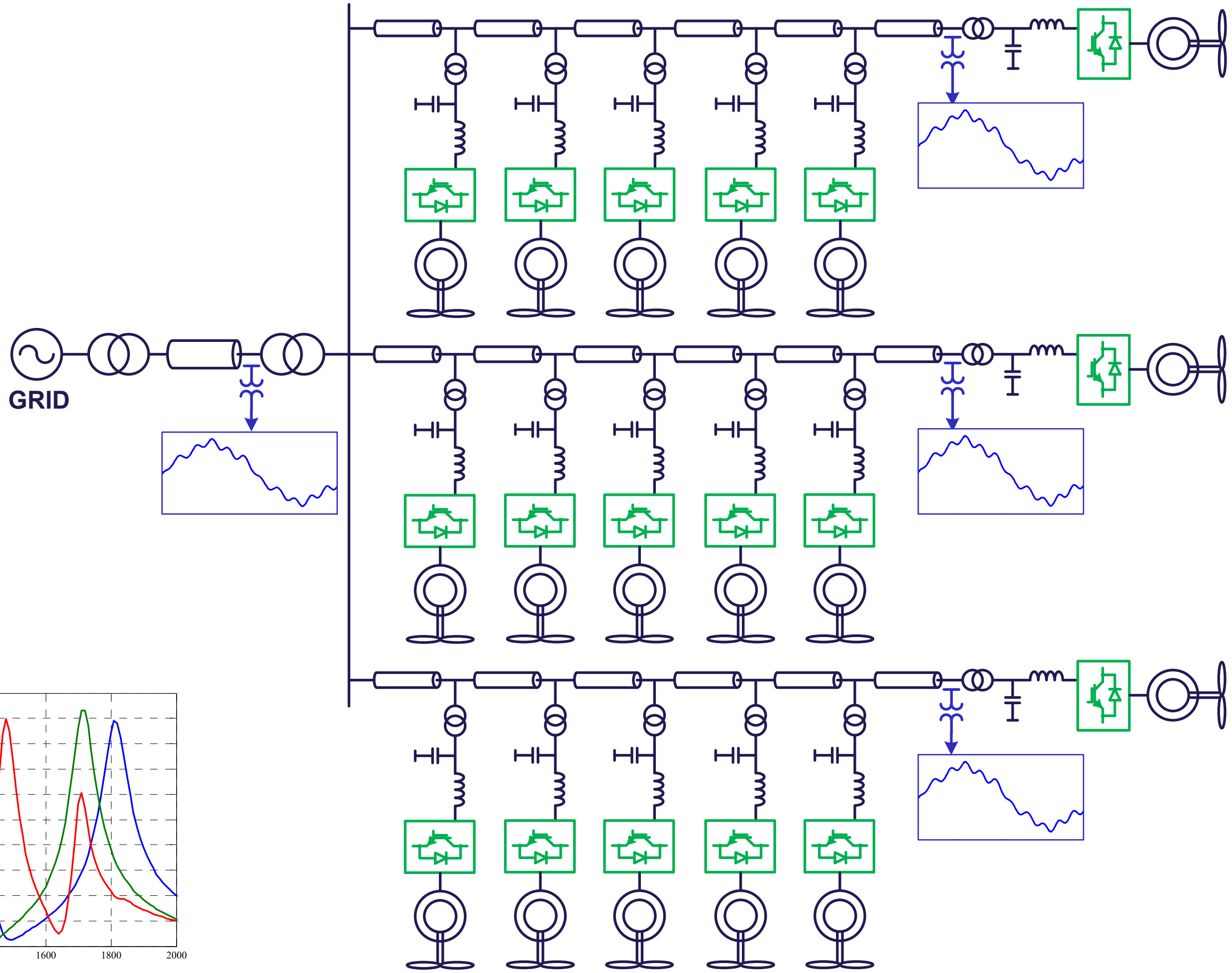

Wind power plant

Real-Life Challenges

Damping: positive (harmonics), negative (instabilities), zero (resonances)

VSC-HVDC + Offshore Wind

Filter resonance in the offshore HVDC converter station

Electrification of railways

Locomotives is out of control because of abnormal harmonics

©CSG

MMC-HVDC Transmission

Transformer resonance with current control of MMC

Real-Life Challenges

Harmonic current generated from offshore wind power plant

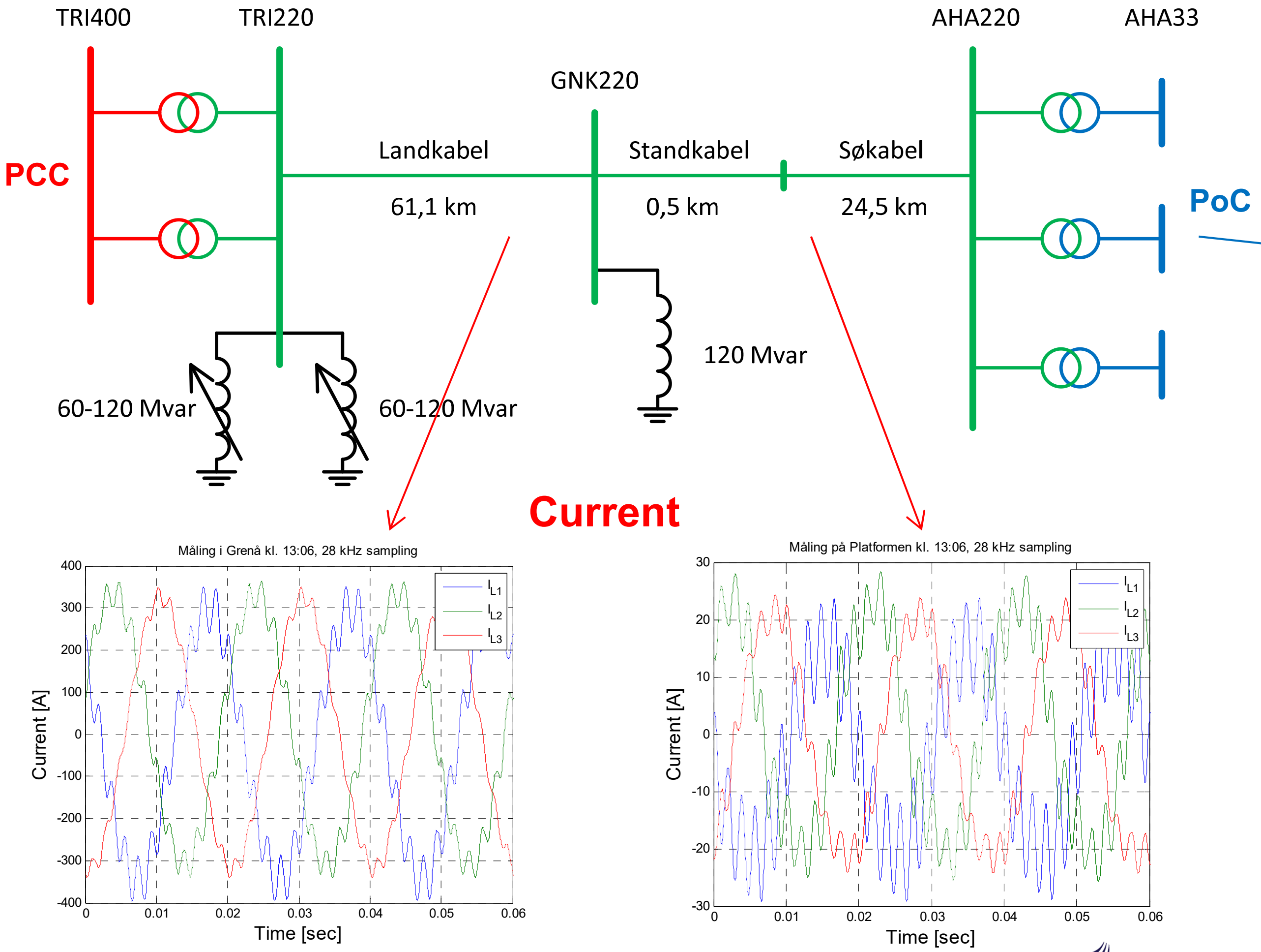

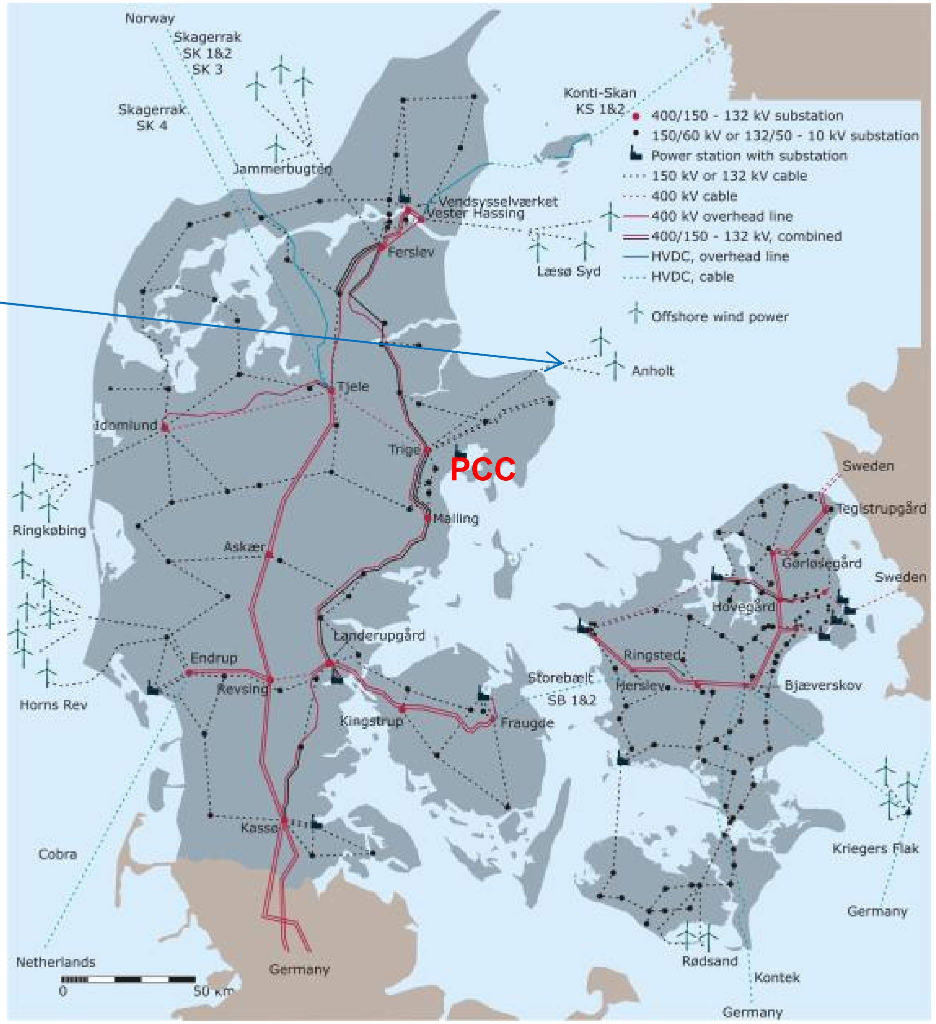

Source: C. F. Jensen, Energinet.dk, "Harmonic assessment in modern transmission network," Harmony Symposium, Aalborg, August 2015.

Grid-Forming/-Following Converters

Synchronization control is the key: from voltage-based to power-based

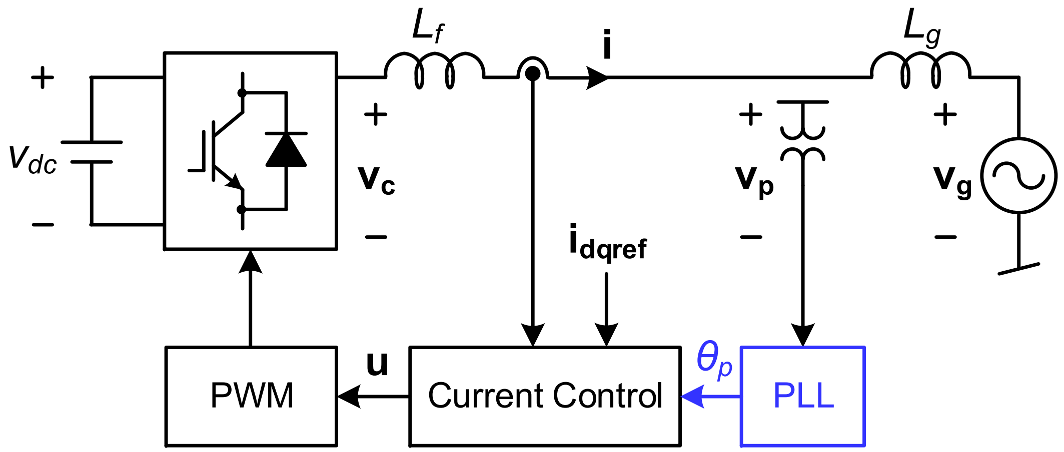

Grid-following control

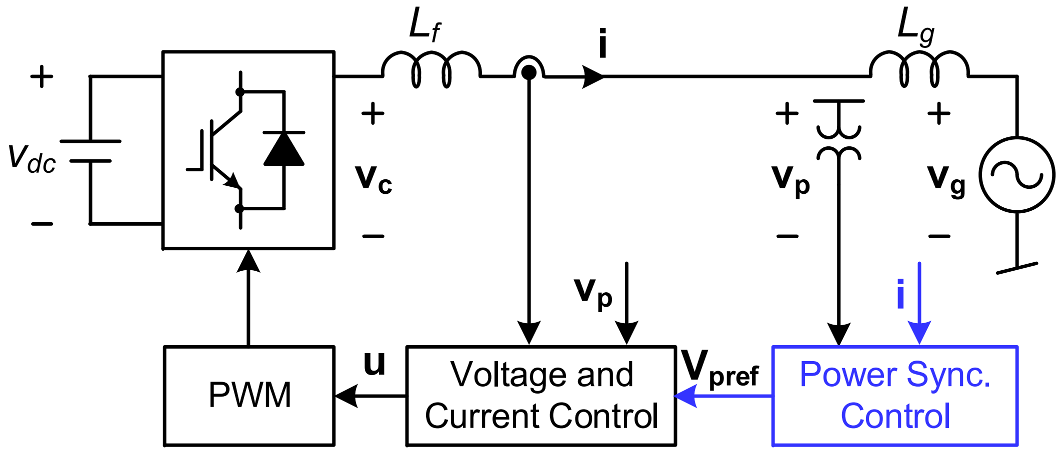

Grid-forming control

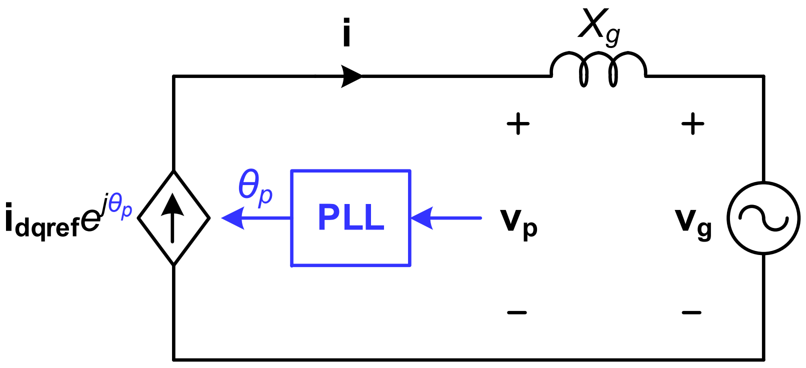

Voltage-based synchronization

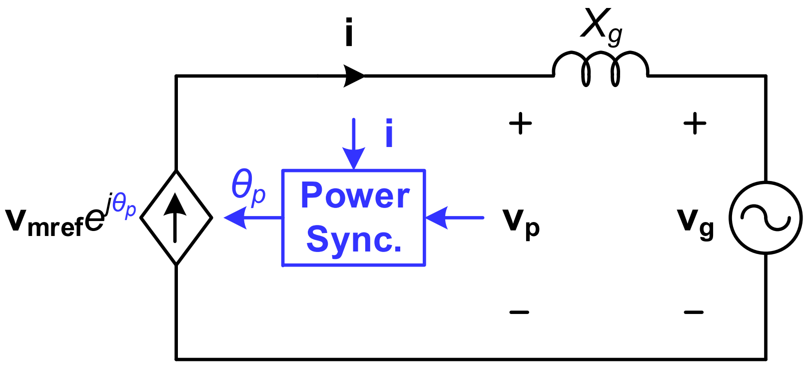

Power-based synchronization

Grid-forming converters

State of the art of power-based synchronization control

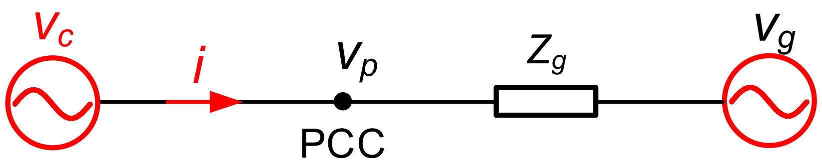

$$v_c = Ve^{j\theta}$$

$$\theta \Rightarrow P$$
$$V \Rightarrow Q$$

$P_{max} \approx 1$ p.u. @ SCR=1

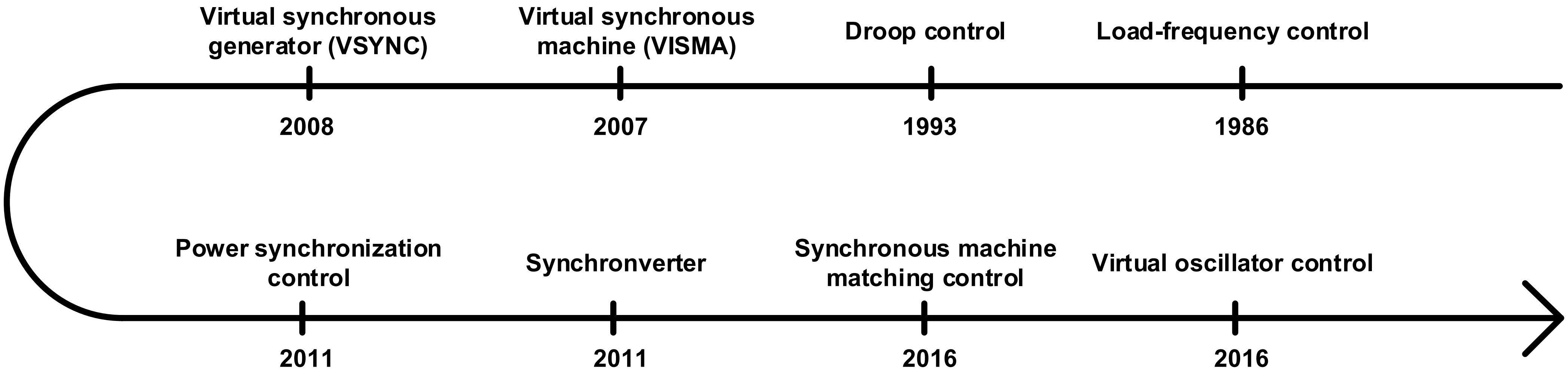

SMALL-SIGNAL MODELING

- Review of small-signal modeling methods
- Dynamic representations

Dynamic Properties of Grid-Connected Converters

Hybrid, nonlinear and time-variant systems

Sources of nonlinearity and time-variance

- **Hybrid:** Both continuous filter dynamics and discrete switching events
- **Nonlinear:** Feedback control - dependence of the duty cycle, i.e. d(t), on the input variables
- **Time-variant:** Switching modulation process and time-periodic operating trajectory

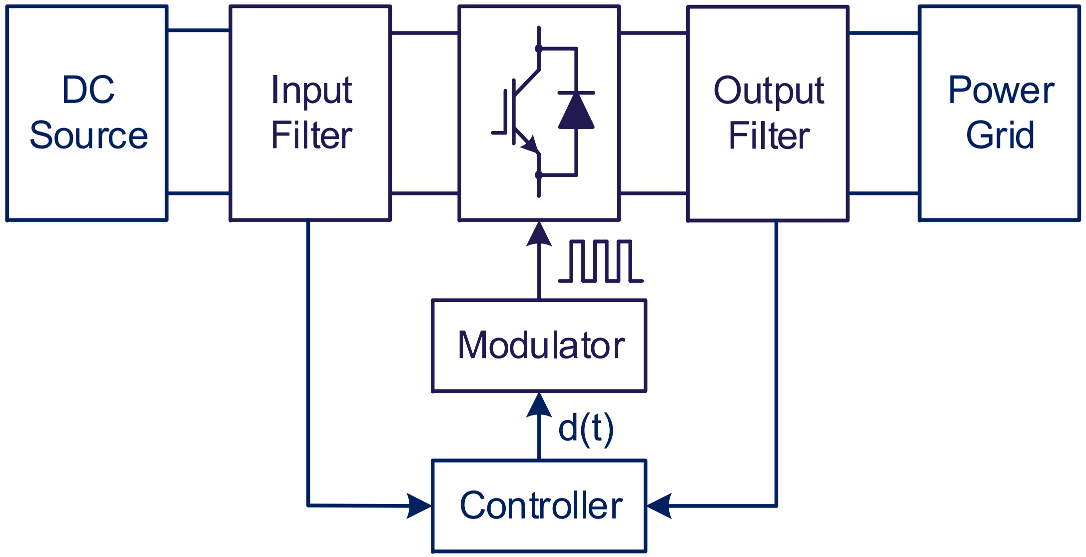

General diagram of grid-connected converters

Historical Review of Small-Signal Models

Harmonic analysis and controller design

1970

Persson [7] - thyristor HVDC
Frequency response analysis
Describing Function with single sinusoidal inputs

For control design

1985

Sakui and Fujita [8] - thyristor rectifier, Switching Function model w/o firing angle variation considered

For harmonic analysis

1986

Ngo [9] - PWM converter
State-Space Averaging with Park transformation
DQ-frame linearized model

For control design

1989

Larson, Baker, McIver [10] – thyristor HVDC, numerical simulations derived Harmonic Cross-Coupling Matrix

For harmonic/control analysis

1997

Mattavelli, Verghese, Stankovic [11] - thyristor FACTS devices
Dynamic Phasor with time-variant Fourier coefficients

For control design

2000

Mollerstedt [12] - locomotive inverter, Harmonic State-Space (HSS) modelling, Harmonic Transfer Matrix

For harmonic stability analysis

2003

Rico, Madrigal, Acha [13] - STATCOM with phase angle control, Extended Harmonic Domain (EHD)

For harmonic analysis

2007

Harnefors [14] - PWM converter
DQ-frame linearized model with the phase variation
Wen, Boroyevich, et, al [15], 2016

For control design

2014

Cespedes and Sun [16] - stability effect of PLL on PWM converter
Harmonic Balance, Multi-Input Describing Functions

For control design

2016

Wang, Harnefors, Blaabjerg [17] - Unified Impedance Model from *dq*-frame to *αβ*-frame, 2nd-order Harmonic Transfer Matrix

For control design

State-Space Averaging with Park Transformation

Averaged *dq*-frame model based on single real space vectors

Three-phase balanced converters

Switching function model → **Averaged (abc) model** → **Averaged (dq) model** → **Linearized (dq) model**

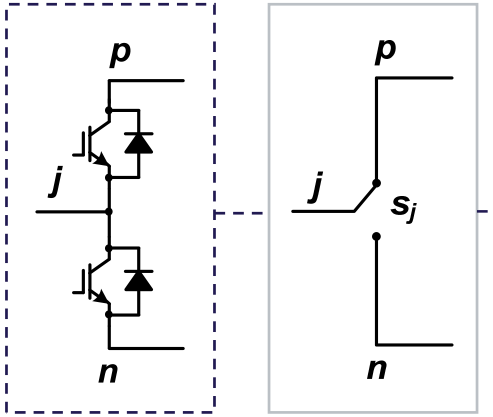

Neglect switching parasitic parameters

Nonlinear, time-variant , continuous

$$d_j(t) = \frac{1}{T_s}\int_{t-T_s}^{t} s_j(t)dt$$

Small-ripple approximation

High pulse ratios ($f_s/f_1 > 20$)

Nonlinear, time-periodic $d_{abc}(t)$

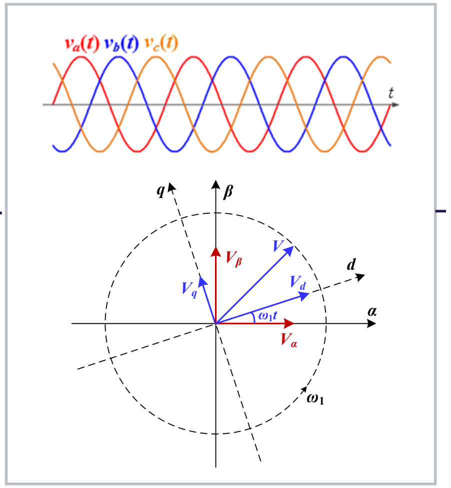

Nonlinear, time-invariant $d_{dq}(t)$

$$A = \begin{bmatrix} \frac{\partial f_1}{\partial x_1} & \cdots & \frac{\partial f_1}{\partial x_n} \\ \vdots & \cdots & \vdots \\ \frac{\partial f_n}{\partial x_1} & \cdots & \frac{\partial f_n}{\partial x_n} \end{bmatrix}$$

Jacobian matrix (Taylor series)

Linear, time-invariant

Generalized Averaging (Dynamic Phasor)

Averaged *dq*-frame model based on multiple complex space vectors

Three-phase unbalanced/single-phase converters

Switching function model → **Generalized averaging over the fundamental frequency ($\pm\omega_1$)** → **Linearized (dq) model**

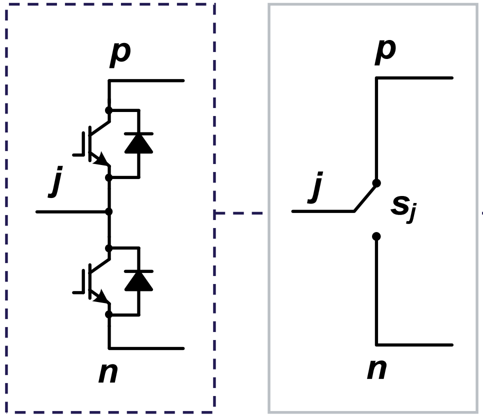

Neglect switching parasitic parameters

Nonlinear, time-variant , continuous

$$d_j(t) = \frac{1}{T}\int_{t-T}^{t} s_j(t)e^{-jk\omega_1 t}dt$$

Small-ripple approximation

Unbalanced three-phase systems ($k = \pm 1$)

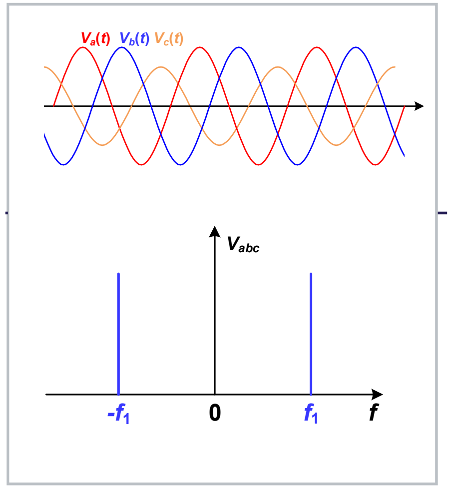

Nonlinear, time-invariant, but

multiple $d_{dq}(t)$

$$A = \begin{bmatrix} \frac{\partial f_1}{\partial x_1} & \cdots & \frac{\partial f_1}{\partial x_n} \\ \vdots & \cdots & \vdots \\ \frac{\partial f_n}{\partial x_1} & \cdots & \frac{\partial f_n}{\partial x_n} \end{bmatrix}$$

Jacobian matrix (Taylor series)

Linear, time-invariant

Harmonic State-Space
Averaged *αβ*-frame model based on multiple real space vectors

Three-phase unbalanced/single-phase converters

Nonlinear time-variant system → **Linear time-periodic (LTP) systems** → **Harmonic state-space (HSS) model**

$$\dot{x}(t) = f\left(x(t), u(t), t\right)$$
$$y(t) = g\left(x(t), u(t), t\right)$$

$$\Delta\dot{x}(t) = A(t)\cdot\Delta x(t) + B(t)\cdot\Delta u(t)$$
$$y(t) = C(t)\cdot\Delta x(t) + D(t)\cdot\Delta u(t)$$

$$s\mathbf{X} = (\mathbf{A}-\mathbf{N})\mathbf{X} + \mathbf{B}\mathbf{U}$$
$$\mathbf{Y} = \mathbf{C}\mathbf{X} + \mathbf{D}\mathbf{U}$$

Linearization about a time-periodically varying trajectory

Fourier series expansion for $A(t)$, $B(t)$, $C(t)$, $D(t)$;

Exponentially modulated periodic (EMP) input $u(t)$

$$A(t) = \sum_{k=-\infty}^{+\infty} A_k e^{jk\omega_1 t}, \quad u(t) = e^{st}\cdot\sum_{k=-\infty}^{+\infty} U_k e^{jk\omega_1 t}$$

Harmonic transfer function:

$$\mathbf{G}(s) = \mathbf{C}\left[s\mathbf{I} - (\mathbf{A}-\mathbf{N})\right]^{-1}\mathbf{B} + \mathbf{D}$$

$$\mathbf{N} = diag[\ldots \quad -j\omega_1 \quad 0 \quad j\omega_1 \quad \ldots]^T$$

Comparisons of Small-Signal Modeling Methods
Linearization around time-invariant/-periodic operating point/trajectory

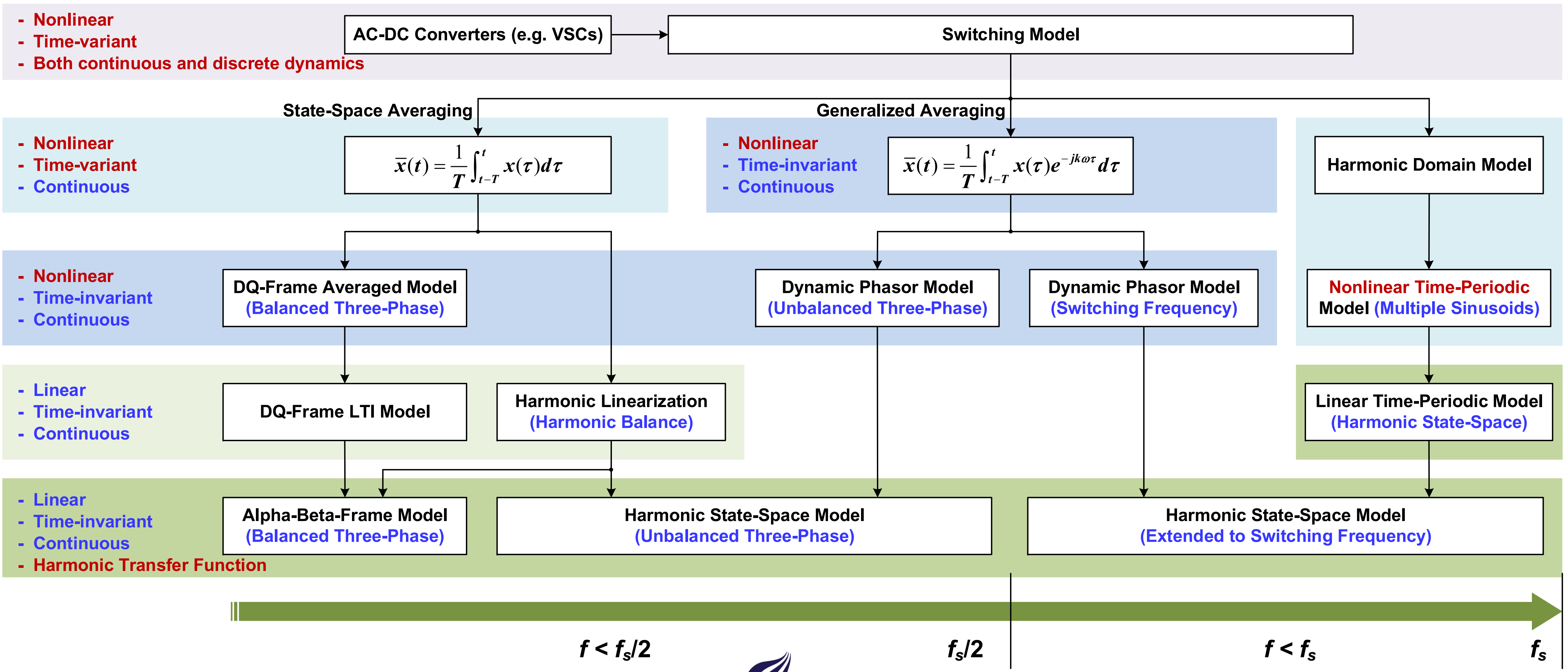

Comparisons of Small-Signal Modeling Methods

Model adequacy for analyzing grid-converter interactions

Model Adequacy	DQ-frame (averaged) Model	Dynamic Phasor Model	Harmonic State-Space Model
Sideband (f_1) oscillations	+	+	+
Harmonic oscillations	+	+	+
Sideband (f_s) oscillations	–	+	+
Low pulse-ratio (f_s/f_1)	–	+	+
Unbalanced three-phase systems	–	+	+

- Dynamic phasor model is a generalization of the *dq*-frame averaged model, which extracts the time-invariant operating point in the frequency domain
- Harmonic state-space model is a generalization of the stationary- (*αβ*-) frame model, which linearizes the system on time-periodic operating trajectories in the time domain

Multiple-Input Multiple-Output (MIMO) Representation
Averaged *dq*-frame model of converter power stage

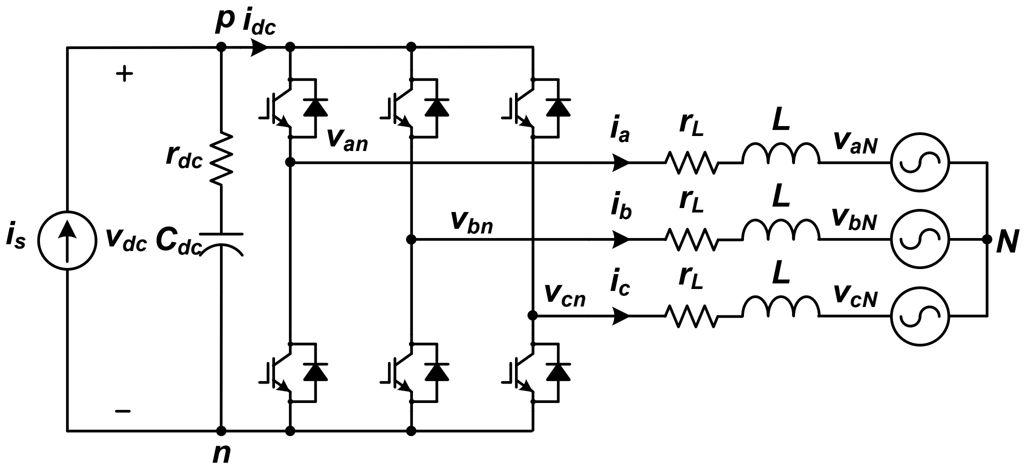

Voltage-Source Converter (VSC) with a non-ideal dc-link

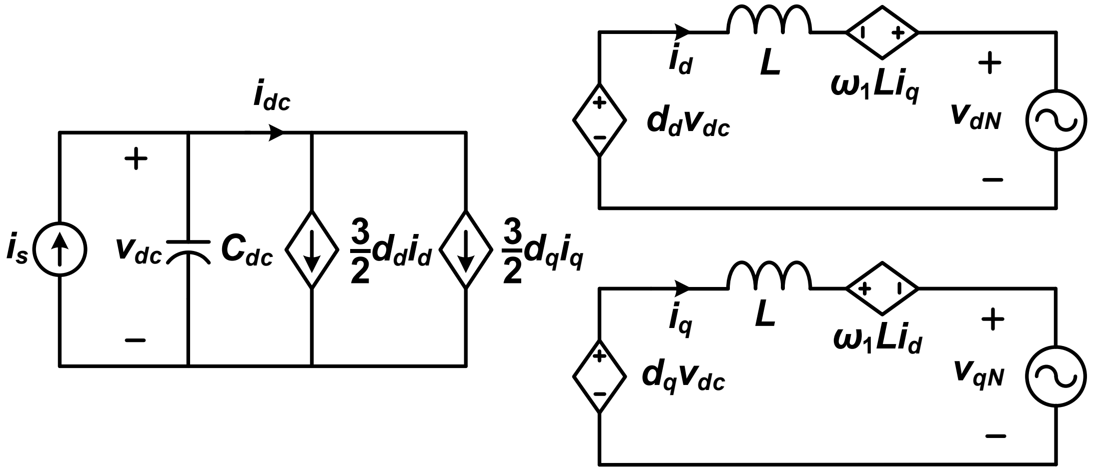

Averaged (*dq*-frame) model for three-phase balanced system

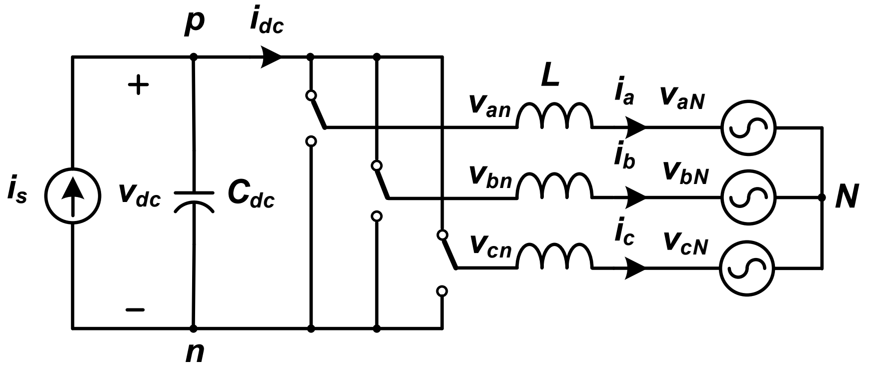

Switching function model of VSC

$$L\frac{d}{dt}\begin{bmatrix} i_d \\ i_q \end{bmatrix} = \begin{bmatrix} d_d \\ d_q \end{bmatrix} v_{dc} - \begin{bmatrix} v_{dN} \\ v_{qN} \end{bmatrix} - \begin{bmatrix} 0 & -\omega_1 L \\ \omega_1 L & 0 \end{bmatrix}\begin{bmatrix} i_d \\ i_q \end{bmatrix}$$

$$C\frac{dv_{dc}}{dt} = i_s - \frac{3}{2}\begin{bmatrix} d_d & d_q \end{bmatrix}\begin{bmatrix} i_d \\ i_q \end{bmatrix}$$

Simplified Model with Symmetrical Dynamics

Linear time-invariant (LTI) approximation with nearly ‘ideal’ dc-link

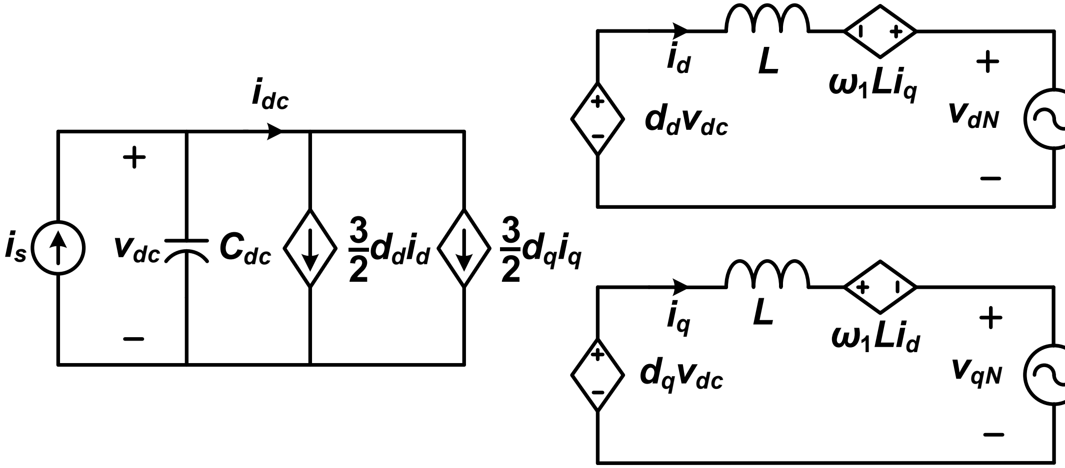

Averaged (*dq*-frame) model for three-phase balanced system

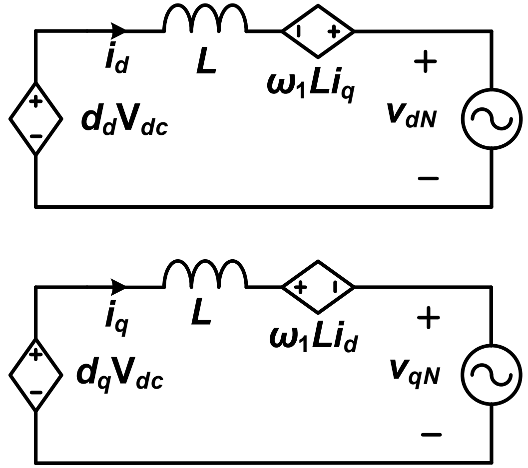

LTI model for vector current control

$$\begin{bmatrix} L\frac{d}{dt} & -\omega_1 L \\ \omega_1 L & L\frac{d}{dt} \end{bmatrix} \begin{bmatrix} i_d \\ i_q \end{bmatrix} = \begin{bmatrix} d_d \\ d_q \end{bmatrix} \mathrm{V}_{dc} - \begin{bmatrix} v_{dN} \\ v_{qN} \end{bmatrix}$$

$$Z_{L\_dq}(s) = \begin{bmatrix} Ls & -\omega_1 L \\ \omega_1 L & Ls \end{bmatrix}$$

Single-Input Single-Output (SISO) Representation
Complex transfer functions ↔ symmetrical transfer matrices

L1: SISO complex transfer functions based on complex vectors equal to symmetrical transfer matrices based on real vectors

- Symmetrical transfer function matrix of L-filter can be represented by SISO complex transfer function:

$$\mathbf{Z}_{\mathbf{L\_dq}}(\mathbf{s}) = \begin{bmatrix} sL & -\omega_1 L \\ \omega_1 L & sL \end{bmatrix} \quad \Leftrightarrow \quad Z_{L\_dq}(s) = (s + j\omega_1)L$$

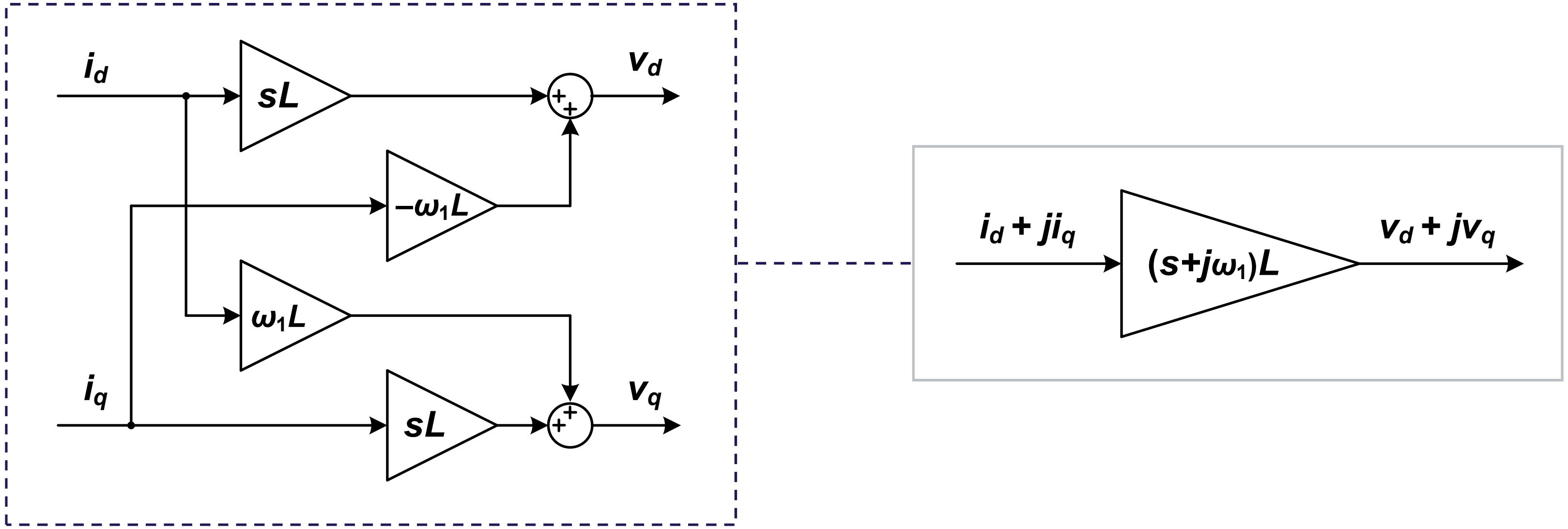

SISO Representation in Stationary Frame

Frequency translation of complex transfer functions from *dq*- to *αβ*-frame

L2: Park transformations for symmetrical transfer matrices equal to frequency shifts for complex transfer functions

- Representing Park transformations by complex exponential functions (Euler's formula)

$$\begin{bmatrix} i_d \\ i_q \end{bmatrix} = \begin{bmatrix} \cos(\omega_1 t) & \sin(\omega_1 t) \\ -\sin(\omega_1 t) & \cos(\omega_1 t) \end{bmatrix} \begin{bmatrix} i_\alpha \\ i_\beta \end{bmatrix} \Leftrightarrow i_d + j i_q = \left[\cos(\omega_1 t) - j\sin(\omega_1 t)\right](i_\alpha + j i_\beta) \Leftrightarrow \begin{cases} i_d + j i_q = e^{-j\omega_1 t}(i_\alpha + j i_\beta) \\ i_\alpha + j i_\beta = e^{j\omega_1 t}(i_d + j i_q) \end{cases}$$

- Frequency shift of complex transfer functions

$$v_d + j v_q = L(s + j\omega_1)(i_d + j i_q) \Leftrightarrow e^{-j\omega_1 t}(v_\alpha + j v_\beta) = L(\frac{d}{dt} + j\omega_1)e^{-j\omega_1 t}(i_\alpha + j i_\beta) \Leftrightarrow v_\alpha + j v_\beta = Ls(i_\alpha + j i_\beta)$$

$$\boxed{Z_{L\_\alpha\beta}(s) \Leftrightarrow Z_{L\_dq}(s - j\omega_1) \qquad Z_{L\_dq}(s) \Leftrightarrow Z_{L\_\alpha\beta}(s + j\omega_1)}$$

SISO Model of Vector Current Control

Constant dc-link voltage and no phase (θ_g) variation

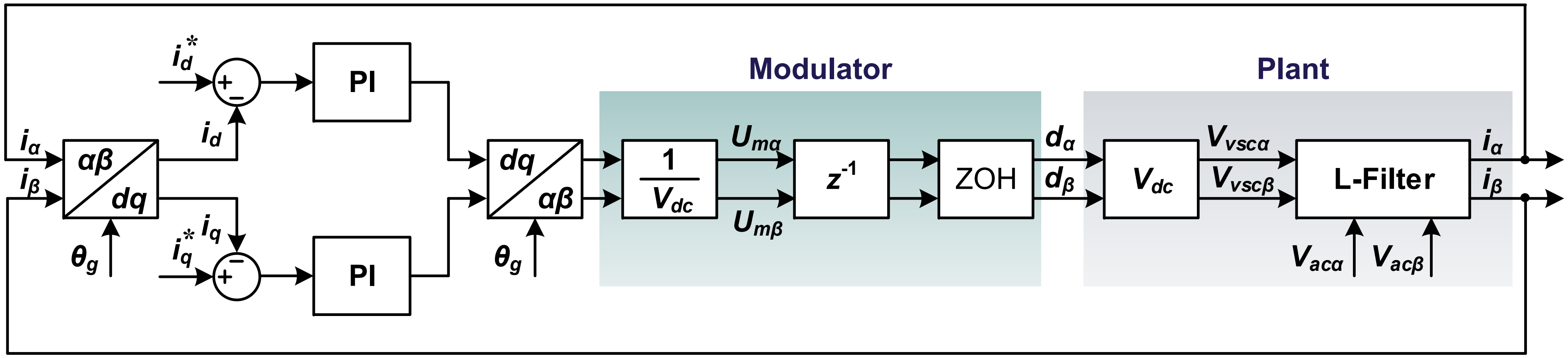

DQ-frame PI current control with digital modulator

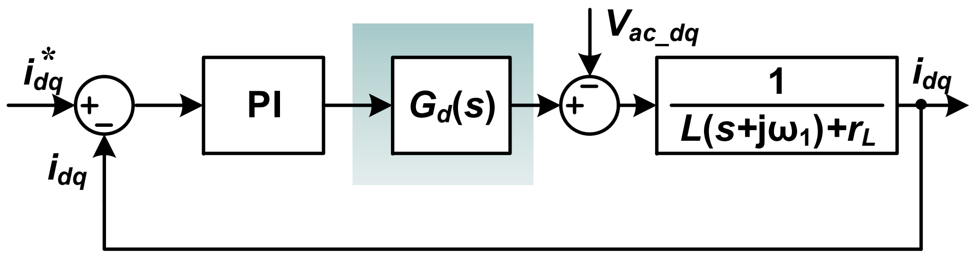

SISO model of *dq*-frame PI current control

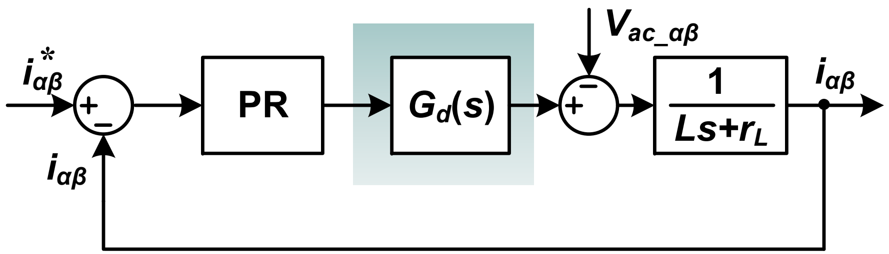

SISO model of *αβ*-frame PR current control

Time Delay of Digital Modulator
1.5 sampling period: ZOH + one sampling period

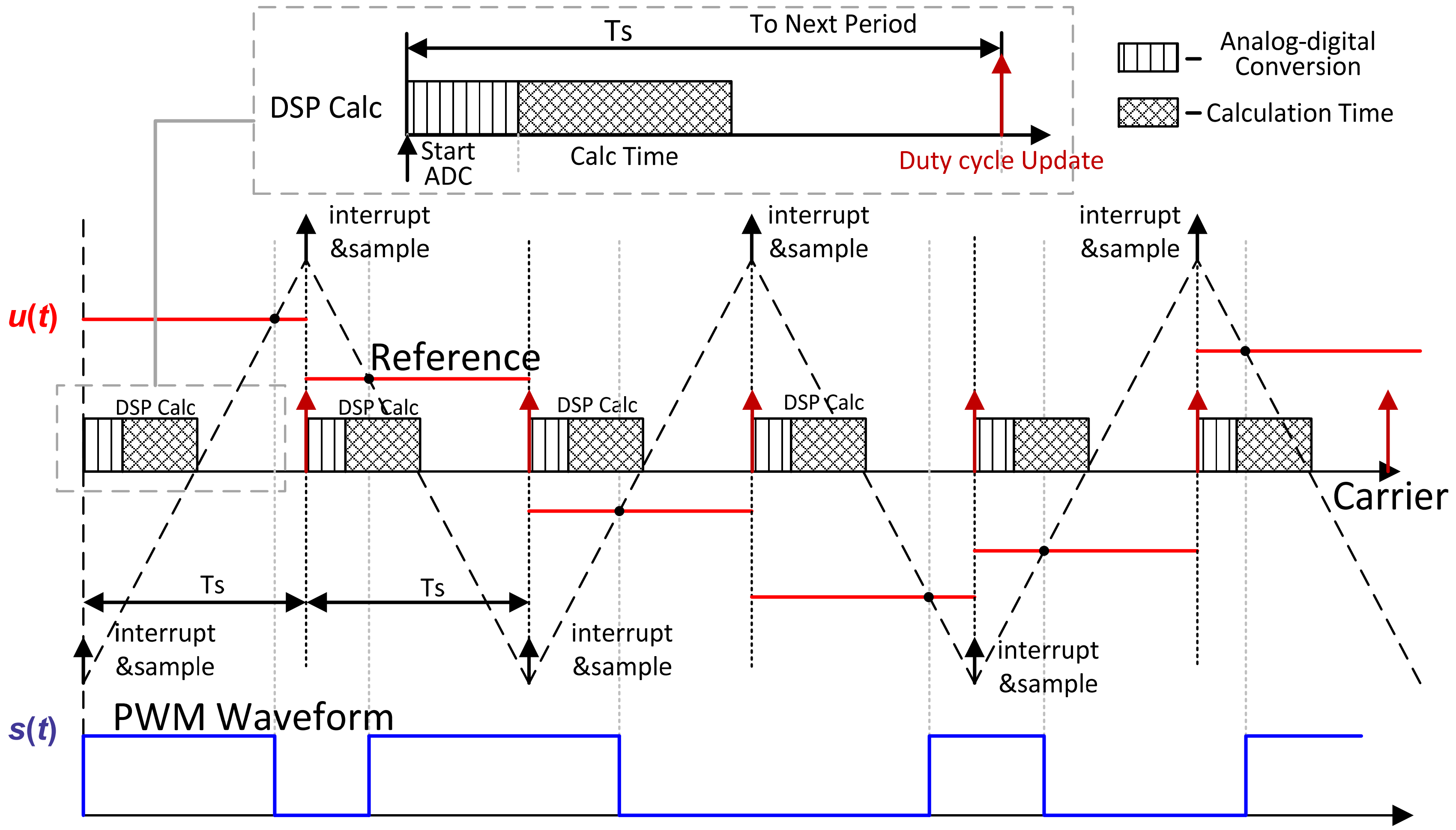

Dynamic Effect of Phase-Locked Loop (PLL)

Including phase (θ_g) variation into current control

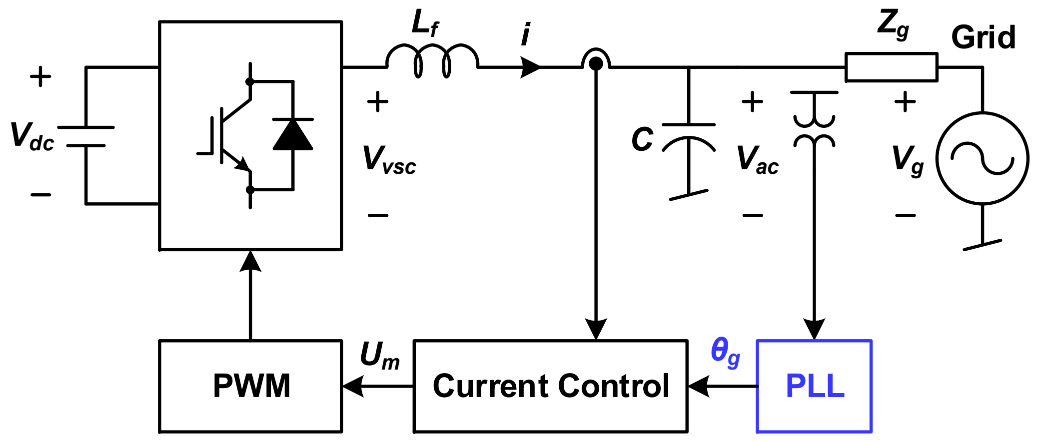

Vector current control with PLL included

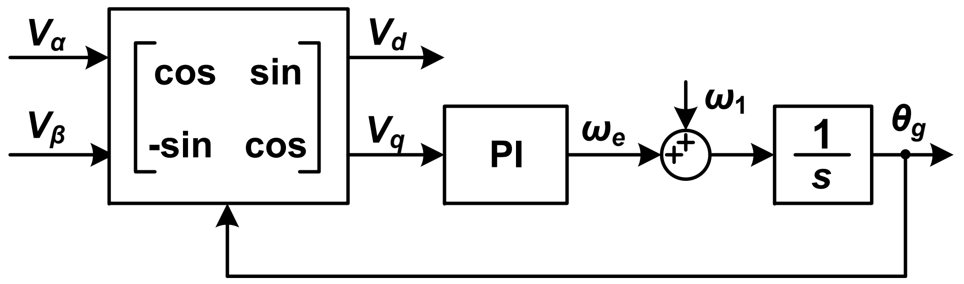

DQ-frame PLL

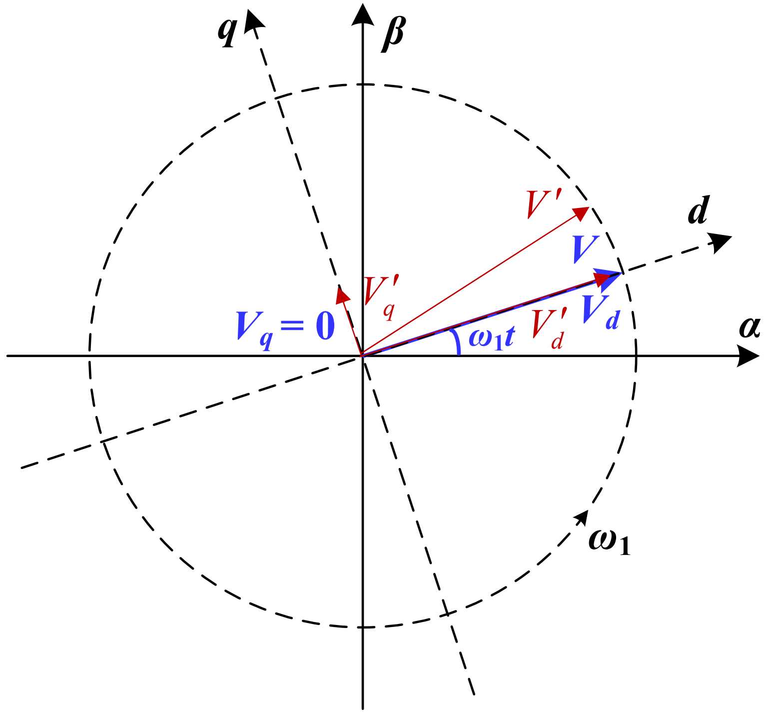

Basic principle

Small-Signal Modeling of PLL

Perturbations on the input voltage vector and the output phase

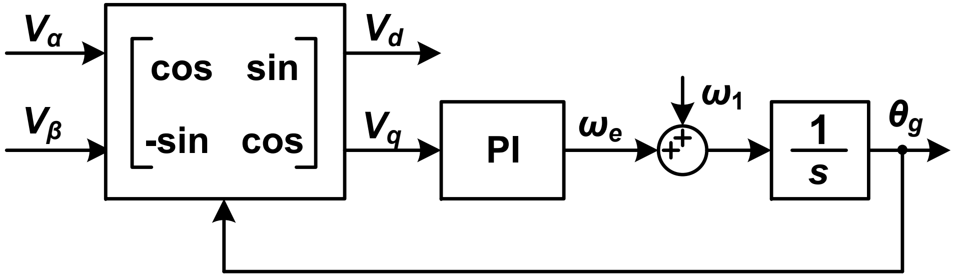

DQ-frame PLL

$$V_{dq0} = V_{d0} + j0, \quad V_{\alpha\beta} = \left(V_{dq0} + \Delta V_{dq}\right) e^{j\omega_1 t}$$

$$\theta_g = \omega_1 t + \delta, \quad V_{dq}^c = V_{\alpha\beta} e^{-j\theta_g}$$

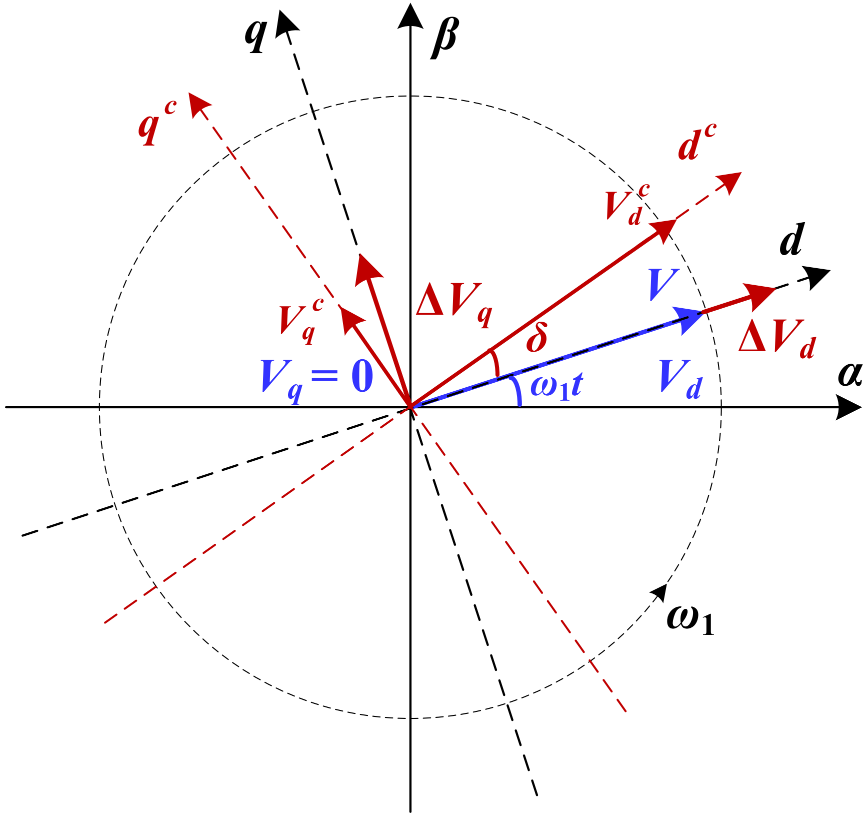

Small-Signal Modeling of PLL

Asymmetrical dynamics between *d*-axis and *q*-axis

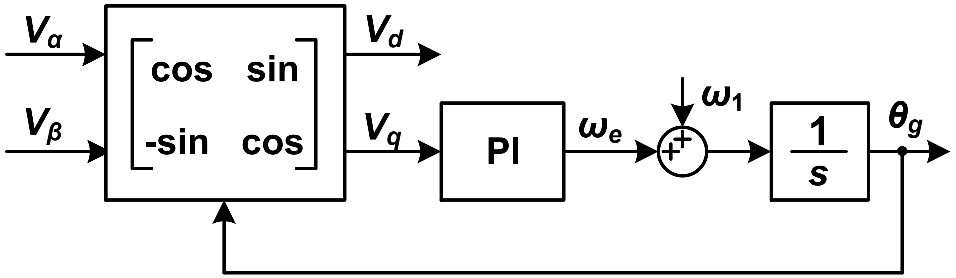

DQ-frame PLL

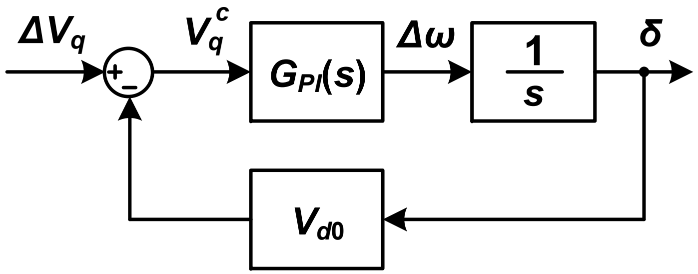

Second-order model of PLL

$$V_{\alpha\beta} = \left(V_{dq0} + \Delta V_{dq}\right) e^{j\omega_1 t}, \quad V_{dq0} = V_{d0} + j0$$

$$\theta_g = \omega_1 t + \delta$$

$$V_{dq}^c = V_{\alpha\beta} e^{-j\theta_g} = \left(V_{dq0} + \Delta V_{dq}\right) e^{j\omega_1 t} \cdot e^{-j(\omega_1 t + \delta)}$$

$$e^{-j\delta} \approx 1 - j\delta, \quad V_q^c = \Delta V_q - V_{d0}\delta$$

$$\delta = H_{PLL}(s)\Delta V_q, \quad H_{PLL}(s) = \frac{G_{PI}(s)}{s + G_{PI}(s) V_{d0}}$$

PLL Bridges Voltage Disturbance Current

Negative damping introduced on the q-q axis

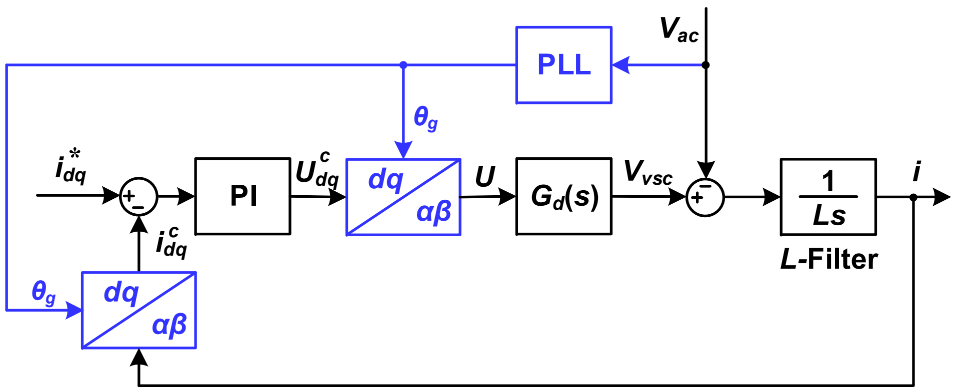

DQ-frame current control with PLL dynamics

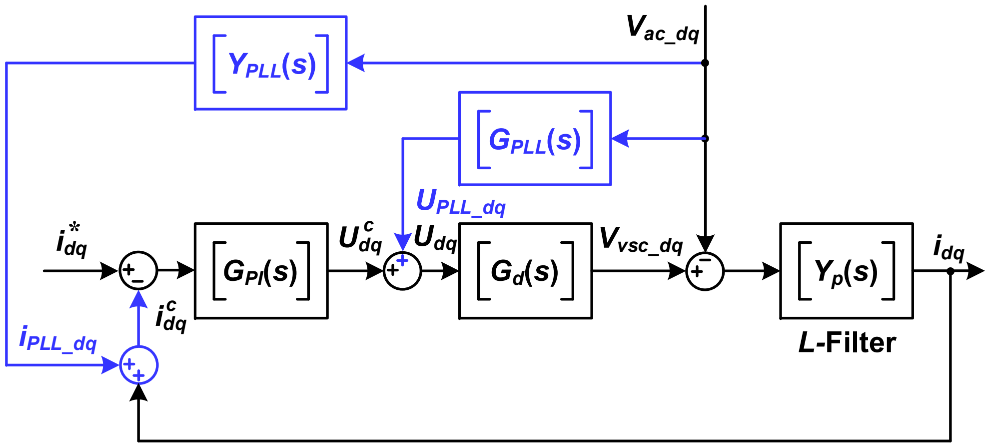

Equivalent block diagram with PLL dynamics

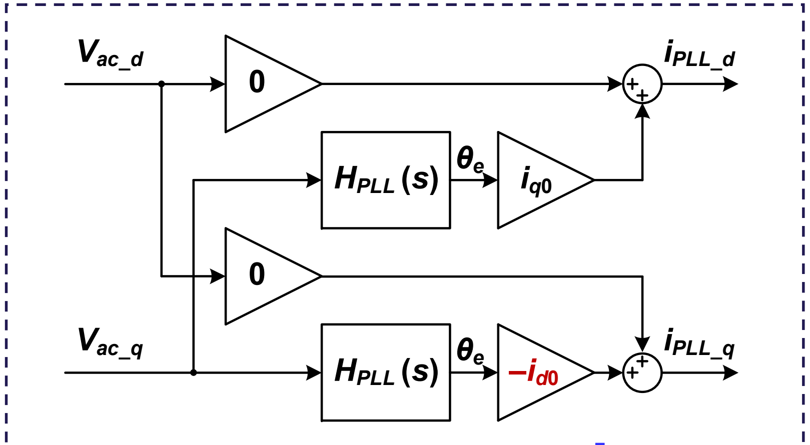

Asymmetrical $[Y_{PLL}(s)]$

$$i_{dq0}+\Delta i^c_{dq} = \underbrace{\left(i_{dq0}+\Delta i_{dq}\right)e^{j\omega_1 t}}_{i_{\alpha\beta}} \cdot e^{-j(\omega_1 t+\delta)} = \left(i_{dq0}+\Delta i_{dq}\right)e^{-j\delta}$$

$$e^{-j\delta} \approx 1-j\delta, \quad \Delta i^c_{dq} = i_{dq0}(1-j\delta)+\Delta i_{dq}(1-j\delta)$$

$$\Delta i_{PLL\_dq} = -ji_{dq0}\delta = -ji_{dq0}H_{PLL}(s)\Delta V_q$$

MIMO Representation of PLL Effect
Asymmetrical transfer function matrices in the *dq*-frame

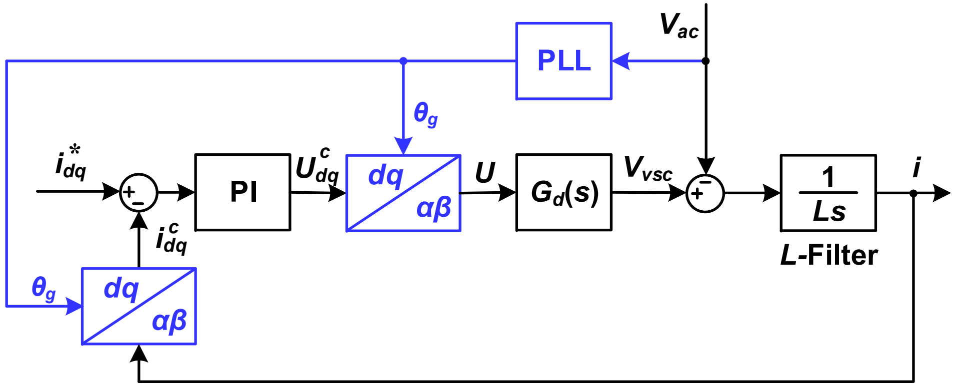

DQ-frame current control with PLL dynamics

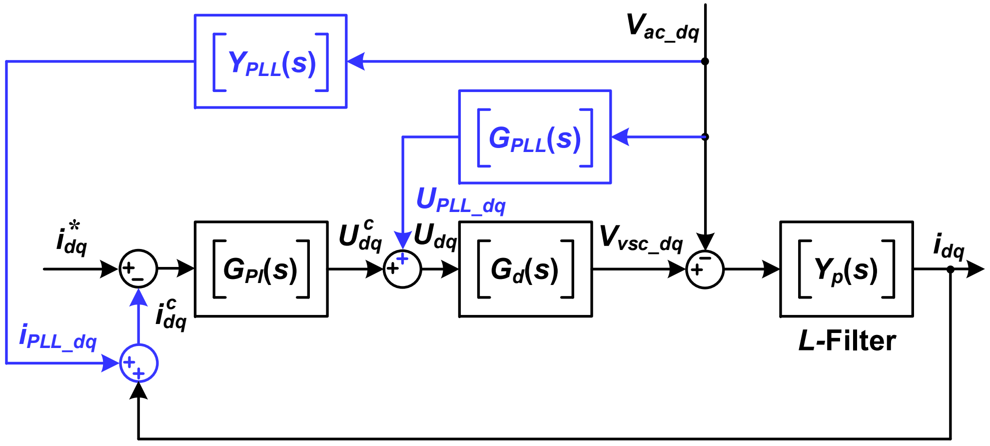

Equivalent block diagram with PLL dynamics

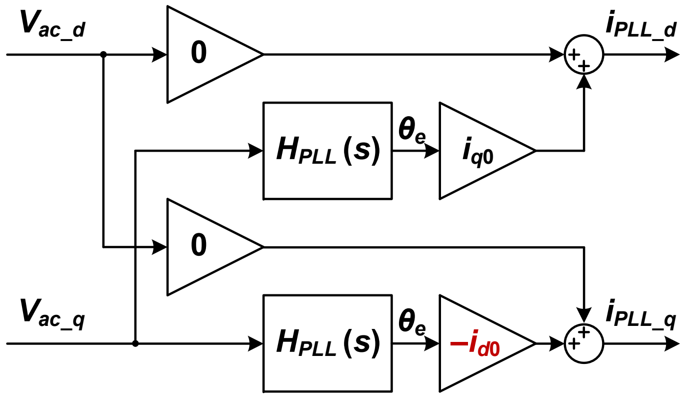

Asymmetrical $[Y_{PLL}(s)]$

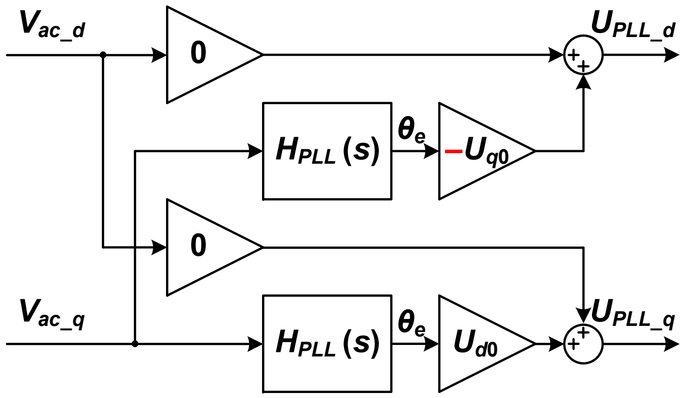

Asymmetrical $[G_{PLL}(s)]$

MIMO Representation of PLL Effect

Complex-valued equivalent of asymmetrical transfer matrices (*dq*-frame)

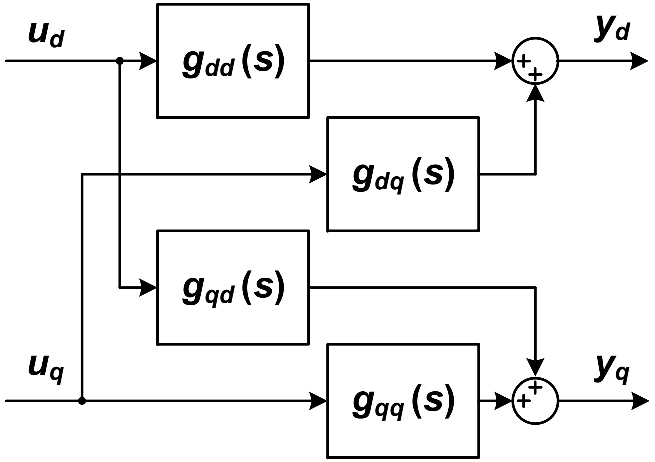

Asymmetrical transfer matrix for real vector (*dq*-frame, *ω*)

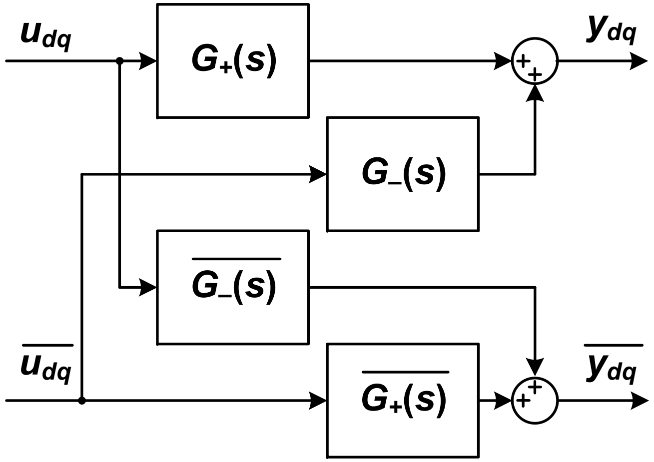

Equivalent transfer matrix for complex vector (*dq*-frame, *ω* → *ω*, −*ω*)

$$G_{+}(s)=\frac{g_{dd}(s)+g_{qq}(s)}{2}+j\frac{g_{qd}(s)-g_{dq}(s)}{2}$$

$$G_{-}(s)=\frac{g_{dd}(s)-g_{qq}(s)}{2}+j\frac{g_{qd}(s)+g_{dq}(s)}{2}$$

$$\overline{u_{dq}}=u_d-ju_q,\quad \overline{y_{dq}}=y_d-jy_q$$

$$\overline{G_{+}(s)}=\frac{g_{dd}(s)+g_{qq}(s)}{2}-j\frac{g_{qd}(s)-g_{dq}(s)}{2}$$

Generalized MIMO Representation
Complex-valued equivalent of asymmetrical transfer matrices ($\alpha\beta$-frame)

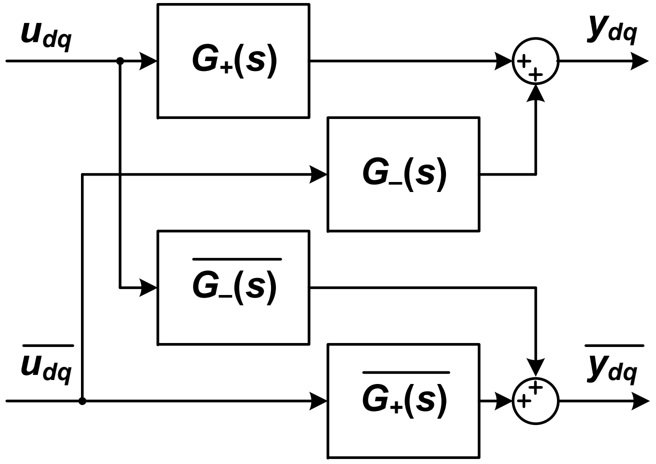

Equivalent transfer matrix for complex vector (*dq*-frame, $\omega \rightarrow \omega, -\omega$)

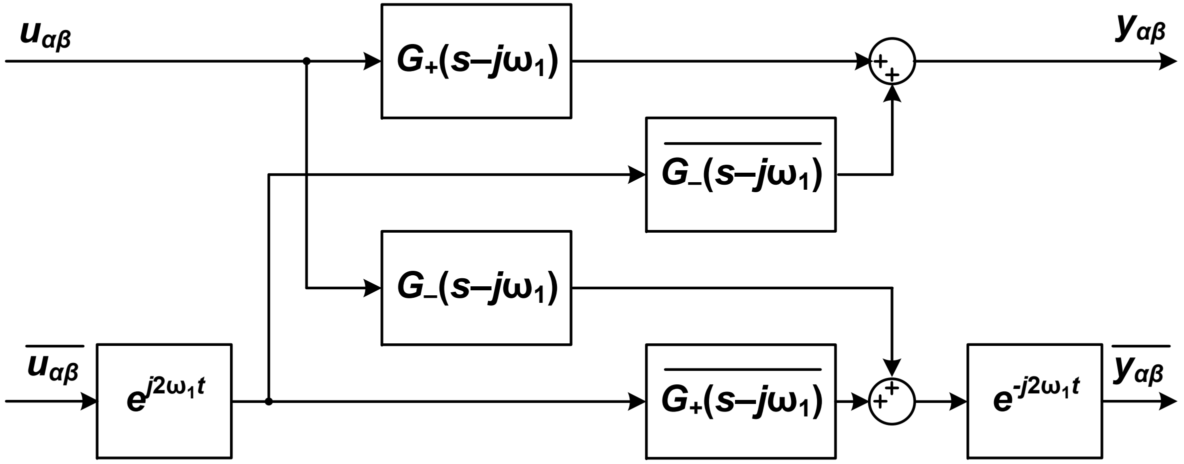

Equivalent transfer matrix for complex vector ($\alpha\beta$-frame, $\omega \rightarrow \omega, 2\omega_1-\omega$)

$$y_{dq} = G_+(s)u_{dq} + G_-(s)\overline{u_{dq}} \Rightarrow e^{-j\omega_1 t} y_{\alpha\beta} = G_+(s)e^{-j\omega_1 t}u_{\alpha\beta} + G_-(s)e^{j\omega_1 t}\overline{u_{\alpha\beta}} \Rightarrow y_{\alpha\beta} = G_+(s-j\omega_1)u_{\alpha\beta} + G_-(s-j\omega_1)e^{j2\omega_1 t}\overline{u_{\alpha\beta}}$$

$$\overline{y_{dq}} = \overline{G_-(s)}u_{dq} + \overline{G_+(s)}\,\overline{u_{dq}} \Rightarrow e^{j\omega_1 t}\overline{y_{\alpha\beta}} = \overline{G_-(s)}e^{-j\omega_1 t}u_{\alpha\beta} + \overline{G_+(s)}e^{j\omega_1 t}\overline{u_{\alpha\beta}} \Rightarrow e^{j2\omega_1 t}\overline{y_{\alpha\beta}} = \overline{G_-(s-j\omega_1)}u_{\alpha\beta} + \overline{G_+(s-j\omega_1)}e^{j2\omega_1 t}\overline{u_{\alpha\beta}}$$

Generalized MIMO Representation

Physical insights revealed by the *αβ*-frame transfer matrices

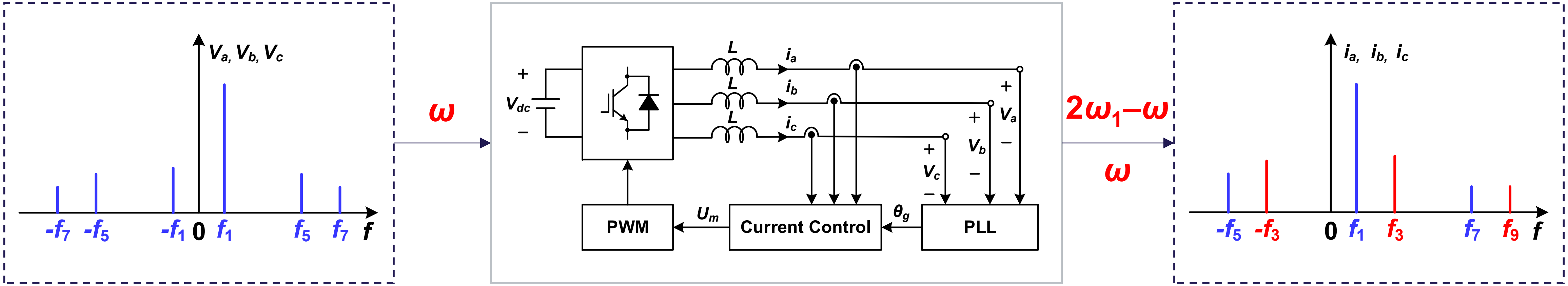

Input voltage perturbation | Three-phase three-wire converter | Output current response

Non-zero-sequence triplen harmonics in the three-phase three-wire converters with asymmetrical control dynamics in the *dq*-frame

Generalized MIMO Representation
Mathematical equivalence between different transfer matrices

DQ-transformation

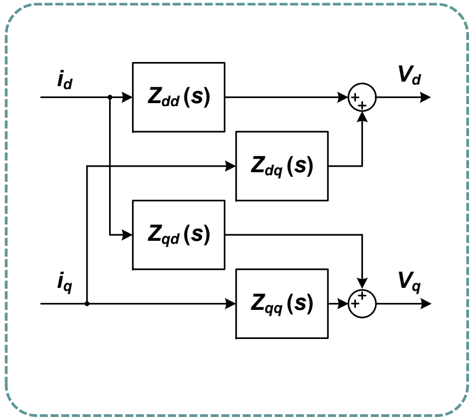

$$\begin{bmatrix} V_d \\ V_q \end{bmatrix} = \begin{bmatrix} Z_{dd}(s) & Z_{dq}(s) \\ Z_{qd}(s) & Z_{qq}(s) \end{bmatrix} \begin{bmatrix} i_d \\ i_q \end{bmatrix}$$

DQ-frame impedance model (real vector)

Complex equivalence

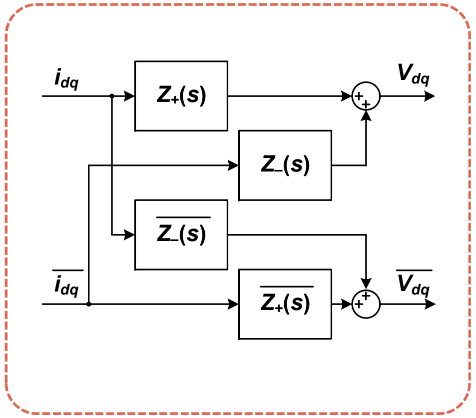

$$\begin{bmatrix} V_{dq} \\ \overline{V_{dq}} \end{bmatrix} = \begin{bmatrix} Z_+(s) & Z_-(s) \\ \overline{Z_-(s)} & \overline{Z_+(s)} \end{bmatrix} \begin{bmatrix} i_{dq} \\ \overline{i_{dq}} \end{bmatrix}$$

DQ-frame impedance model (complex vector)

Frequency translation

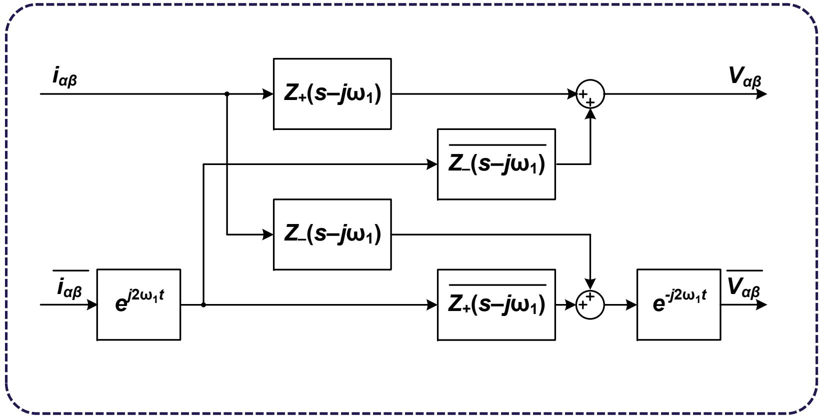

$$\begin{bmatrix} V_{\alpha\beta} \\ e^{j2\omega_1 t}\overline{V_{\alpha\beta}} \end{bmatrix} = \begin{bmatrix} Z_+(s-j\omega_1) & Z_-(s-j\omega_1) \\ \overline{Z_-(s-j\omega_1)} & \overline{Z_+(s-j\omega_1)} \end{bmatrix} \begin{bmatrix} i_{\alpha\beta} \\ e^{j2\omega_1 t}\overline{i_{\alpha\beta}} \end{bmatrix}$$

Stationary (αβ)-frame impedance model (complex vector)

IMPEDANCE-BASED STABILITY ANALYSIS

- Basic principle: minor feedback loop and Nyquist criterion
- Stability effects of different control loops

SISO Impedance-Based Stability Analysis
Minor-feedback loop gain and Nyquist criterion

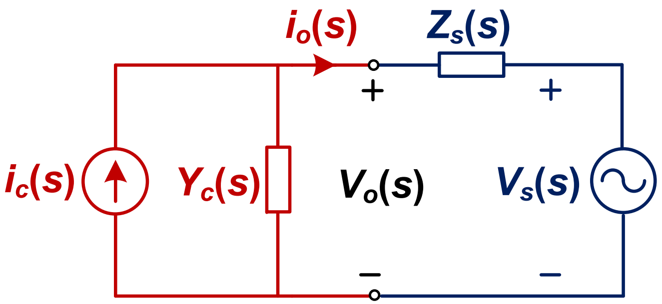

Equivalent circuit of grid converter

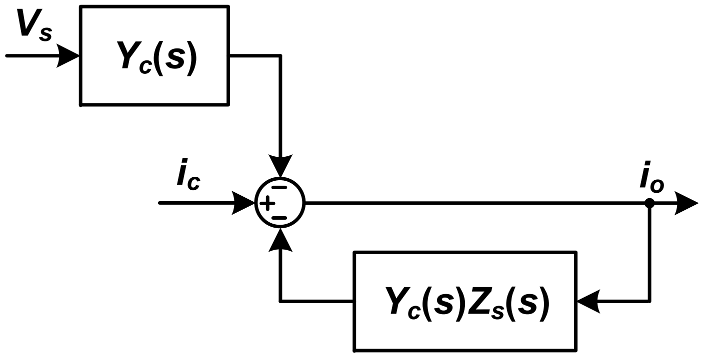

Concept of minor feedback loop

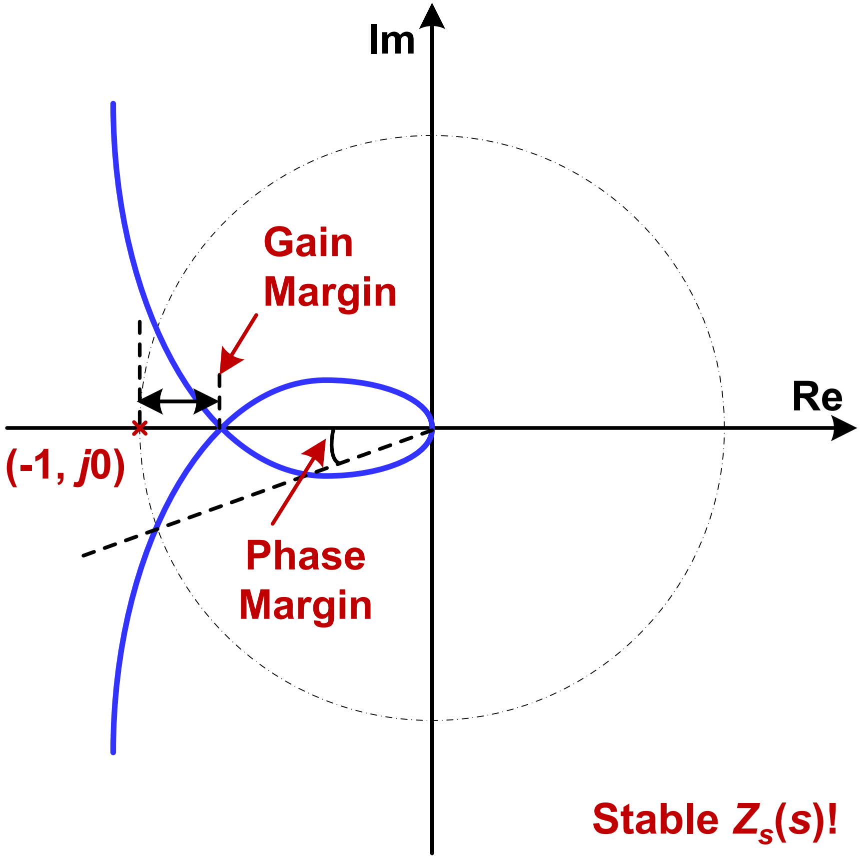

$T(s) = Y_c(s)Z_s(s)$

MIMO Impedance-Based Stability Analysis
Return-ratio matrix and generalized Nyquist criterion

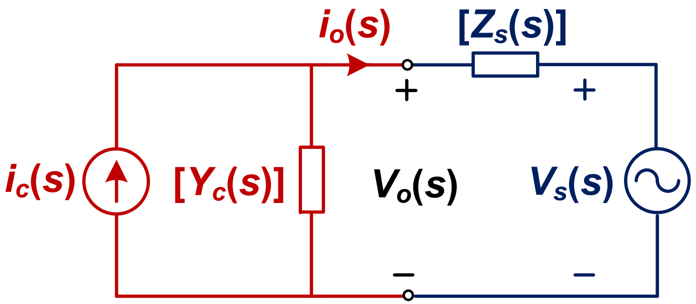

Equivalent circuit of grid converter

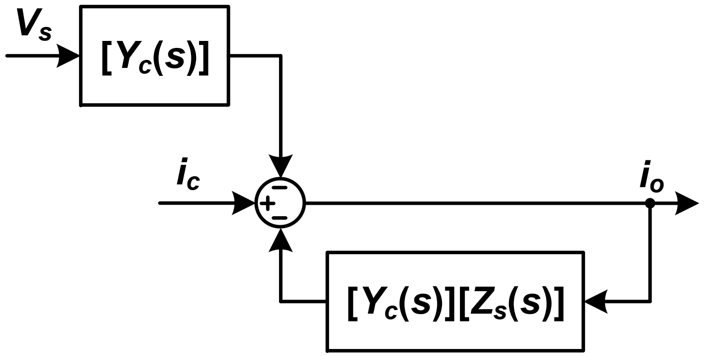

MIMO minor feedback loop

- **Generalized Nyquist stability criterion**

$$\det\left\{\lambda \mathrm{I} - \left[Y_c(s)\right]\left[Z_s(s)\right]\right\} = 0$$

- **Nyquist diagrams of λ_1 and λ_2**

Current Control for Grid-Following Converters
Time delay destabilizes the stability of current control with L-filter

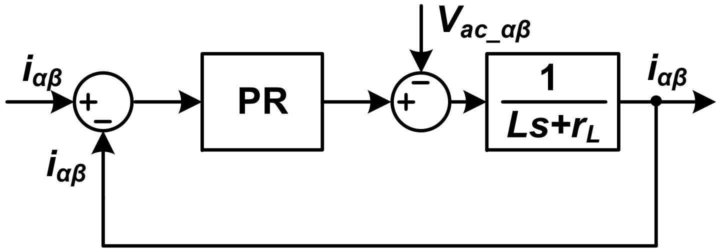

Current control w/o time delay - always stable!
Phase response within 180˚

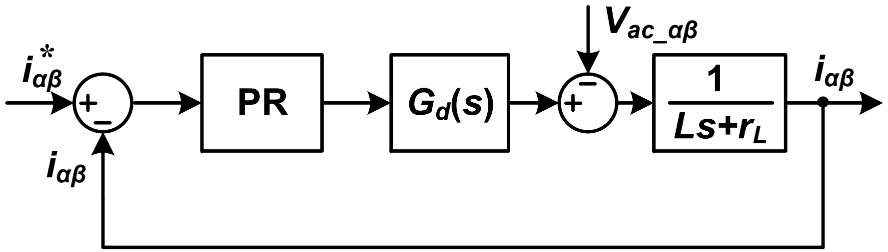

Current control w/ time delay - adding phase lag
Phase response out of 180˚

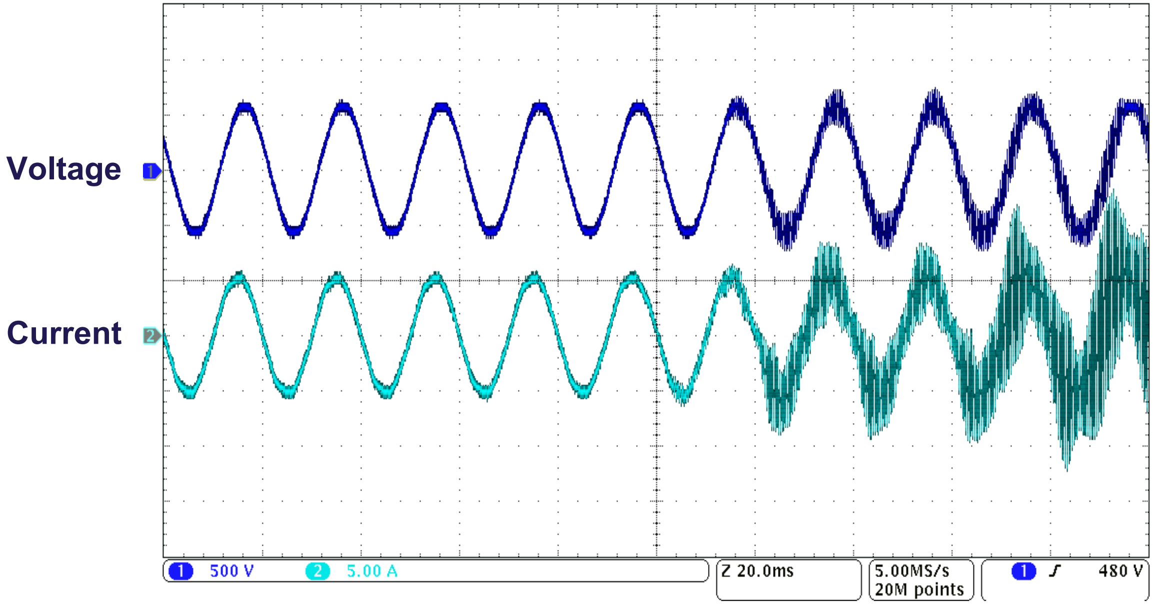

Measured waveforms for current control

Current Control for Grid-Following Converters
Time delay introduces a frequency-dependent negative resistance

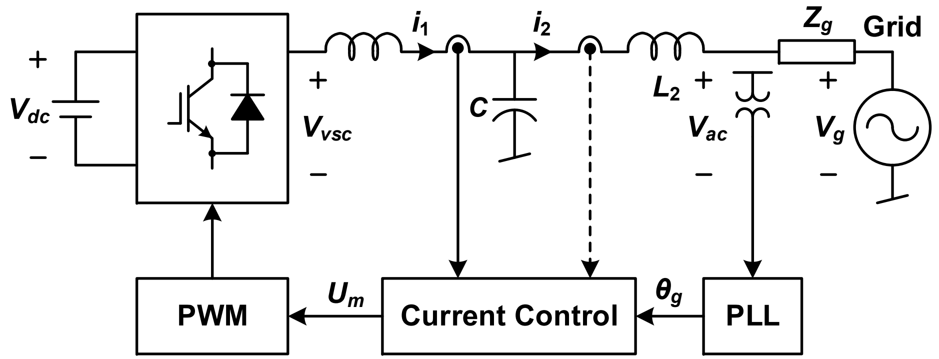

Current control with LCL-filter (i_1)

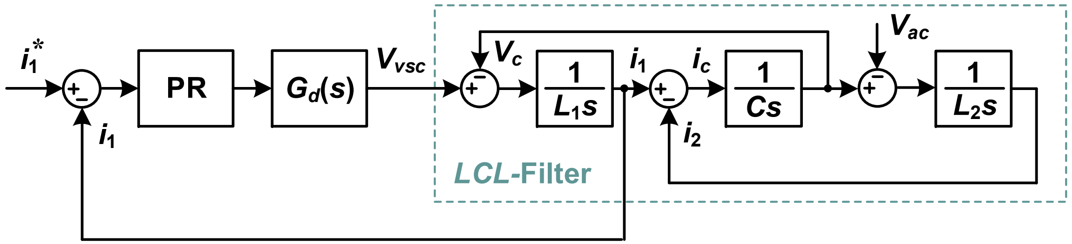

Single-loop converter current control

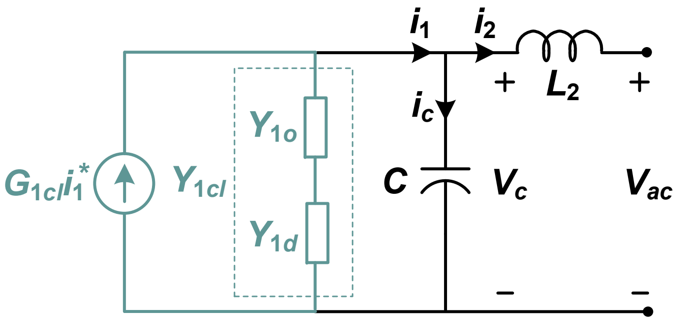

Impedance model

- *L*-filter plant and open-loop gain

$$Y_{1p} = Y_{1o} = \frac{1}{Z_{L1}}, \quad T_1 = G_c G_d Y_{1p}$$

- Closed-loop gain and output admittance

$$G_{1cl} = \frac{T_1}{1+T_1}, \quad Y_{1cl} = \frac{Y_{1o}}{1+T_1} = \frac{1}{\frac{1}{Y_{1o}} + \boxed{\frac{1}{Y_{1d}}}}, \quad Y_{1d} = \frac{1}{G_c G_d}$$

$$Y_{1d} = \frac{1}{k_p} e^{j\omega T_d} = \frac{1}{k_p}\left[\cos(T_d \omega) + j\sin(T_d \omega)\right]$$

Current Control for Grid-Following Converters
Impedance-based stability analysis with LCL-filter only

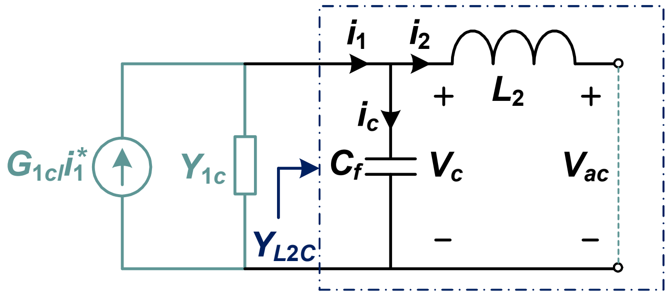

$$i_1 = \frac{1}{1+Y_{1c}/Y_{L2C}} G_{1cl} i_1^* - \frac{Y_{1c}/Y_{L2C}}{1+Y_{1c}/Y_{L2C}} \frac{V_{ac}}{Z_{L2}}$$

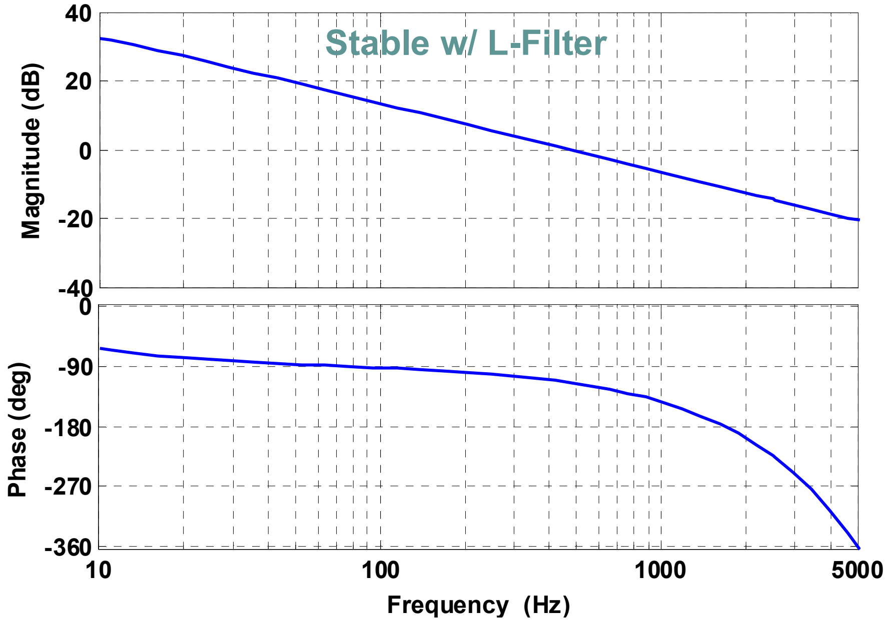

Open-loop gain T_1

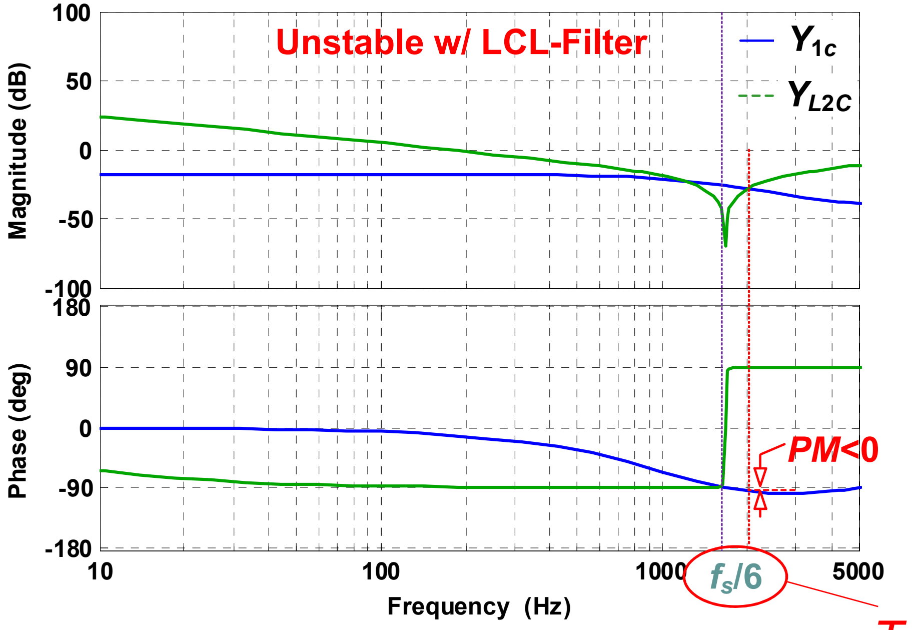

Impedance ratio Y_{1c}/Y_{L2C}

$T_d = 1.5T_s$

Current Control for Grid-Following Converters

Reducing time delay for robust stability of current control

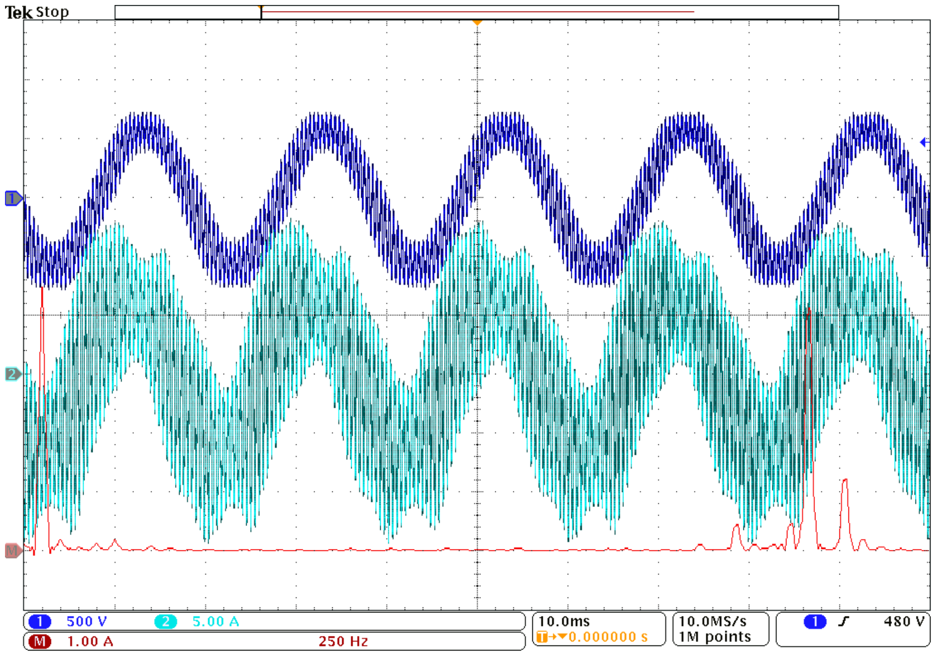

$$G_d(s) = e^{-1.5T_s s} \Rightarrow \omega \in (\omega_s/6, \omega_s/2]$$

T_s: computation delay; $0.5T_s$: PWM delay

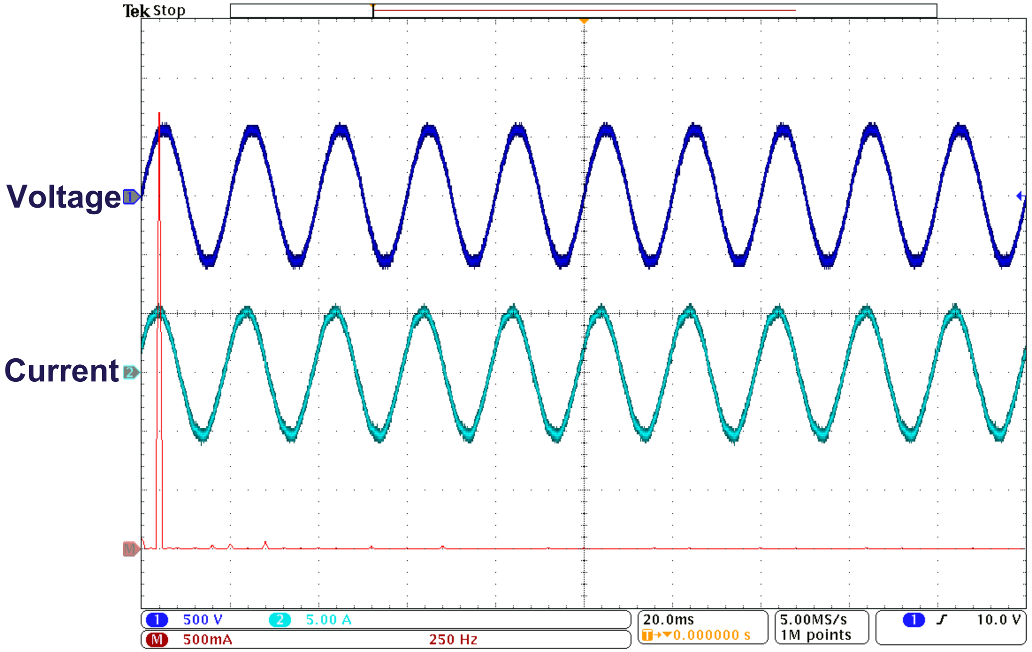

$$G_d(s) = e^{-T_s s} \Rightarrow \omega \in (\omega_s/6, \omega_s/2]$$

$0.5T_s$: computation delay; $0.5T_s$: PWM delay

Interrupt shift with $0.5T_s$

Voltage Control for Grid-Forming Converters
Dual-loop voltage and current control scheme

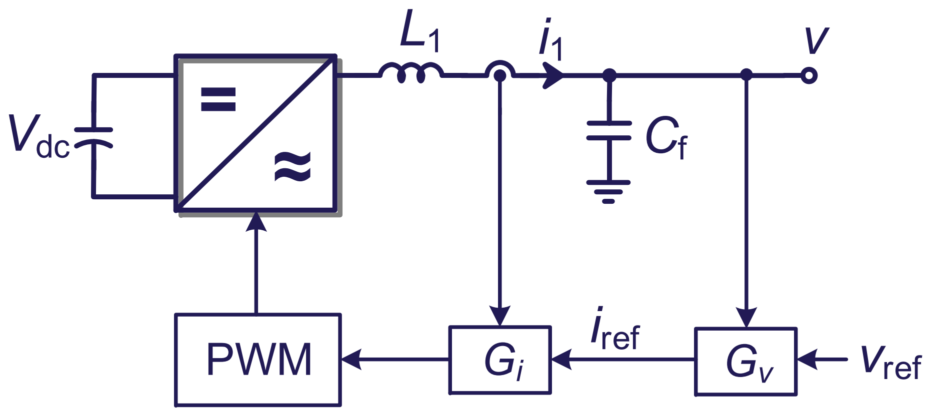

Dual-loop voltage Control

Voltage controller (G_v):

$$G_v = K_{pv} + \frac{K_{rv} s}{s^2 + \omega_1^2}$$

Current controller (G_i):

$$G_i = K_{pi}$$

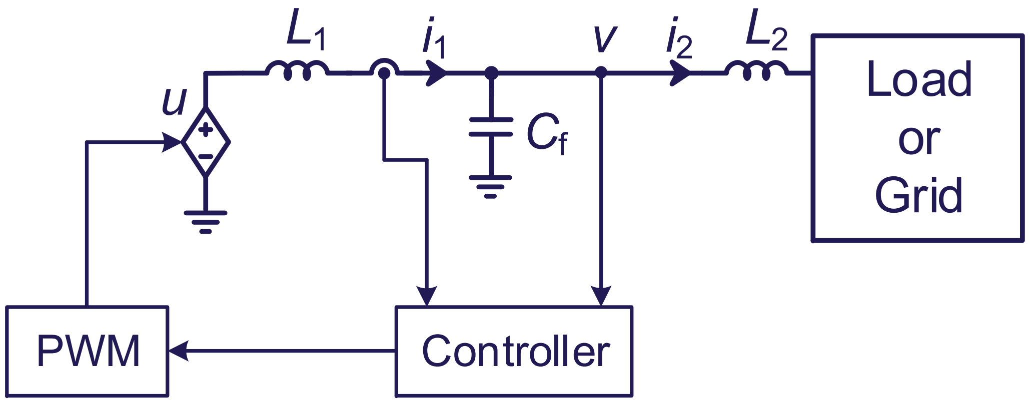

Small-signal model of power stage

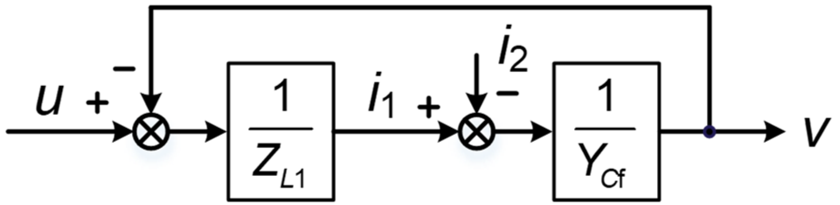

Block diagram of LC-filter

Voltage Control for Grid-Forming Converters
Small-signal modeling of dual-loop voltage control

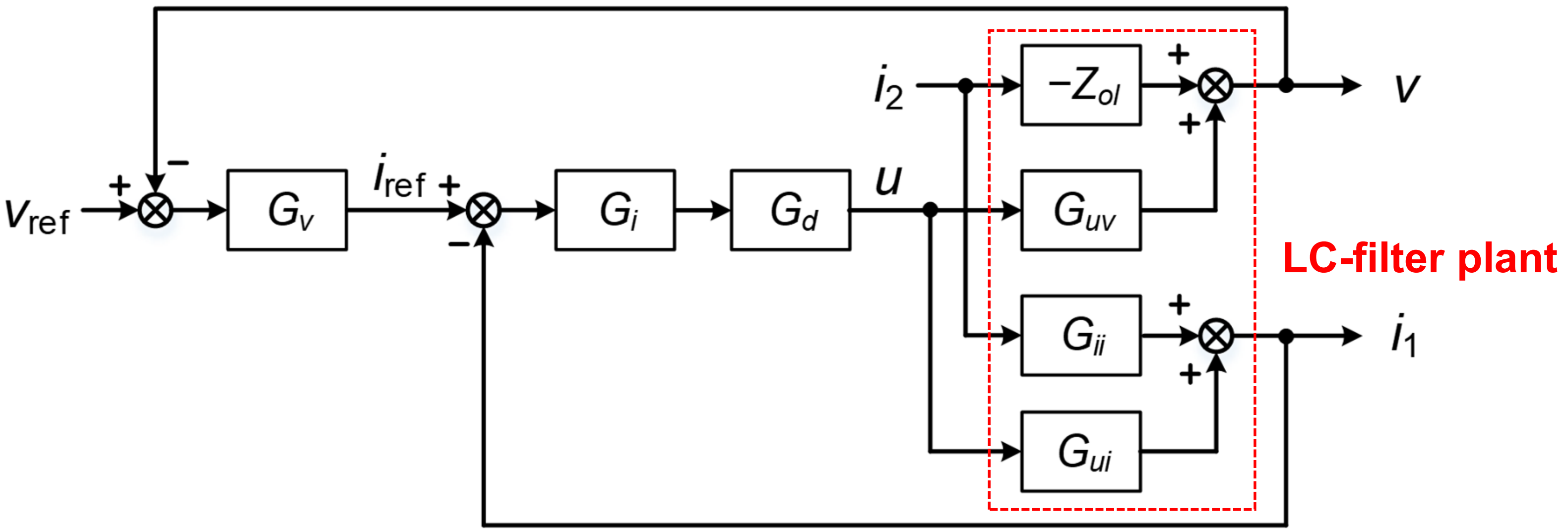

Small-signal model of dual-loop voltage control

Current loop gain: $T_i(s) = T_1$

Voltage loop gain: $T_v(s) = \dfrac{T_2}{1+T_i}$ $\quad T_2(s) = G_{uv}G_dG_iG_v$

Output impedance: $Z_o(s) = \dfrac{Z_{ol}(1+T_1) + G_{uv}G_dG_iG_{ii}}{1+T_1+T_2}$

$$Z_{ol} = \frac{Z_{L1}}{1+Z_{L1}Y_{Cf}} \qquad G_{uv} = \frac{1}{1+Z_{L1}Y_{Cf}}$$

$$G_{ii} = \frac{1}{1+Z_{L1}Y_{Cf}} \qquad G_{ui} = \frac{Y_{Cf}}{1+Z_{L1}Y_{Cf}}$$

Voltage Control for Grid-Forming Converters
Stability of inner current loop, $f_{LC} < f_s/6$

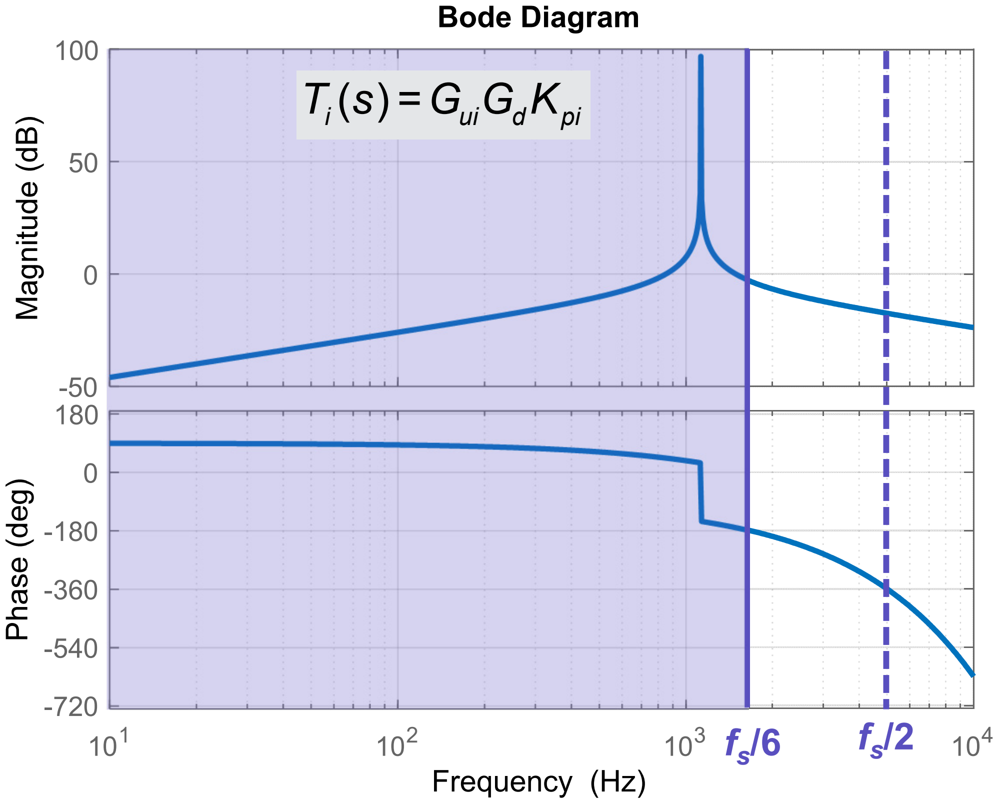

$$G_{ui} = \frac{Y_{Cf}}{1 + Z_{L1} Y_{Cf}} = \frac{sC_f}{1 + s^2 L_1 C_f}$$

Phase lag: 90° → −90°

$$G_d = \cos \omega T_d - j \sin \omega T_d$$

Additional phase lag of 90° at $\omega_s/6$

Phase crossing over −180° at $\omega_s/6$

Critcal K_{pi} for stable current loop:

$$\left| T_i\left(j\frac{\omega_s}{6}\right) \right| \le 10^{-\frac{GM}{20dB}} \quad 0 < K_{pi} \le \frac{10^{-\frac{GM}{20dB}}}{\left| G_{ui}\left(j\frac{\omega_s}{6}\right) \right|}$$

Lager K_{pi} → smaller GM

Voltage Control for Grid-Forming Converters

Stability of outer voltage loop, $f_{LC} < f_s/6$

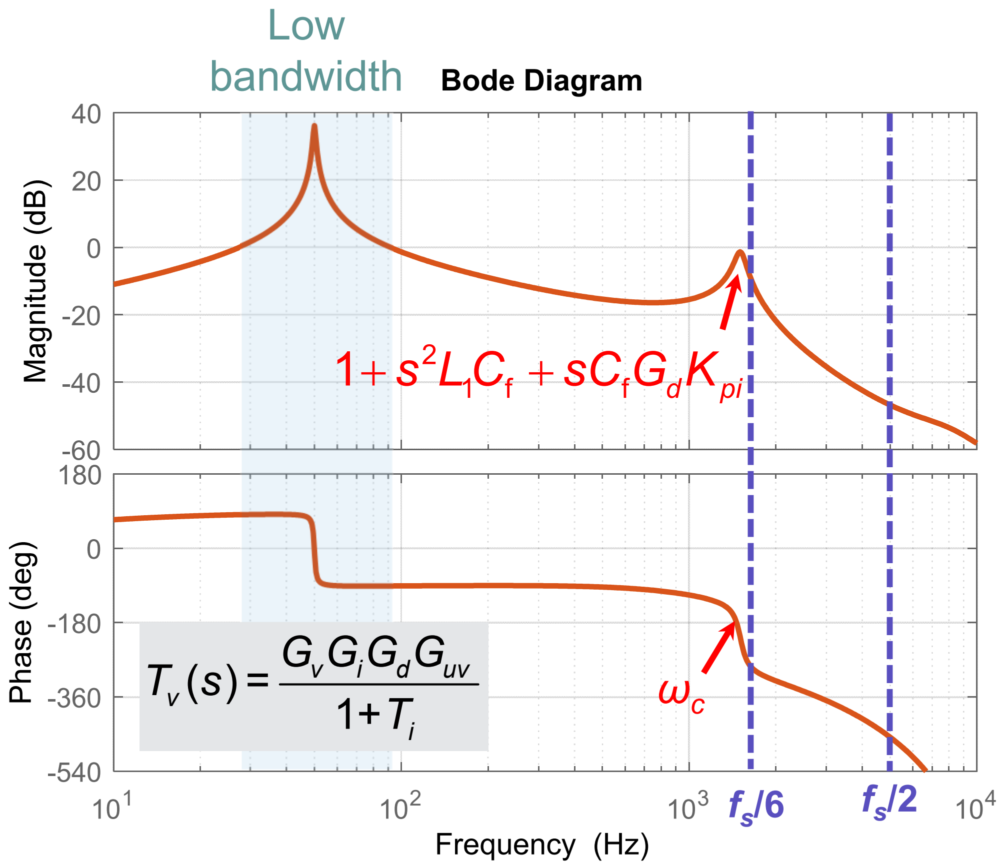

$$T_v = \frac{G_vG_iG_dG_{uv}}{1+T_i} = \frac{G_dK_{pi}}{1+Z_{L1}Y_{Cf}+Y_{Cf}G_dK_{pi}}G_v$$

$$1+s^2L_1C_f+sC_fG_dK_{pi}$$

Larger K_{pi} → more damping to the LC resonance

$$G_v = K_{pv} + \frac{K_{rv}s}{s^2+\omega_1^2} \approx K_{pv} + \frac{K_{rv}}{s}$$

K_{pv}, K_{rv} → $\quad \left|T_v\left(j\omega_c\right)\right| \le 10^{-\frac{\mathrm{GM}}{20\mathrm{dB}}}$

Voltage Control for Grid-Forming Converters

Unstable inner current loop leads to unstable voltage control, $f_{LC} < f_s/6$

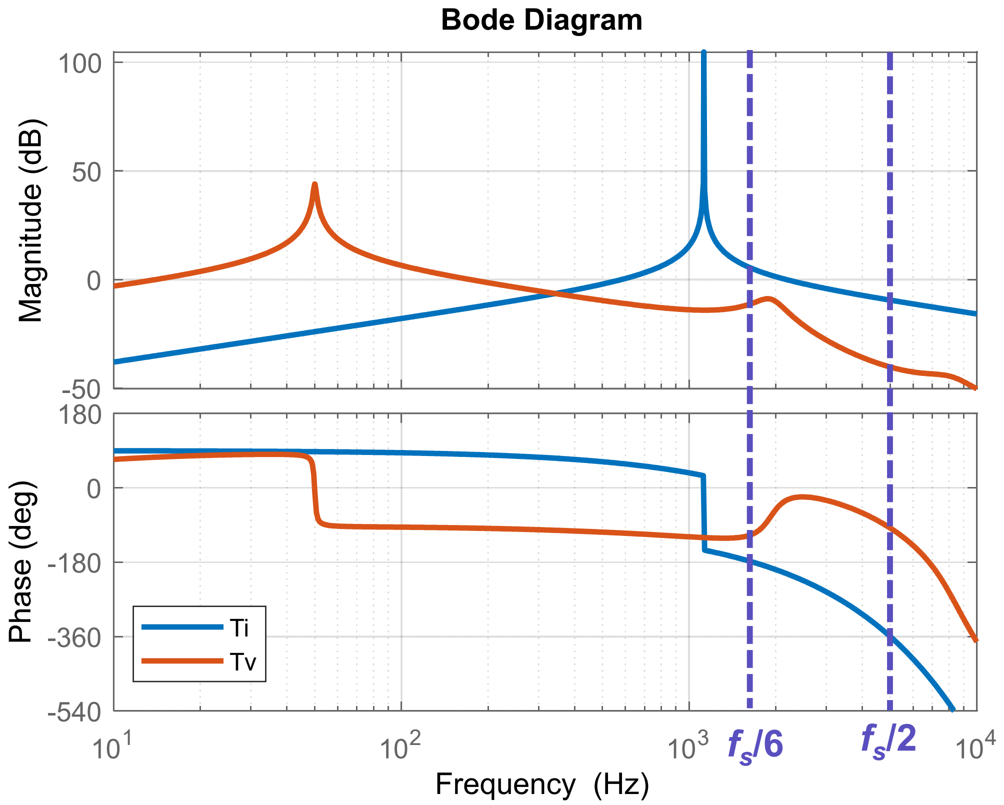

- Current loop, GM<0, unstable
- Voltage loop, 2 RHP poles → phase leading → no crossing over ±180° within the bandwidth

Entire system unstable !

Voltage Control for Grid-Forming Converters

Unstable inner current loop, $f_s/6 < f_{LC} < f_s/2$

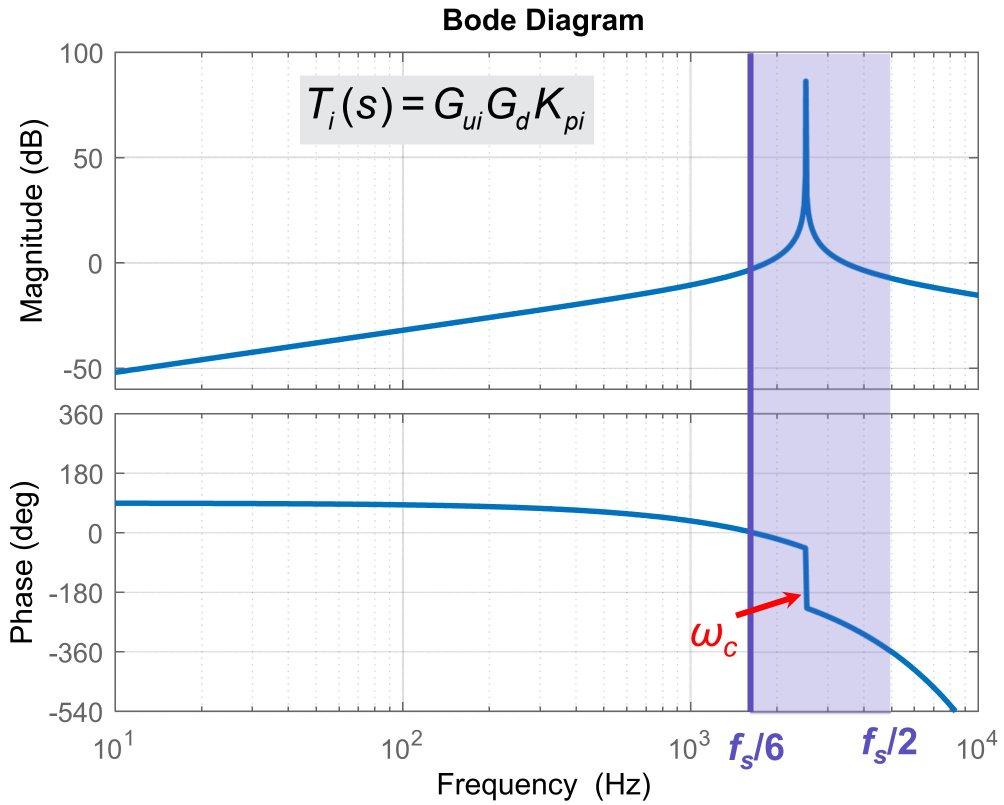

$K_{pi} > 0$

G_d

G_{ui}

Phase crossing over 0° at $f_s/6$

Phase crossing over −180° at f_{LC}

Phase crossing over −360° at $f_s/2$

Current loop and consequently entire system unstable !

Voltage Control for Grid-Forming Converters

Impedance-based stability analysis

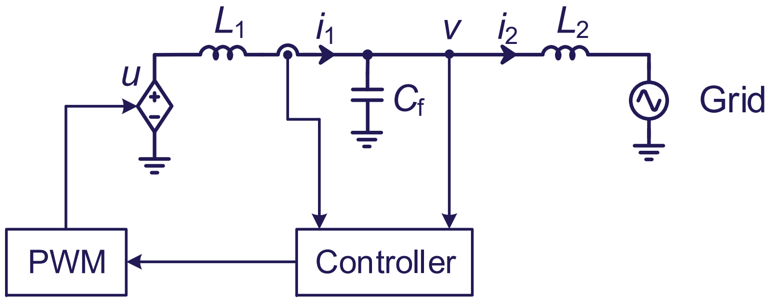

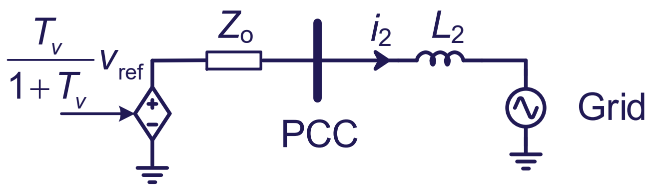

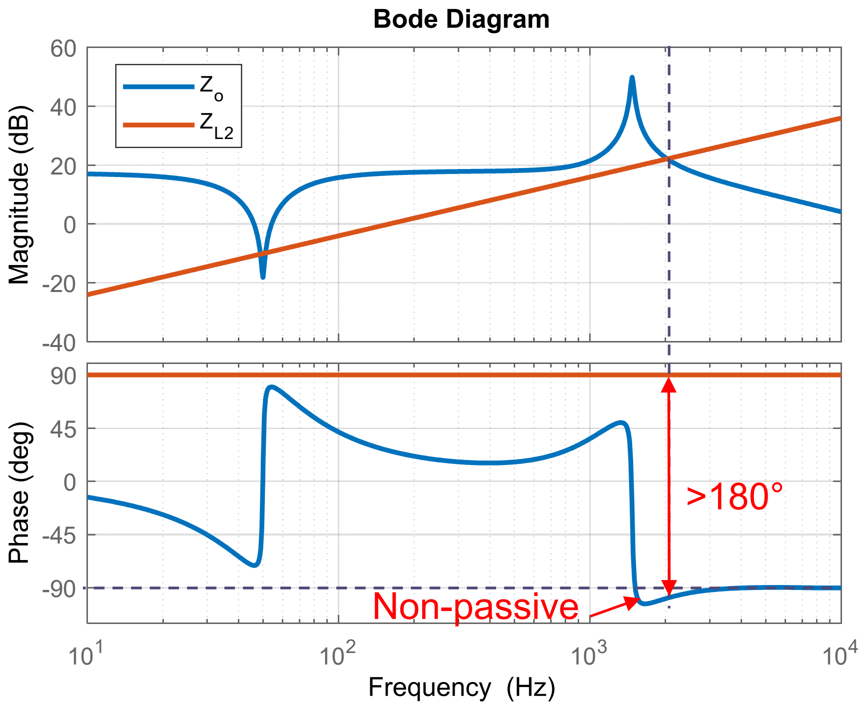

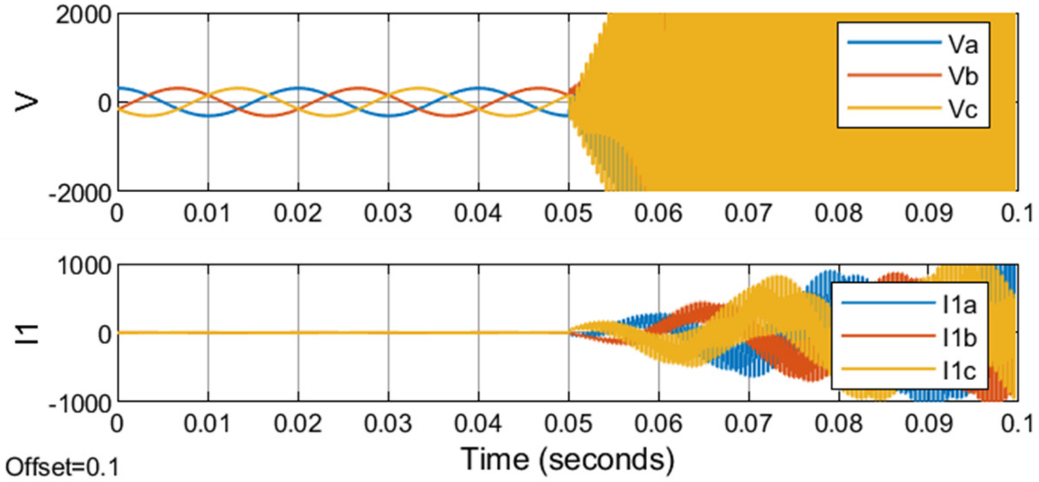

Instability Effect of PLL for Grid-Following Converters

Impedance model of current control with PLL dynamics

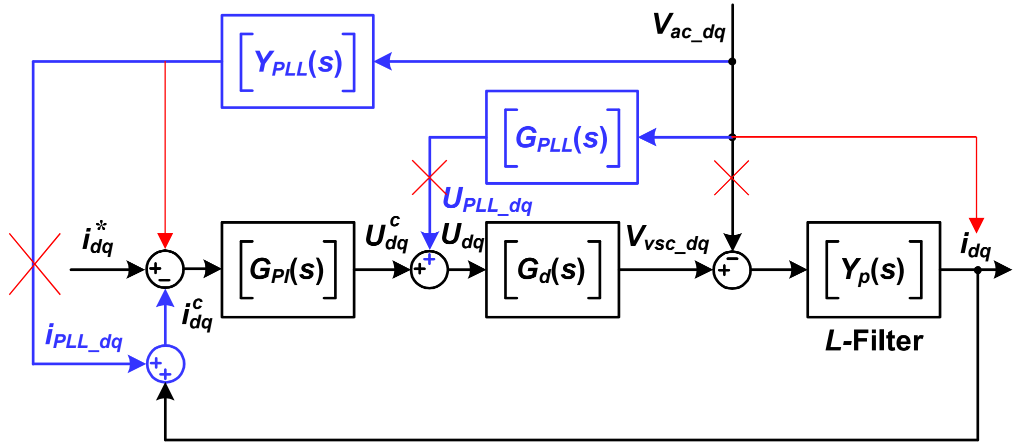

Structural characterization of PLL effect

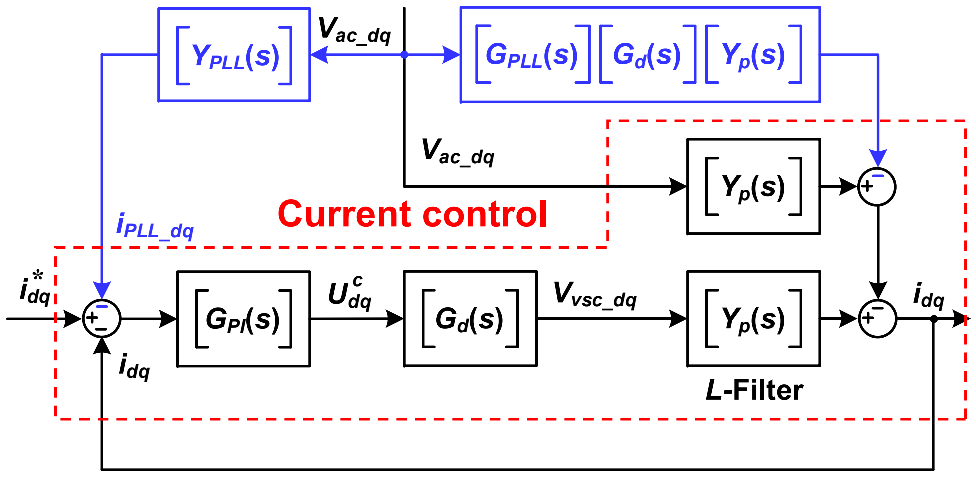

Equivalent block diagram

Instability Effect of PLL for Grid-Following Converters

Two paralleled admittances added by the PLL

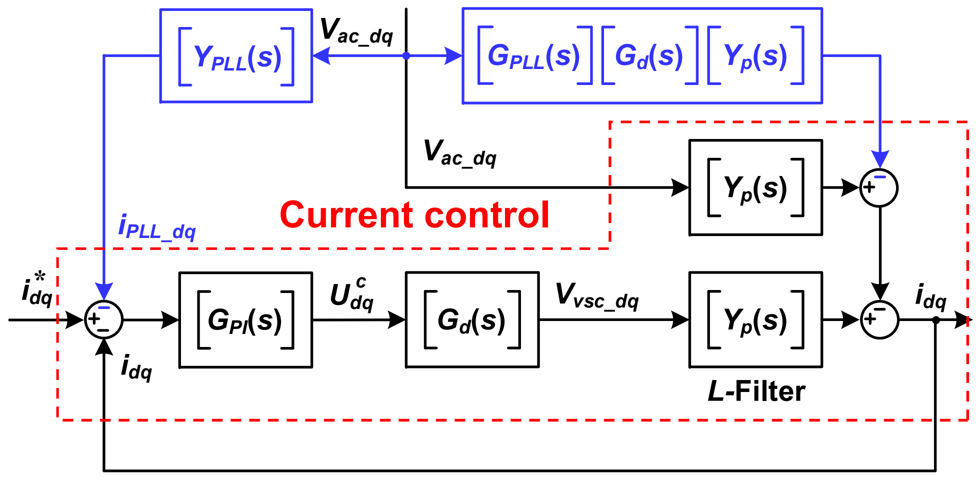

Equivalent block diagram

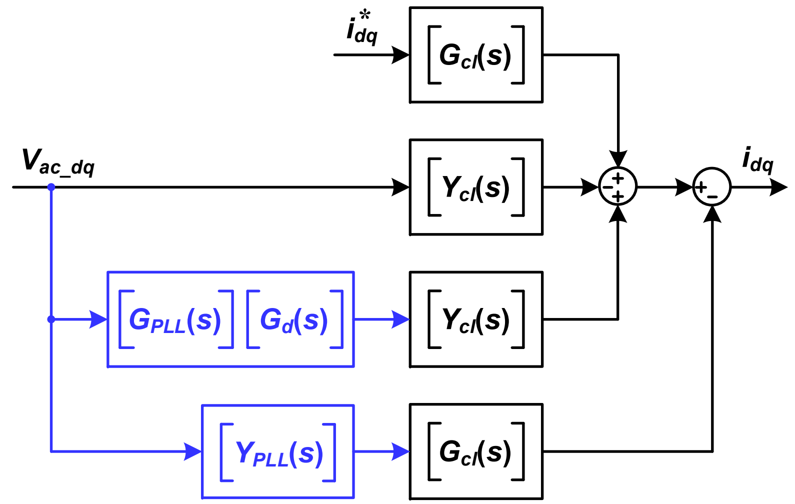

Block diagram of impedance model

$$[G_{cl}(s)] = \left\{ \mathrm{I} + [Y_p(s)][G_d(s)][G_{PI}(s)] \right\}^{-1} [Y_p(s)][G_d(s)][G_{PI}(s)]$$

$$[Y_{cl}(s)] = \left\{ \mathrm{I} + [Y_p(s)][G_d(s)][G_{PI}(s)] \right\}^{-1} [Y_p(s)]$$

$$[Y_{PLL,1}(s)] = -[G_{PLL}(s)][G_d(s)][Y_{cl}(s)]$$

$$[Y_{PLL,2}(s)] = [Y_{PLL}(s)][G_{cl}(s)]$$

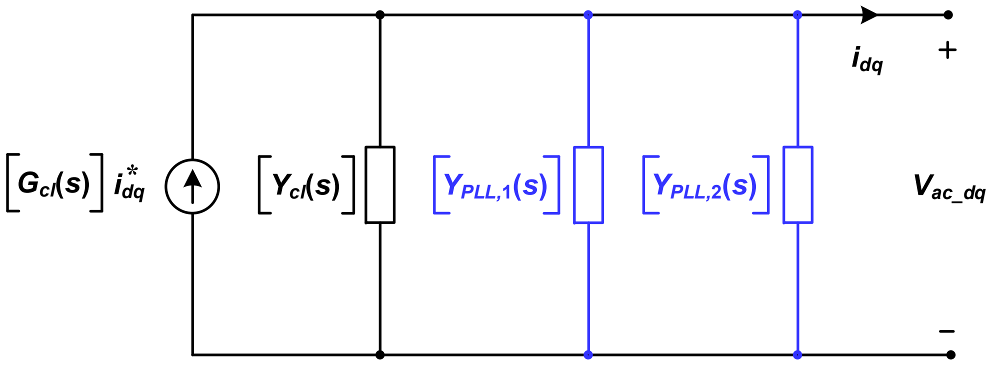

Impedance model

Instability Effect of PLL for Grid-Following Converters
Low-frequency negative resistance on the q-q axis

- **Closed-loop output admittance matrix**

$$\left[Y_{cl,t}(s)\right]=\left[Y_{cl}(s)\right]+\left[Y_{PLL,1}(s)\right]+\left[Y_{PLL,2}(s)\right]$$

- **Low-frequency approximation $Y_{cl,t}(s)$ with unity current loop gain**

$$\left[Y_{cl,t}(s)\right]\approx\left[Y_{PLL,2}(s)\right]\approx\left[Y_{PLL}(s)\right]=\begin{bmatrix}0 & H_{PLL}(s)i_{q0}\\ 0 & -H_{PLL}(s)i_{d0}\end{bmatrix}$$

Negative resistance

- **Grid impedance matrix**

$$\left[Z_g(s)\right]=\begin{bmatrix}sL_g & -\omega_1 L_g\\ \omega_1 L_g & sL_g\end{bmatrix}$$

- **Generalized Nyquist stability criterion**

$$\det\left\{\lambda\mathrm{I}-\left[Z_g(s)\right]\left[Y_{cl,t}(s)\right]\right\}=0$$

- **Nyquist diagrams of λ_1 and λ_2**

Instability Effect of PLL for Grid-Following Converters

DQ-frame impedance matrices - PLL bandwidth 330 Hz, SCR = 7

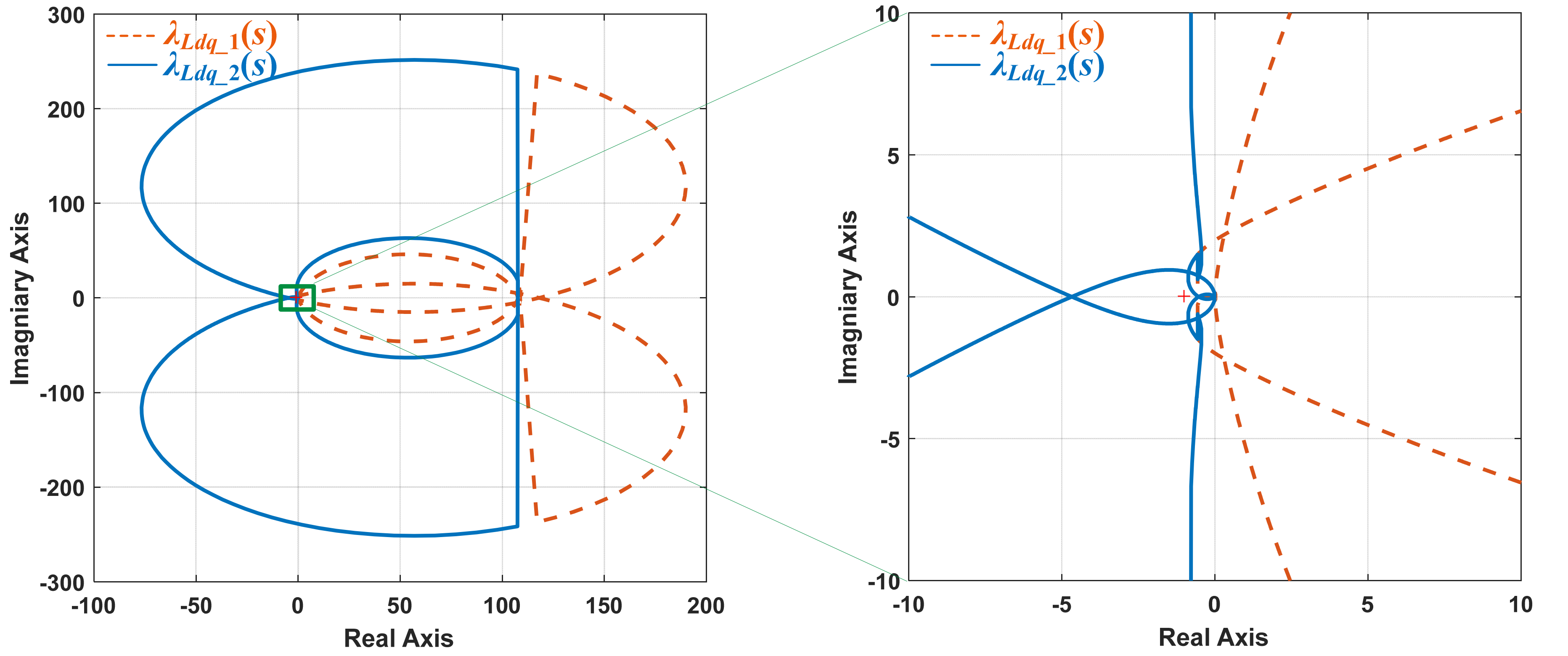

Nyquist diagrams of eigenvalue transfer functions in the *dq*-frame

Instability Effect of PLL for Grid-Following Converters
Stationary-frame impedance matrices - PLL bandwidth 330 Hz, SCR = 7

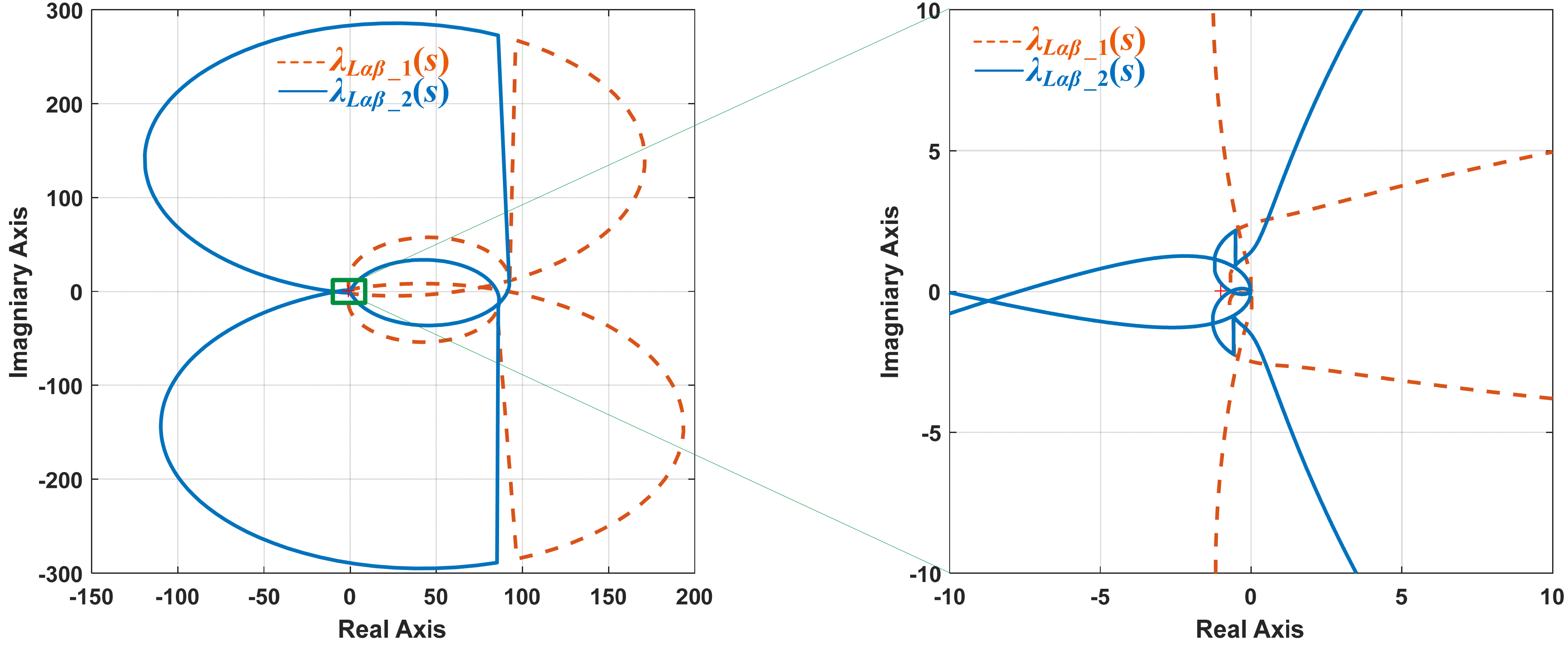

Nyquist diagrams of eigenvalue transfer functions in the *αβ*-frame

Instability Effect of PLL for Grid-Following Converters

Simulations - PLL bandwidth 330 Hz, 175 Hz, 20 Hz, SCR = 7

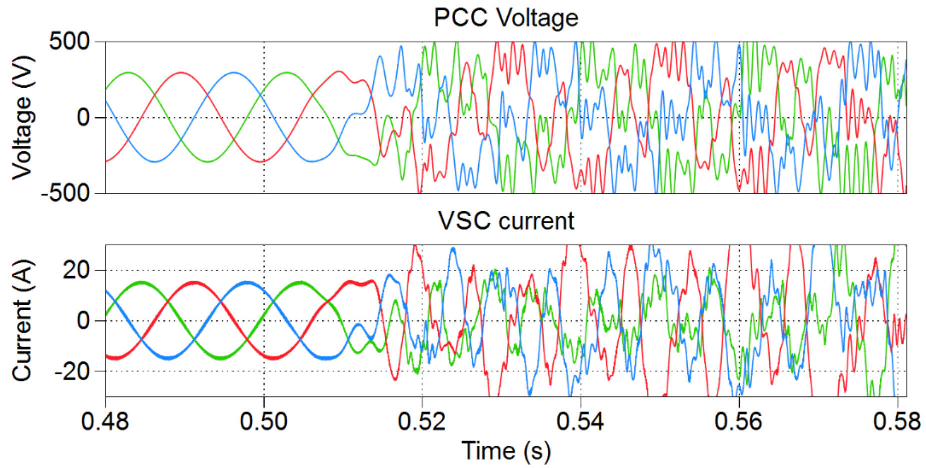

PLL_{BW} = 330 Hz

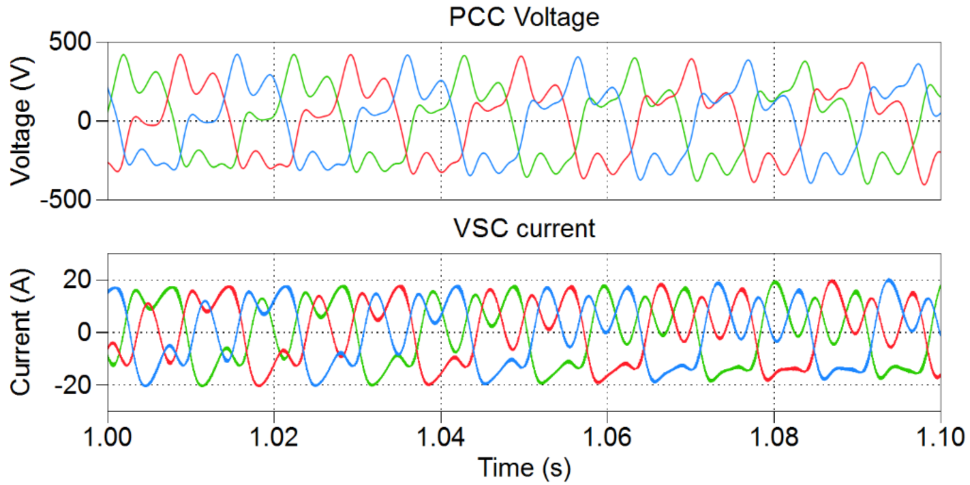

PLL_{BW} = 175 Hz

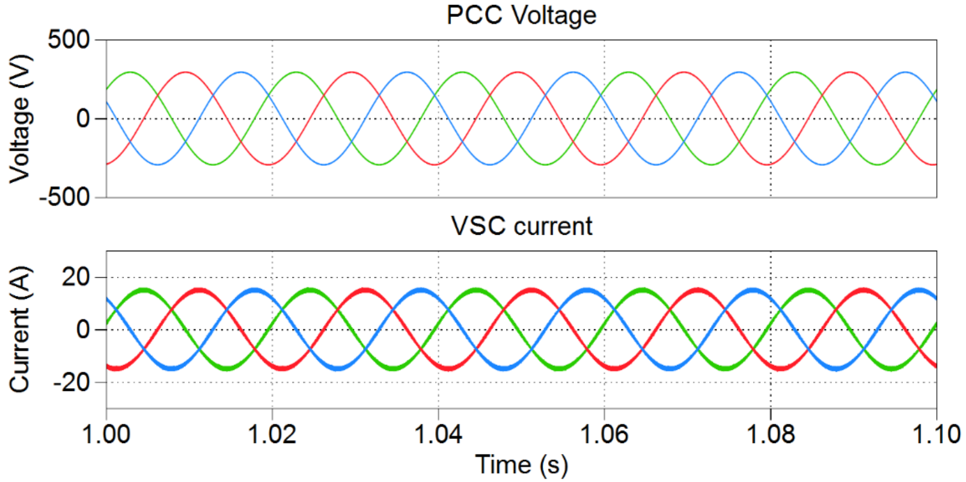

PLL_{BW} = 20 Hz

Instability Effect of PLL for Grid-Following Converters
Experiments - PLL bandwidth 175 Hz, 20 Hz, SCR = 7

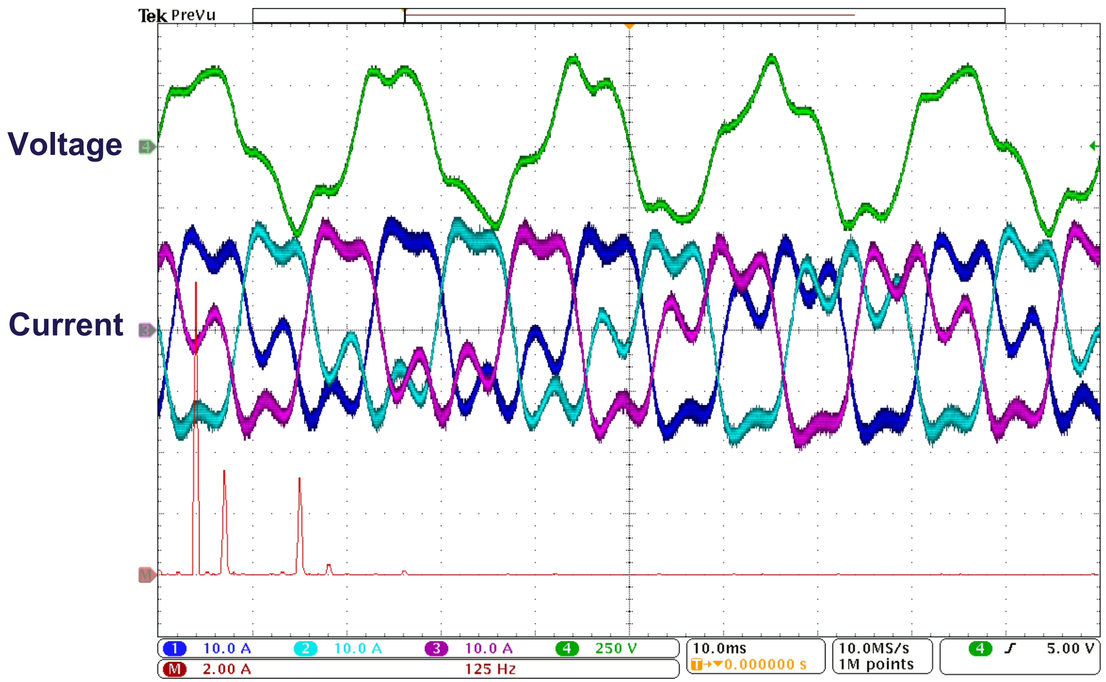

PLL_{BW} = 175 Hz

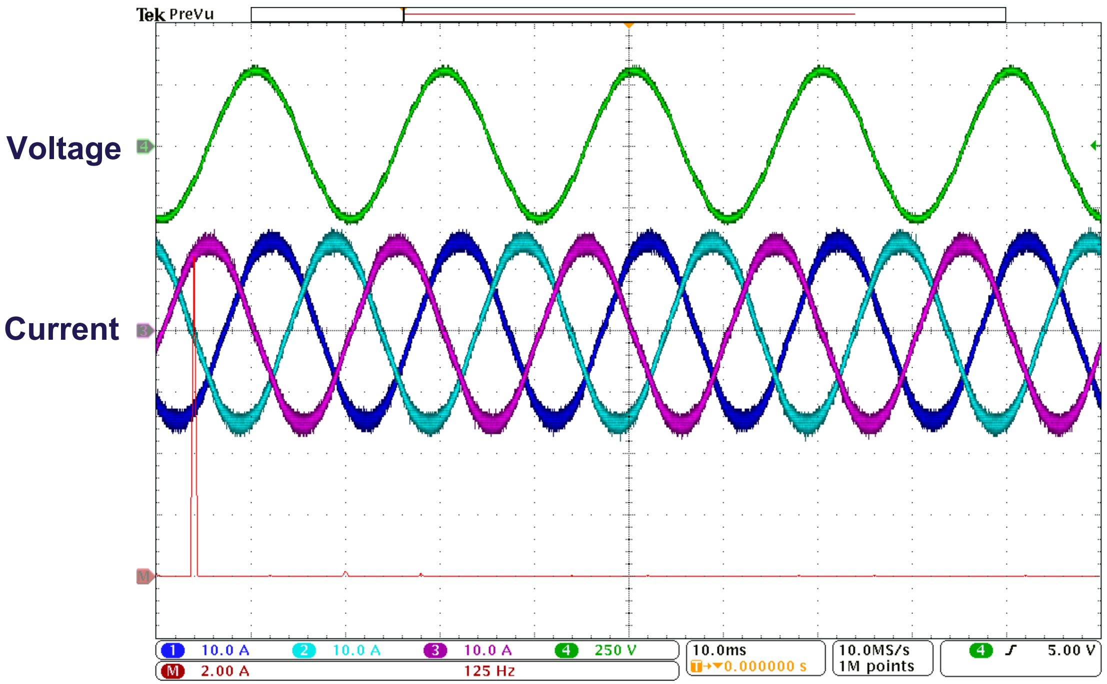

PLL_{BW} = 20 Hz

Instability Effect of PLL for Grid-Following Converters
Three paralleled grid-following inverters with different SCRs

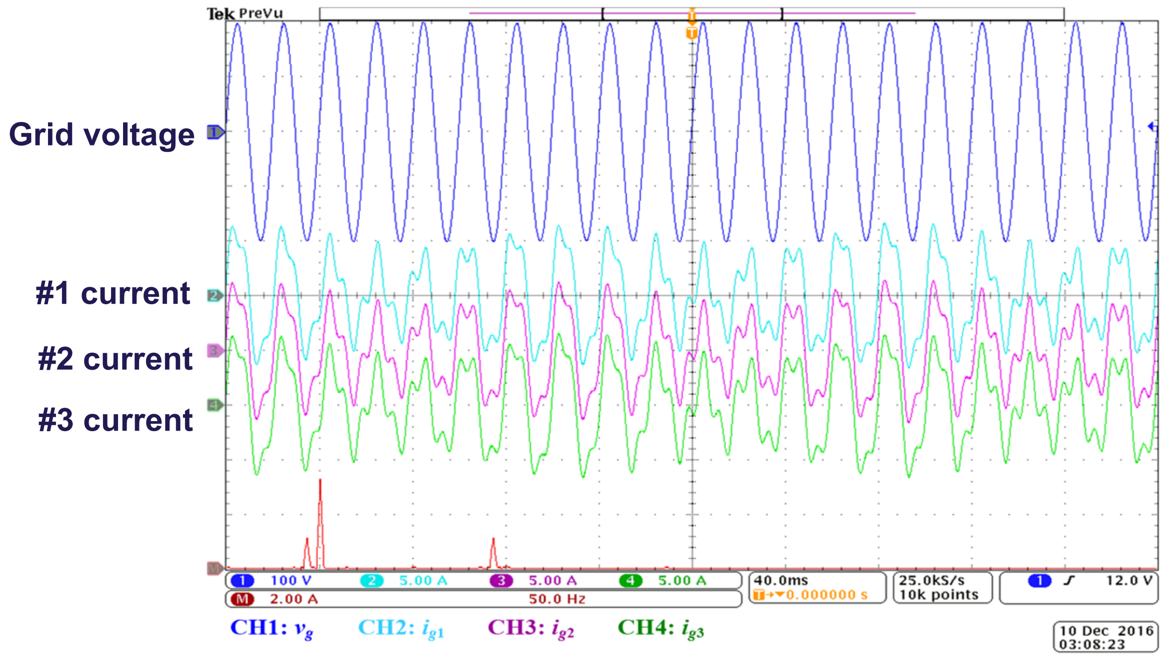

SCR = 8.4

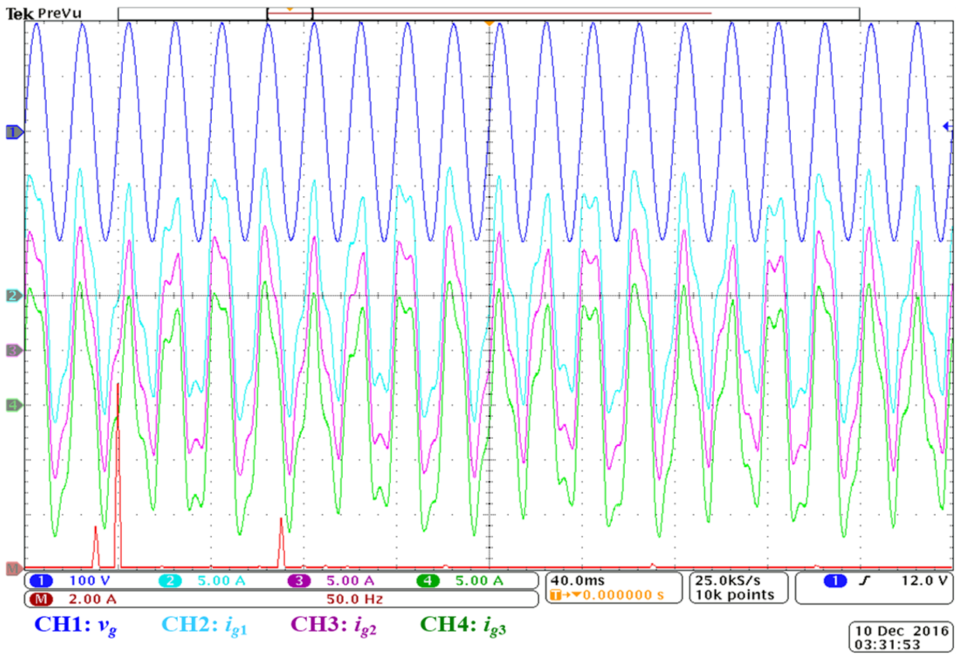

SCR = 4.2

Instability Effect of DC-Link Voltage Control
DC-link Voltage Control (DVC) for grid-following converters (rectifier mode)

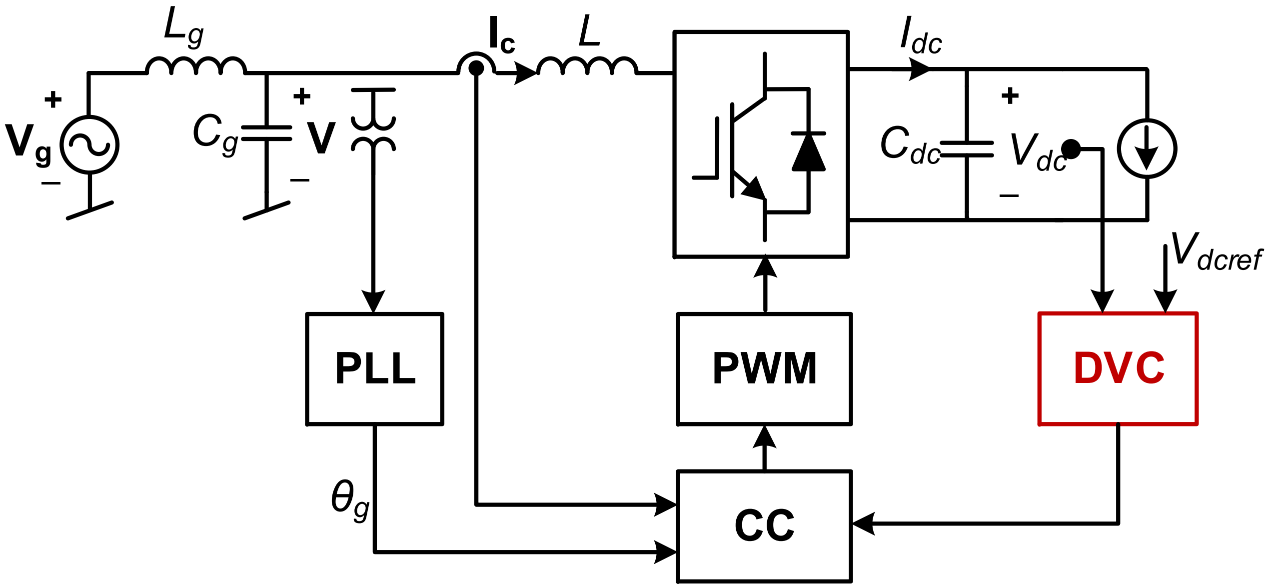

- **Unified power factor operation** ($I_{q,ref}$=0)
- $\mathbf{V_g}$, $\mathbf{I_c}$, **V** are space vectors of three-phase voltages and currents
- **PLL dynamic is not modeled**
- **The coupling between dc-link and ac-side dynamics**
- **Explicit analytical model of DVC loop**

Instability Effect of DC-Link Voltage Control

Closed-loop model with four input and three output variables

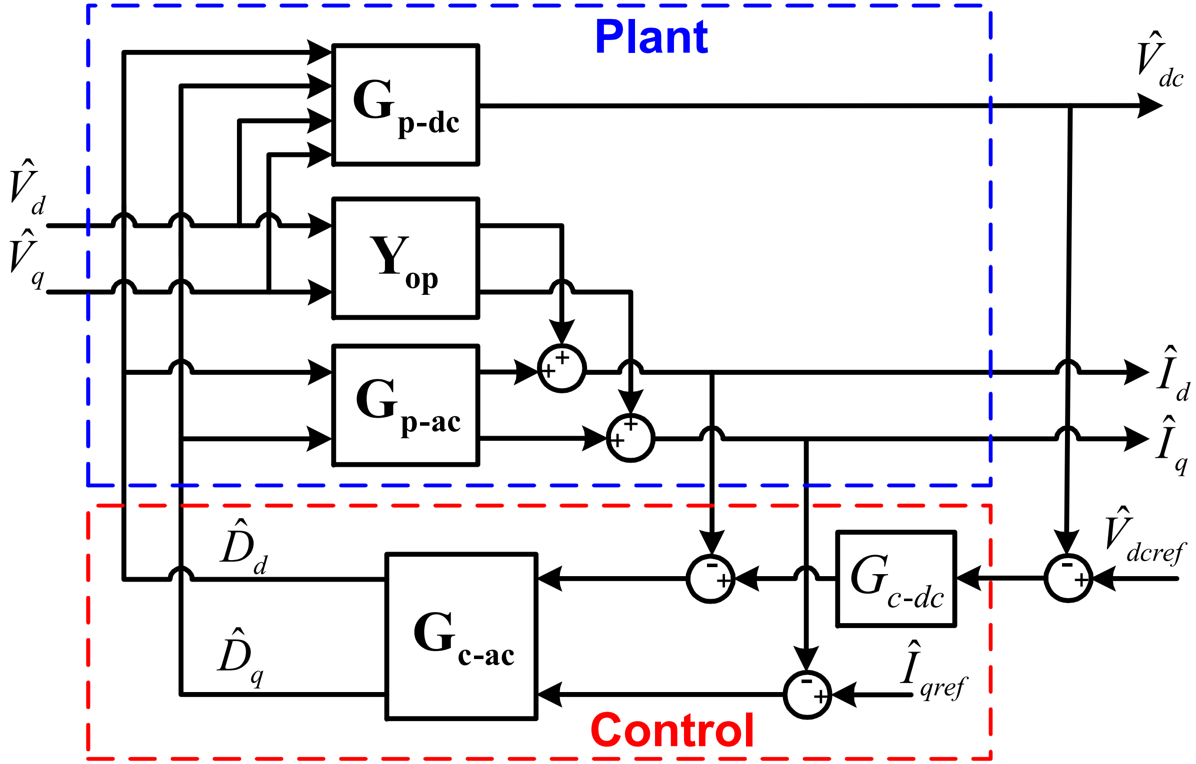

- $\mathbf{G}_{\mathbf{c\text{-}ac}}$: current controller in matrix form; $G_{c\text{-}dc}$: dc-link voltage controller
- $\mathbf{G}_{\mathbf{p\text{-}ac}}$: control plant of CC loop; $\mathbf{G}_{\mathbf{p\text{-}dc}}$: control plant of DVC loop;
- $\mathbf{Y}_{\mathbf{op}}$: open-loop output admittance;

Instability Effect of DC-Link Voltage Control

Plant of dc-link voltage loop, $\mathbf{G}_{\text{p-dc}}$

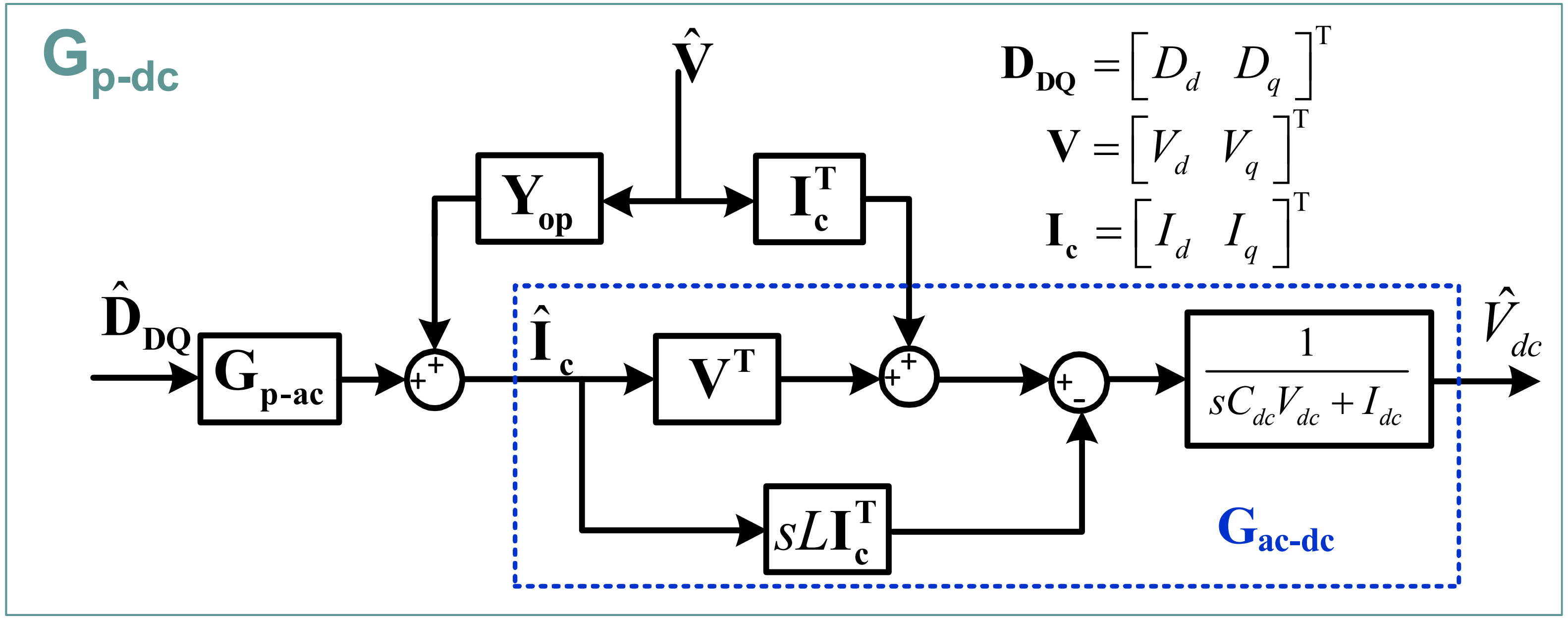

- The dynamic coupling between dc-link and ac-side, $\mathbf{G}_{\text{ac-dc}}$ is derived from the instantaneous power balance, i.e.

$$V_d\hat{I}_d + V_q\hat{I}_q + \hat{V}_d I_d + \hat{V}_q I_q + LI_d\frac{d\hat{I}_d}{dt} + LI_q\frac{d\hat{I}_q}{dt} = C_{dc}V_{dc}\frac{d\hat{V}_{dc}}{dt} + \hat{V}_{dc}I_{dc}$$

$$\mathbf{G}_{\text{ac-dc}} = \begin{bmatrix} \dfrac{LI_d}{C_{dc}V_{dc}} \dfrac{-s + \dfrac{V_d}{LI_d}}{s + \dfrac{I_{dc}}{C_{dc}V_{dc}}} & 0 \end{bmatrix}$$

RHP zero

Instability Effect of DC-Link Voltage Control
Closed-loop input admittance for the rectifier mode

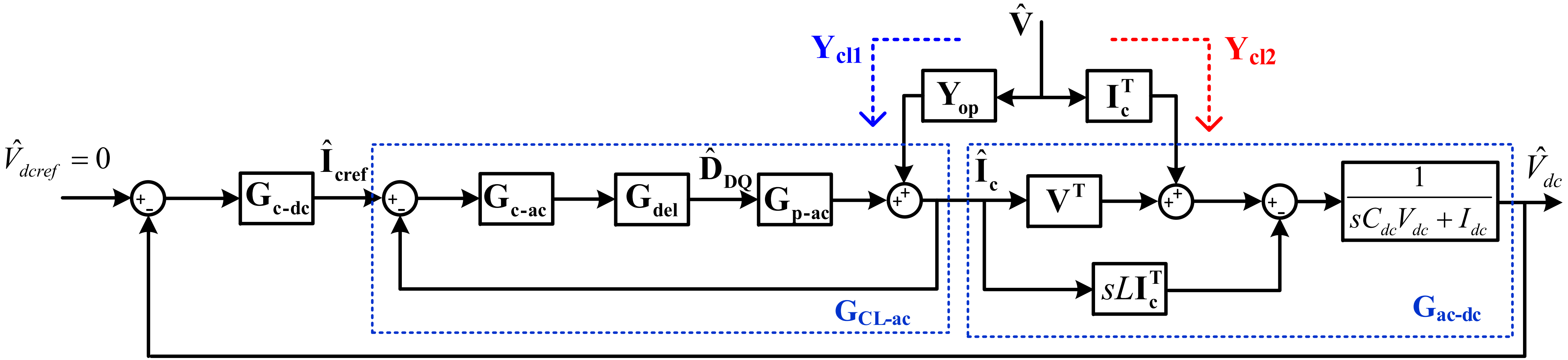

- **$\mathbf{G}_{\text{del}}$**: time delay effect of PWM in matrix form; **E**: unity gain matrix;

$$\mathbf{Y}_{\text{cl}} = \mathbf{Y}_{\text{cl1}} + \mathbf{Y}_{\text{cl2}}$$

Instability Effect of DC-Link Voltage Control

Closed-loop input admittance – Y_{cl1}

- Y_{cl1}: closed-loop output admittance with Y_{op}

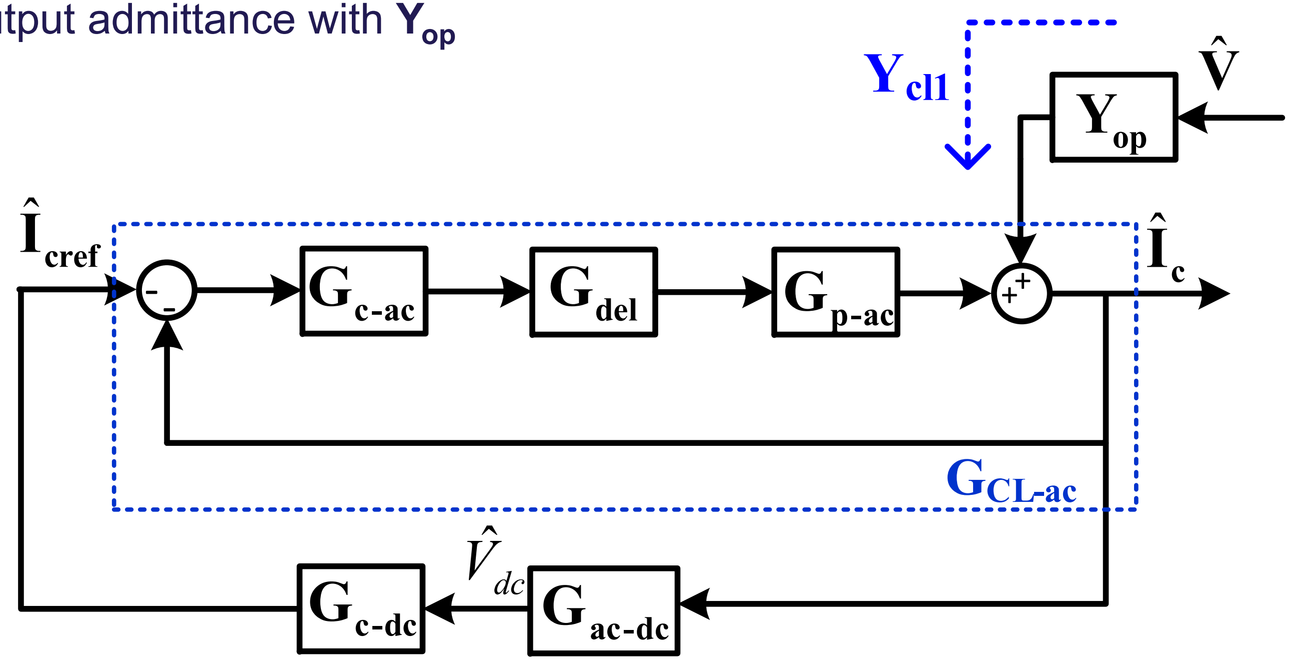

$$G_{Y1} = G_{p\text{-}ac} G_{del} G_{c-ac} G_{c\text{-}dc} G_{ac\text{-}dc} \qquad Y_{cl1} = \frac{\hat{V}}{\hat{I}_c} = \left(I + G_{Y1} + G_{p\text{-}ac} G_{del} G_{c-ac} \right)^{-1} Y_{op}$$

Instability Effect of DC-Link Voltage Control

Closed-loop input admittance – $\mathbf{Y}_{cl2}$

- $\mathbf{Y}_{cl2}$: closed-loop output admittance with the steady-state operating point $I^T=[I_d, I_q]$

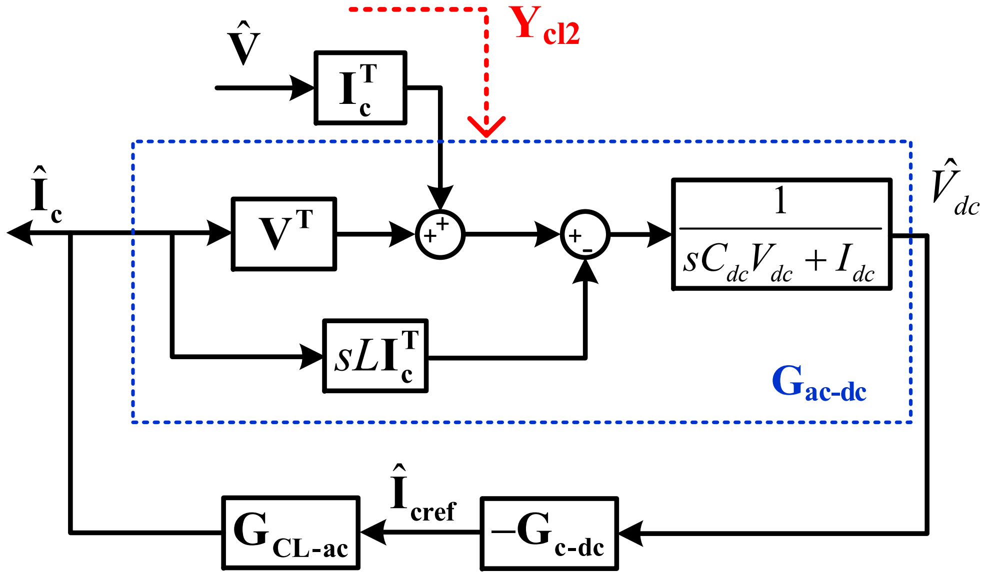

$$\mathbf{G}_{CL\text{-}ac} = \mathbf{G}_{c-ac}\mathbf{G}_{del}\mathbf{G}_{p\text{-}ac}\left(\mathbf{I}+\mathbf{G}_{c-ac}\mathbf{G}_{del}\mathbf{G}_{p\text{-}ac}\right)^{-1}$$

$$\mathbf{G}_{Y2o} = \mathbf{G}_{CL\text{-}ac}\mathbf{G}_{c-dc}\frac{1}{(sC_{dc}V_{dc}+I_{dc})}$$

$$\mathbf{Y}_{cl2} = \frac{\hat{\mathbf{V}}}{\hat{\mathbf{I}}_c} = \mathbf{G}_{Y2o}\left[1-\left(-sL\mathbf{I}_c^T+\mathbf{V}^T\right)\mathbf{G}_{Y2o}\right]^{-1}\mathbf{I}_c^T$$

Instability Effect of DC-Link Voltage Control

Impacts of DVC bandwidth on the closed-loop input admittance

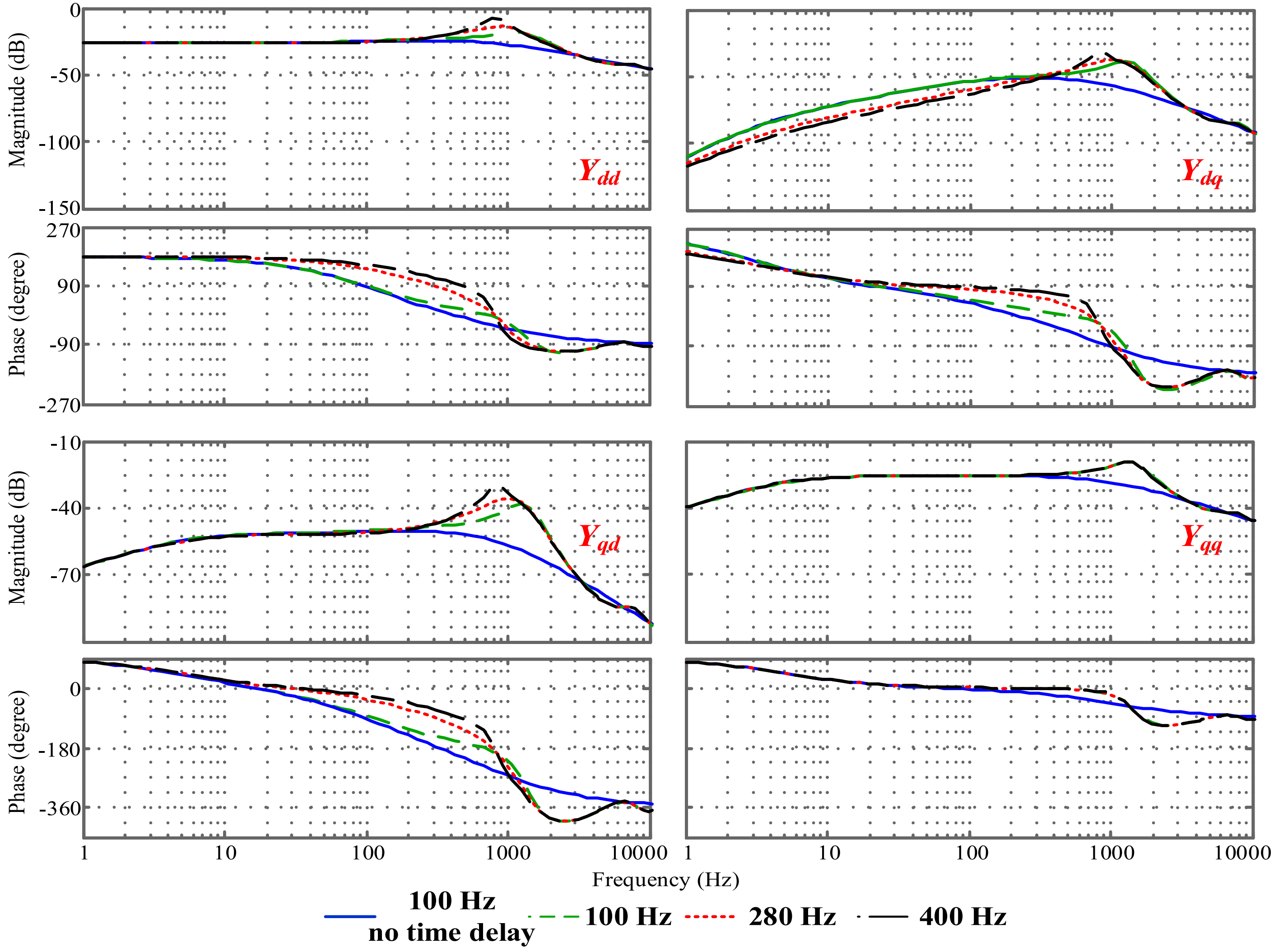

Instability Effect of DC-Link Voltage Control

Converter-grid interaction with L_g=5mH, C_g=20μF

Frequency responses of eigenvalue transfer functions

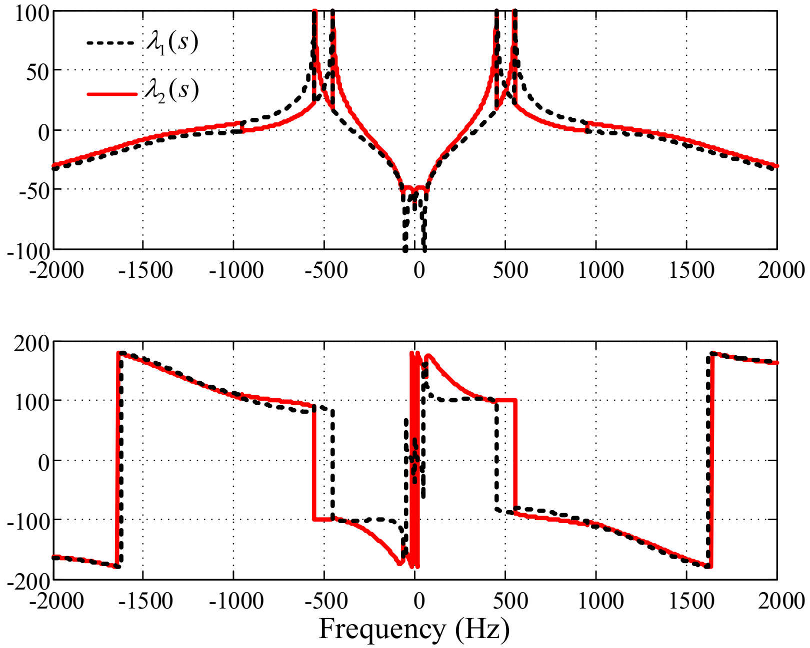

DLC Bandwidth 100Hz

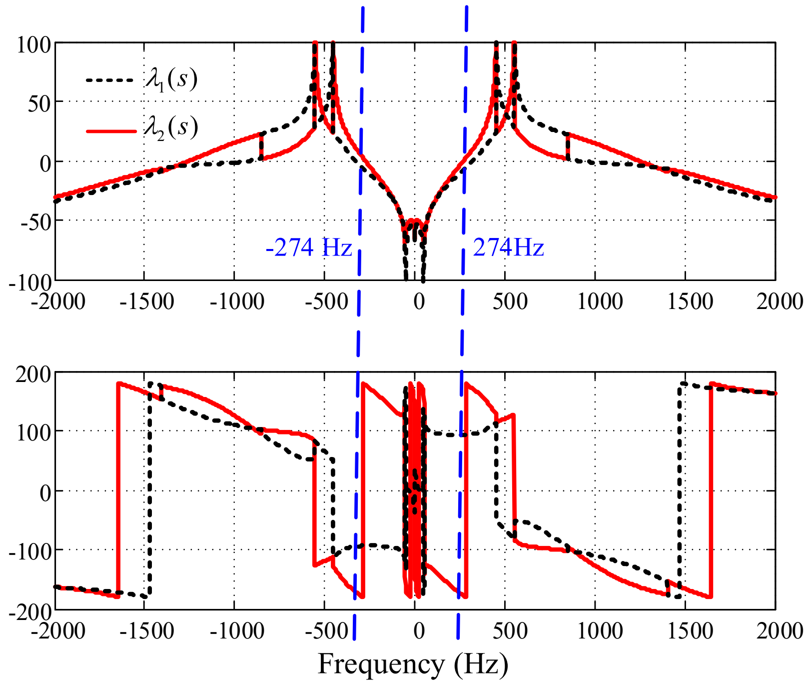

DLC Bandwidth 280Hz

Instability Effect of DC-Link Voltage Control

Converter-grid interaction with L_g=5mH, C_g=20µF

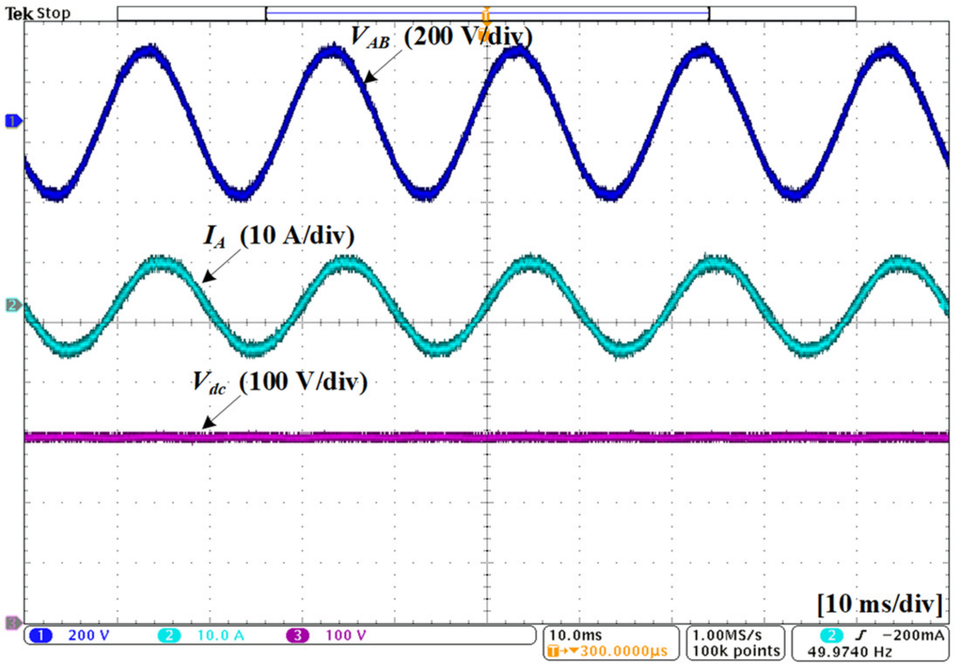

DVC Bandwidth 100Hz

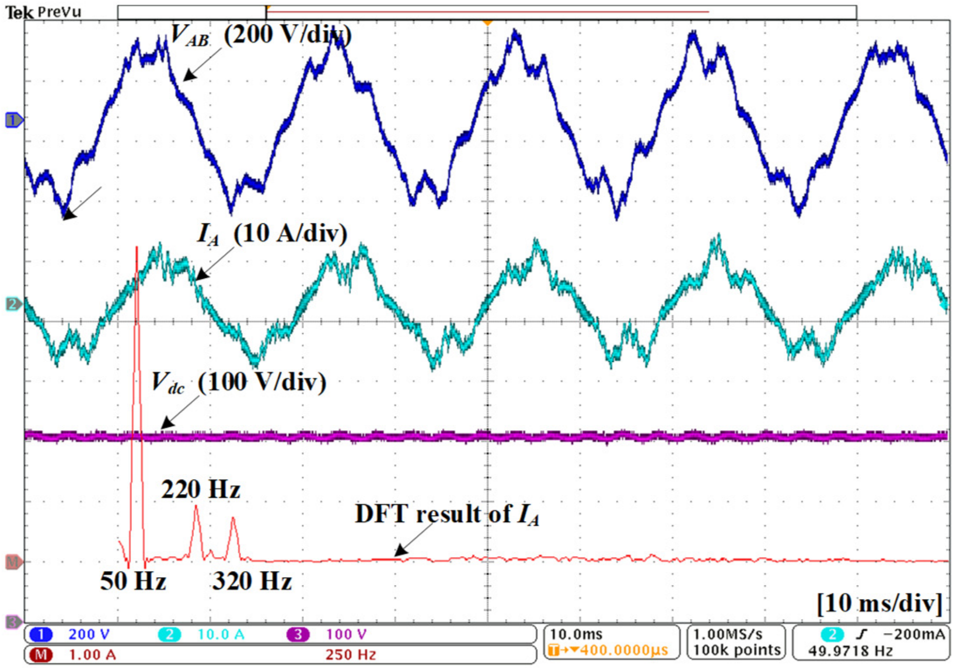

DVC Bandwidth 280Hz

Stability of Power Control for Grid-Forming Converters

Small-signal modeling of power-based synchronization control

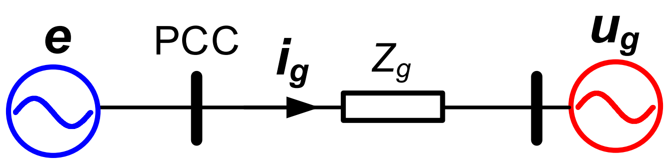

Equivalent circuit

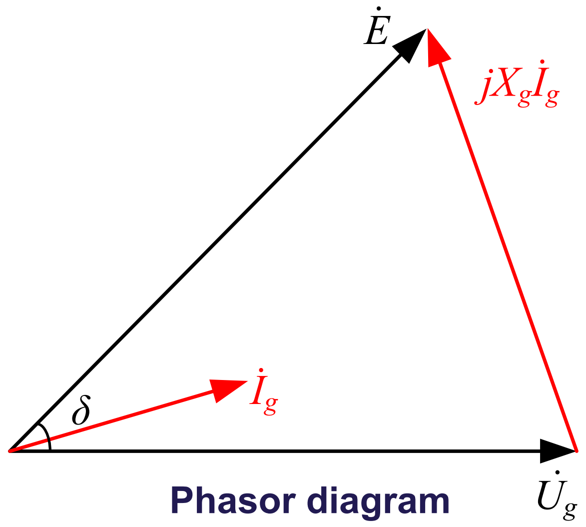

Phasor diagram

$$\dot{U}_g = Ue^{j0} \quad \dot{E} = Ee^{j\delta} \quad Z_g = j\omega_1 L_g = jX_g$$

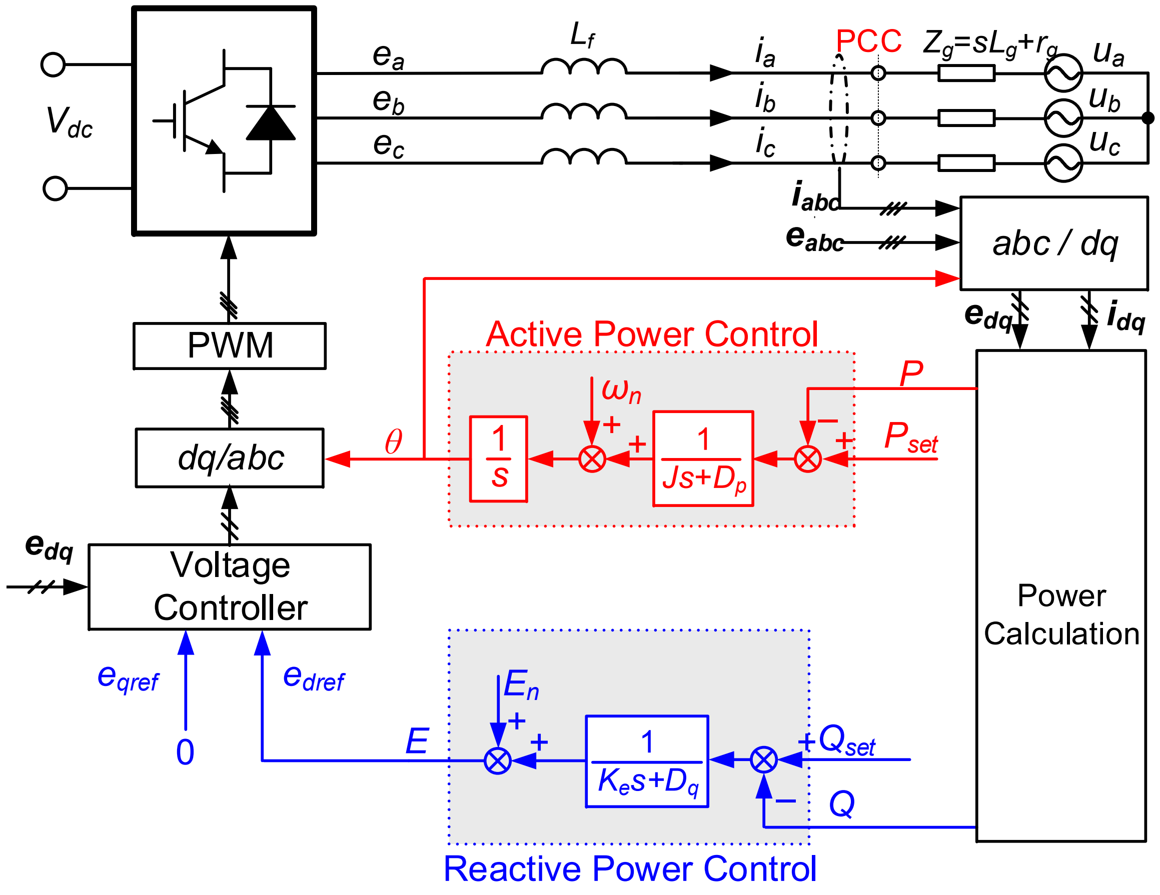

General control diagram of grid-forming converters

Stability of Power Control for Grid-Forming Converters

Small-signal modeling of power-based synchronization control

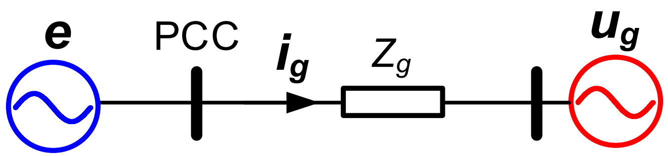

Equivalent circuit

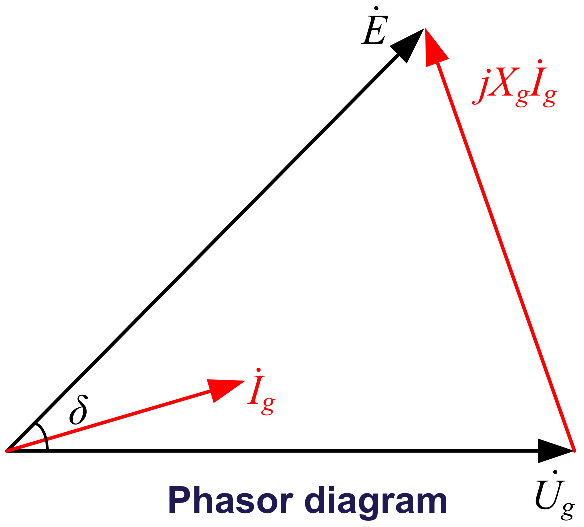

Phasor diagram

$$\dot{U}_g = Ue^{j0} \quad \dot{E} = Ee^{j\delta} \quad Z_g = j\omega_1 L_g = jX_g$$

$$P = \frac{EU}{X_g}\sin\delta \qquad Q = \frac{E\left(E - U\cos\delta\right)}{X_g}$$

Linearization

$$\hat{P} = \frac{E_0 U_0 \cos\delta_0}{X_g}\cdot\hat{\delta} + \frac{U_0\sin\delta_0}{X_g}\cdot\hat{E}$$

$$\hat{Q} = \frac{EU_0\sin\delta_0}{X_g}\cdot\hat{\delta} + \frac{\left(2E_0 - U_0\cos\delta_0\right)}{X_g}\cdot\hat{E}$$

Stability of Power Control for Grid-Forming Converters
Small-signal modeling of power-based synchronization control

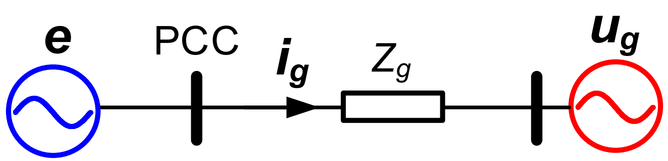

Equivalent circuit

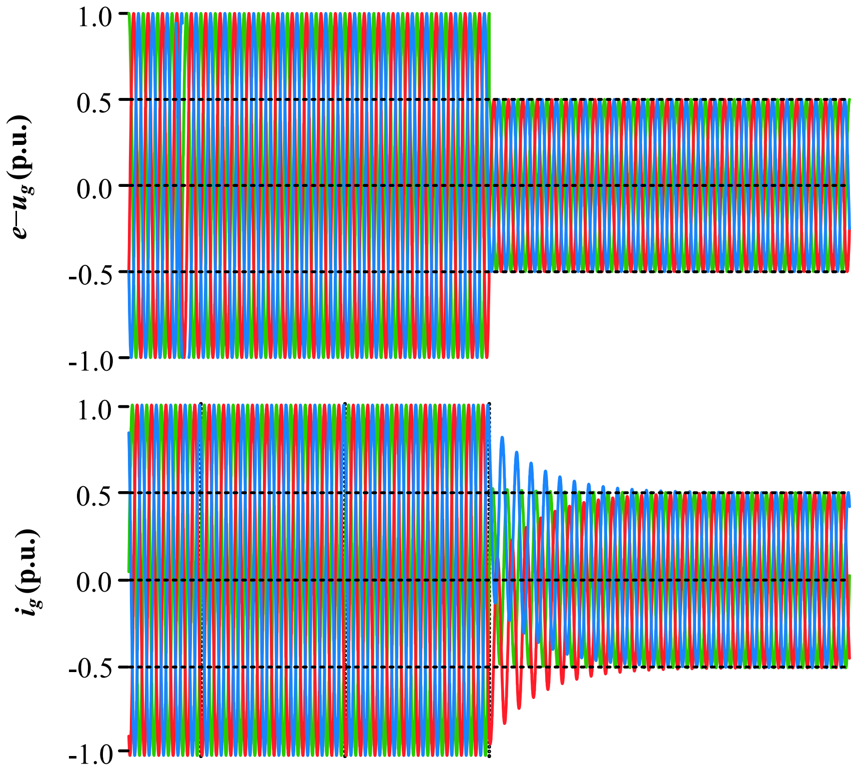

$$P = \frac{EU}{X_g}\sin\delta \qquad Q = \frac{E\left(E - U\cos\delta\right)}{X_g}$$

Linearization

$$\hat{P} = \frac{E_0 U_0 \cos\delta_0}{X_g}\cdot\hat{\delta} + \frac{U_0\sin\delta_0}{X_g}\cdot\hat{E}$$

$$\hat{Q} = \frac{EU_0\sin\delta_0}{X_g}\cdot\hat{\delta} + \frac{\left(2E_0 - U_0\cos\delta_0\right)}{X_g}\cdot\hat{E}$$

Only valid in low frequency range!

Stability of Power Control for Grid-Forming Converters
Small-signal modeling of power-based synchronization control

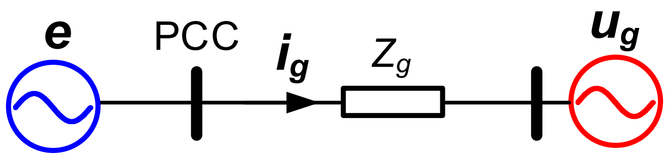

Equivalent circuit

$$\mathbf{e_{dq}} = e_d + je_q = Ee^{j\delta}$$

$$\mathbf{u_{gdq}} = u_{gd} + ju_{gq} = Ue^{j0}$$

$$\mathbf{Z_{gdq}} = sL_g + j\omega_1 L_g = sL_g + jX_g$$

$$\mathbf{s} = p + jq = \mathbf{e_{dq}}\mathbf{i}^*_{\mathbf{gdq}}$$

$$\hat{\mathbf{s}} = \mathbf{E_{dq0}}\hat{\mathbf{i}}^*_{\mathbf{gdq}} + \hat{\mathbf{e}}_{\mathbf{dq0}}\mathbf{I}^*_{\mathbf{gdq0}}$$

$$\hat{\mathbf{e}}_{\mathbf{dq}} = E_0 e^{j(\delta_0 + \hat{\delta})} + \hat{E}e^{j\delta_0} = E_0 e^{j\delta_0}(1 + j\hat{\delta})$$

$$\hat{\mathbf{i}}_{\mathbf{dq}} = \hat{\mathbf{e}}_{\mathbf{dq}} / \mathbf{Z_{gdq}}$$

$$\hat{p} = \left(\frac{X_g E_0}{\boxed{(sL_g)^2 + X_g^2}} - \frac{E_0 - U_0\cos\delta_0}{X_g}\right)E_0 \cdot \hat{\delta} + \left(\frac{sL_g E_0}{\boxed{(sL_g)^2 + X_g^2}} + \frac{U_0 \sin\delta_0}{X_g}\right)\cdot \hat{E}$$

$$\hat{q} = \left(\frac{U_0 \sin\delta_0}{X_g} - \frac{sL_g E_0}{\boxed{(sL_g)^2 + X_g^2}}\right)E_0 \cdot \hat{\delta} + \left(\frac{X_g E_0}{\boxed{(sL_g)^2 + X_g^2}} + \frac{E_0 - U_0\cos\delta_0}{X_g}\right)\cdot \hat{E}$$

Synchronous resonance!

Stability of Power Control for Grid-Forming Converters

Open-loop gains of the power control loops with different parasitic R_g

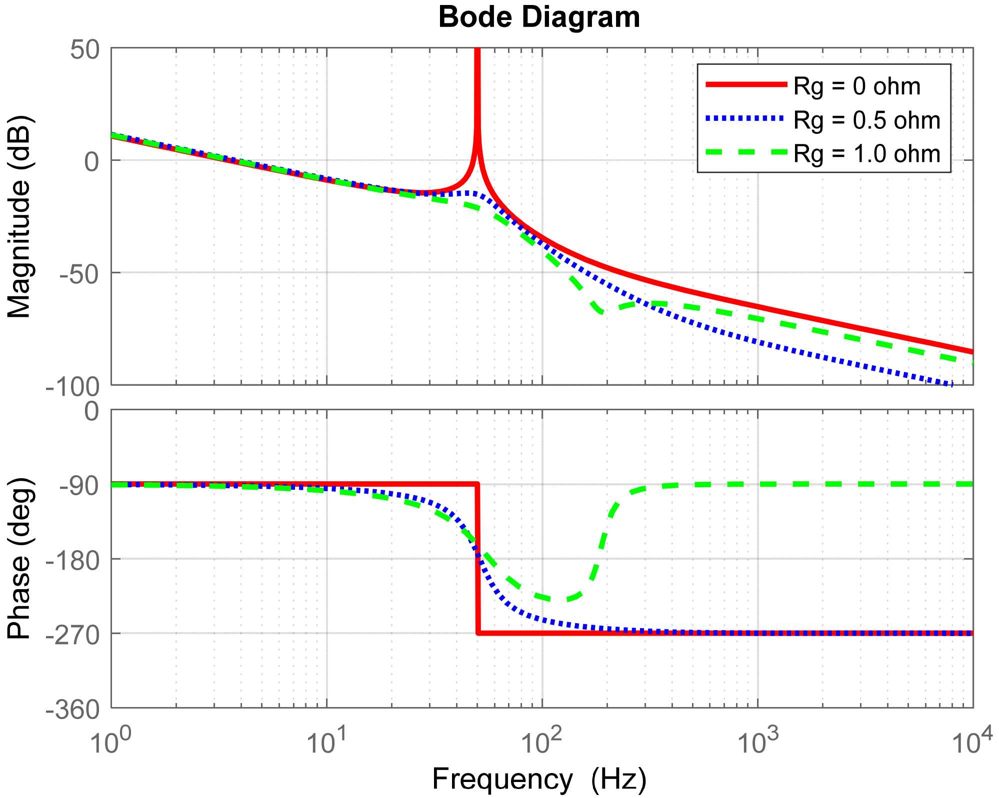

Active power-angle (*P*-*δ*) loop

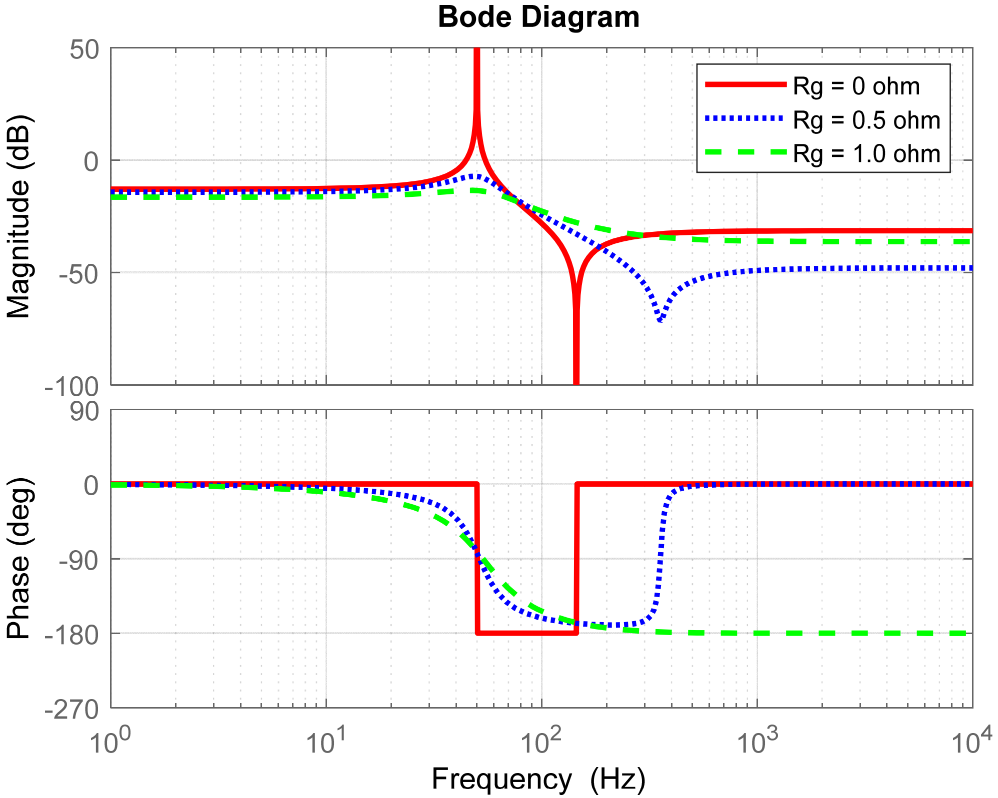

Reactive power-voltage (*Q*-*E*) loop

Stability of Power Control for Grid-Forming Converters

Closed-loop poles – reactive power loop is more robust than active power loop

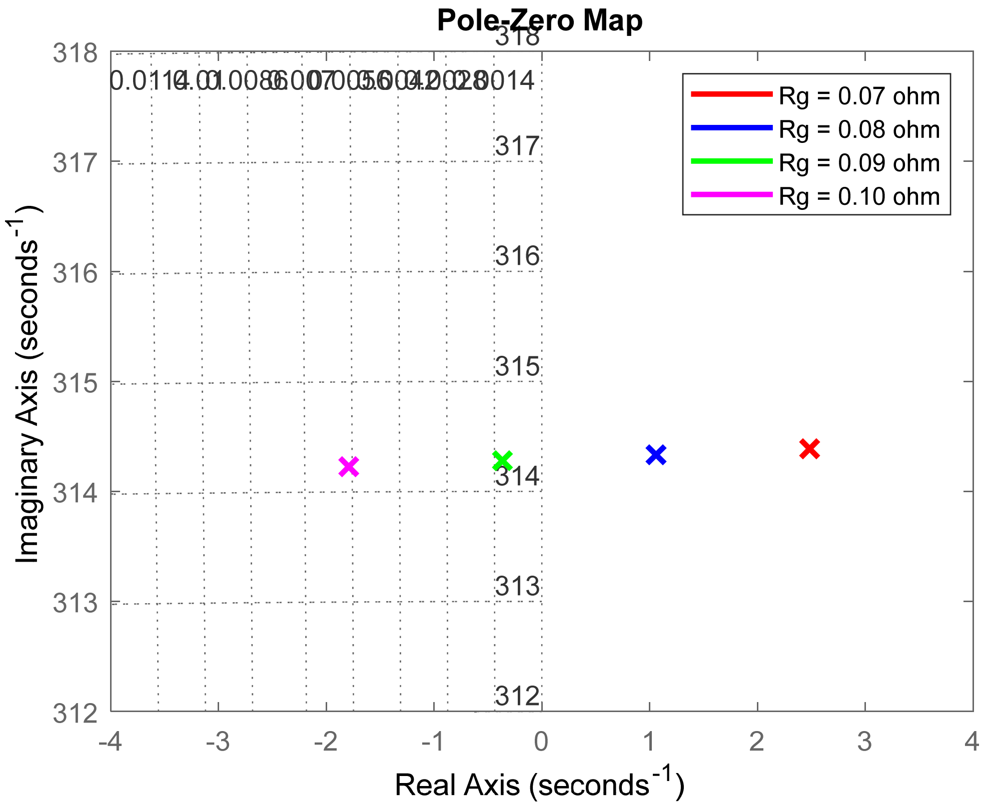

Active power-angle (*P*-*δ*) loop

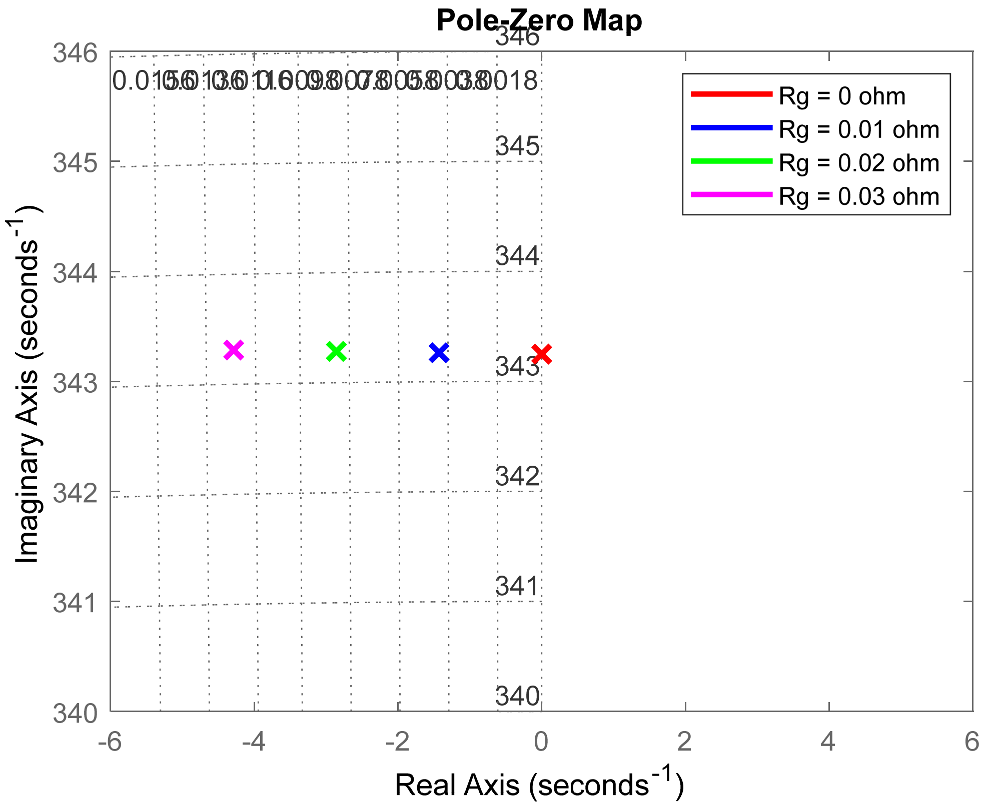

Reactive power-voltage (*Q*-*E*) loop

Stability of Power Control for Grid-Forming Converters

Simulation tests for R_g changed at the time instant of 2.0 s

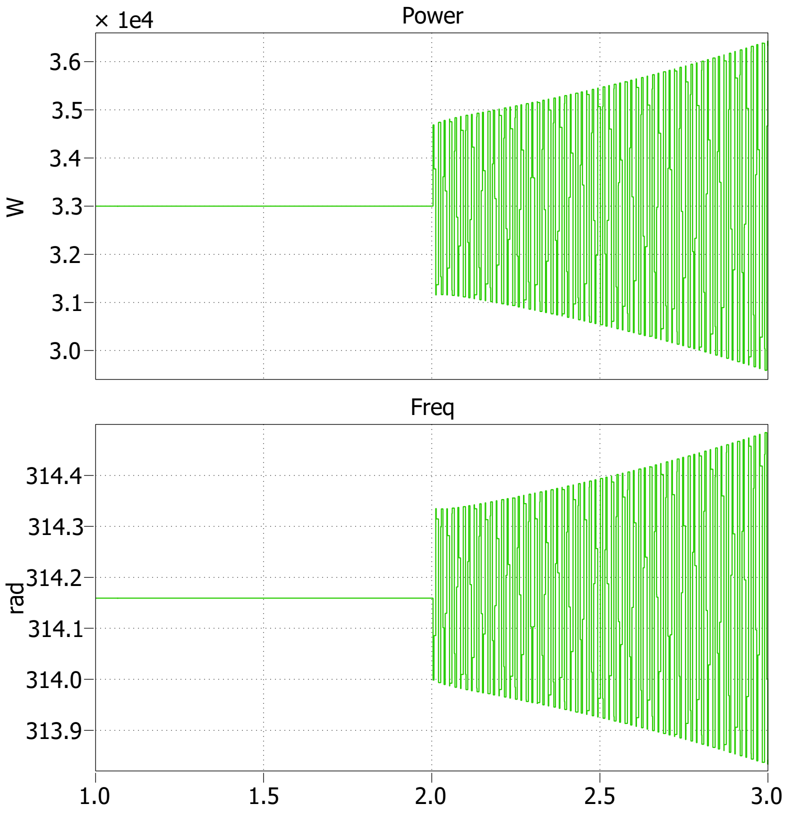

$R_g \rightarrow 0.08\ \Omega$

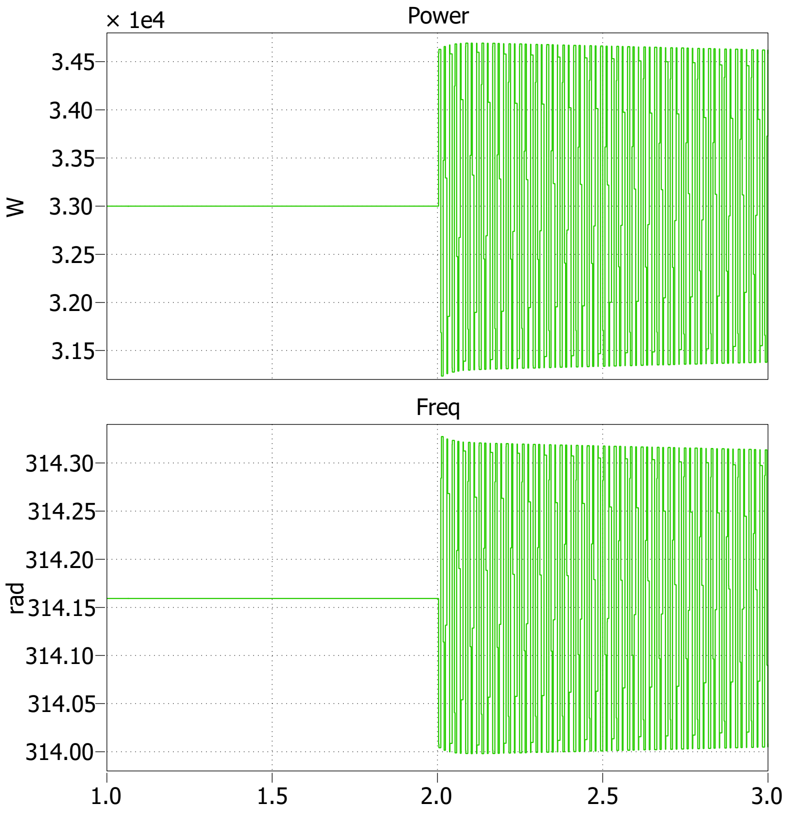

$R_g \rightarrow 0.09\ \Omega$

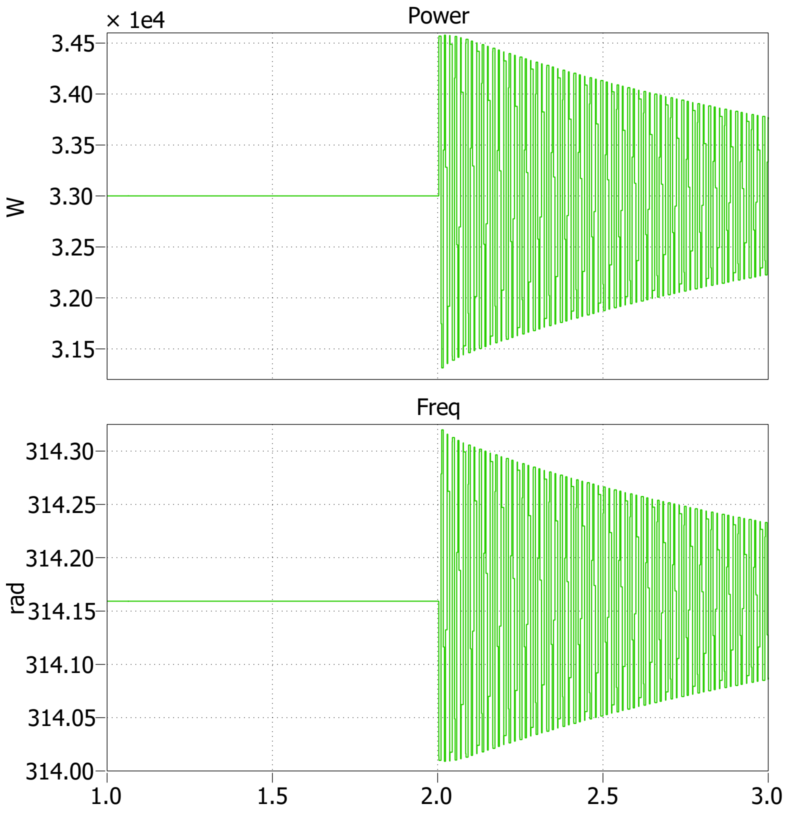

$R_g \rightarrow 0.1\ \Omega$

Stability of Power Control for Grid-Forming Converters

Damping of synchronous resonance - active resistor

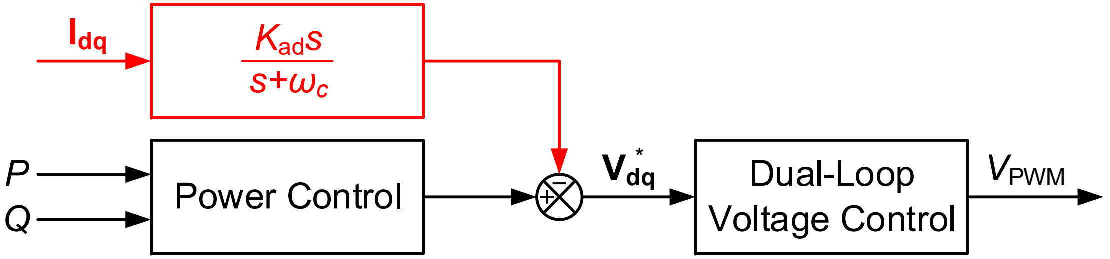

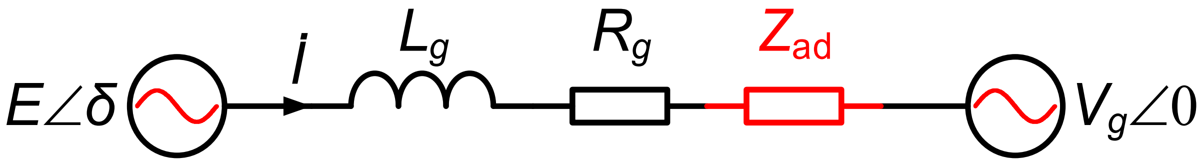

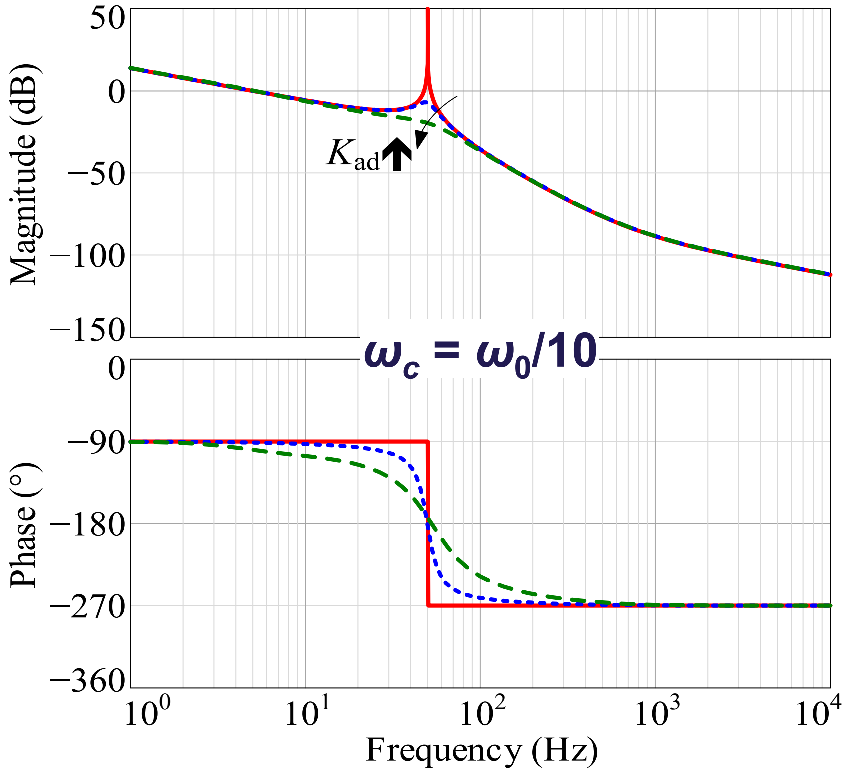

Active power-angle (P-δ) loop

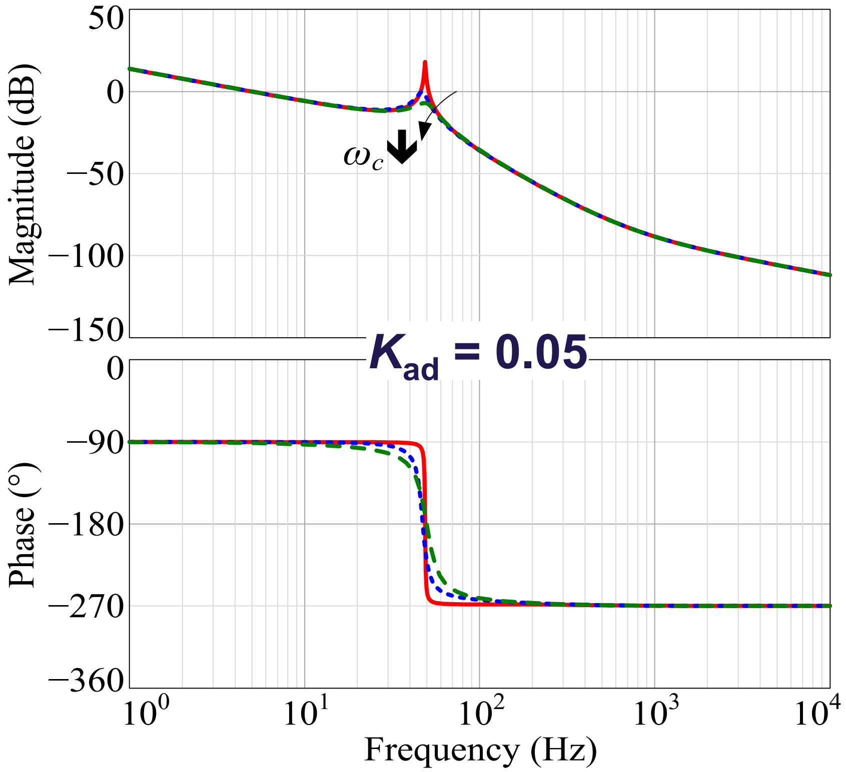

Stability of Power Control for Grid-Forming Converters

Damping of synchronous resonance - active resistor

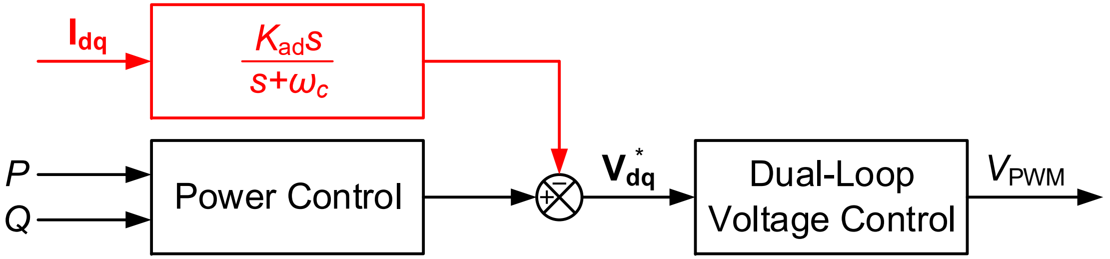

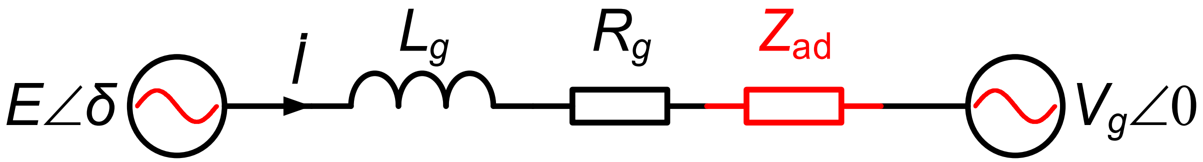

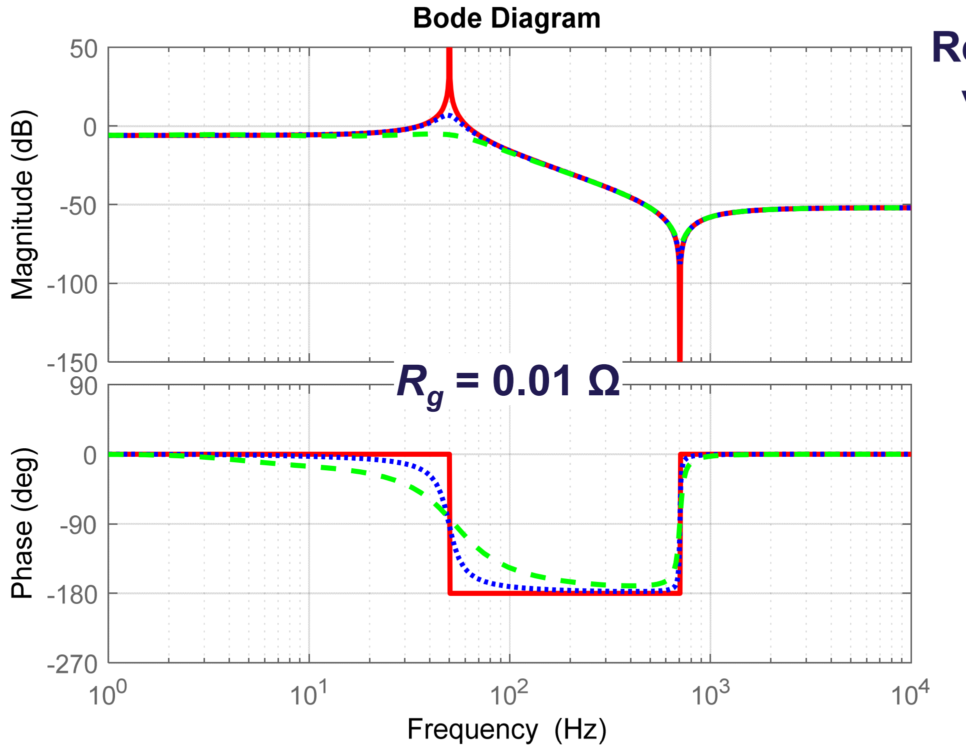

Reactive power-voltage (*Q*-*E*) loop

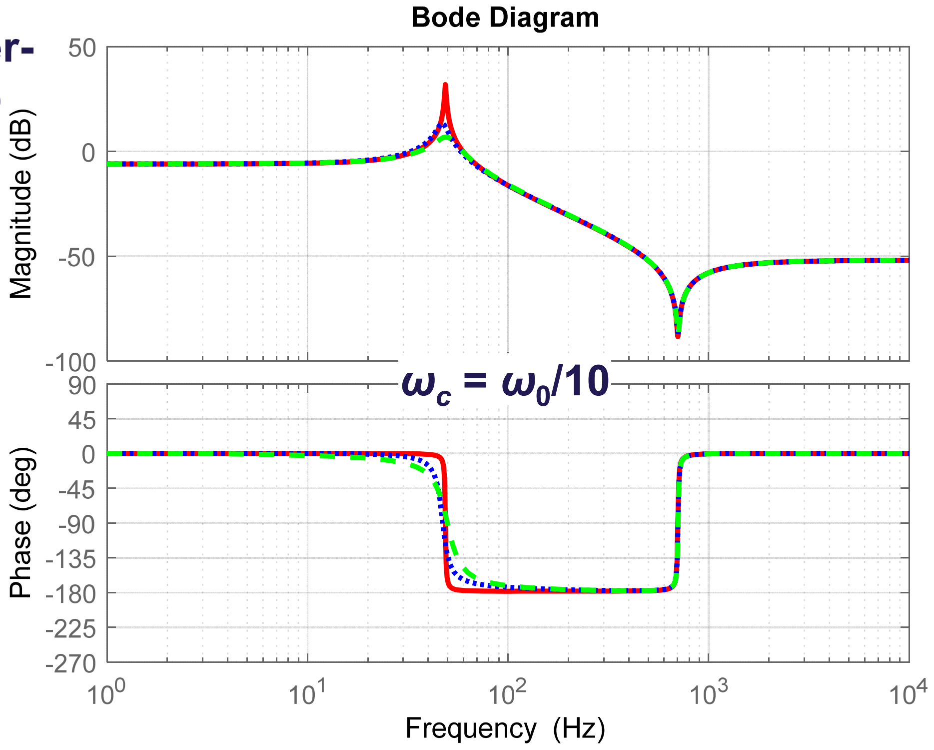

Stability of Power Control for Grid-Forming Converters

Damping of synchronous resonance - active resistor

K_{ad} = 0.05 & $\omega_c = \omega_0/10$ *v.s.* R_g = 0.05 Ω

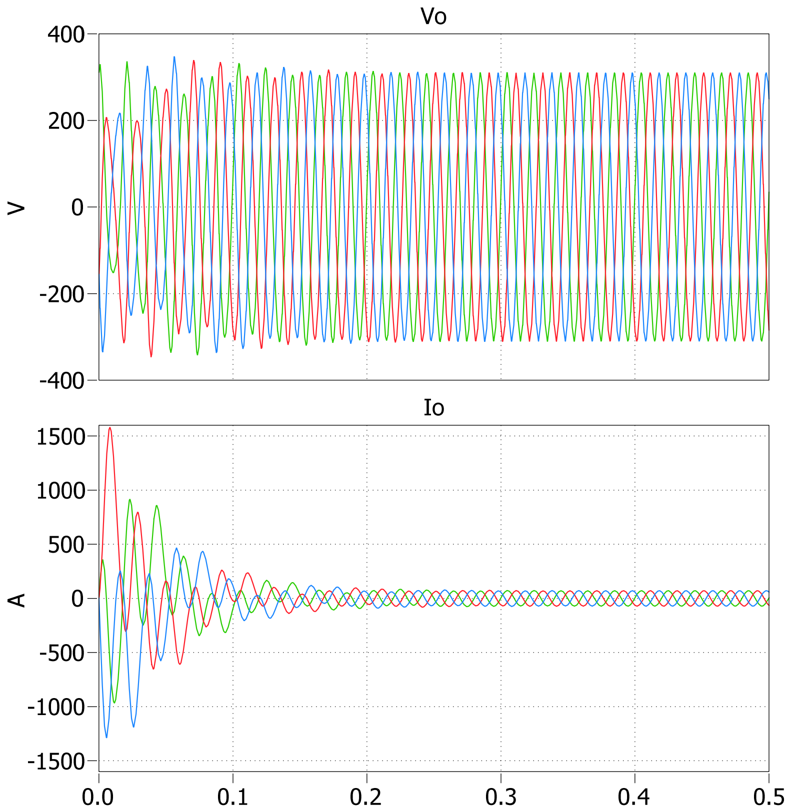

K_{ad} = 0.05, $\omega_c = \omega_0/10$

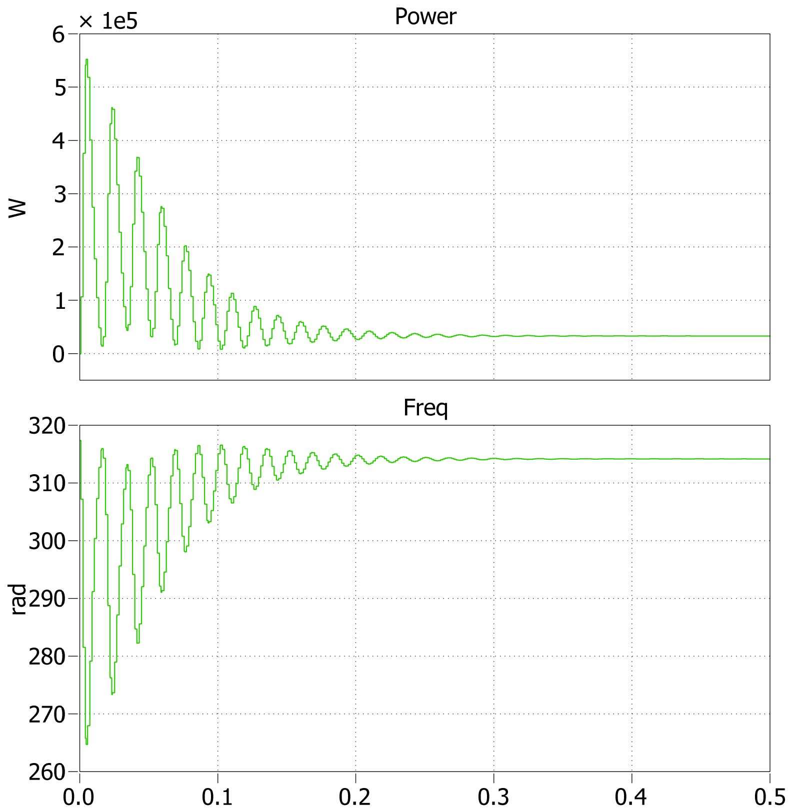

K_{ad} = 0.05, $\omega_c = \omega_0/10$

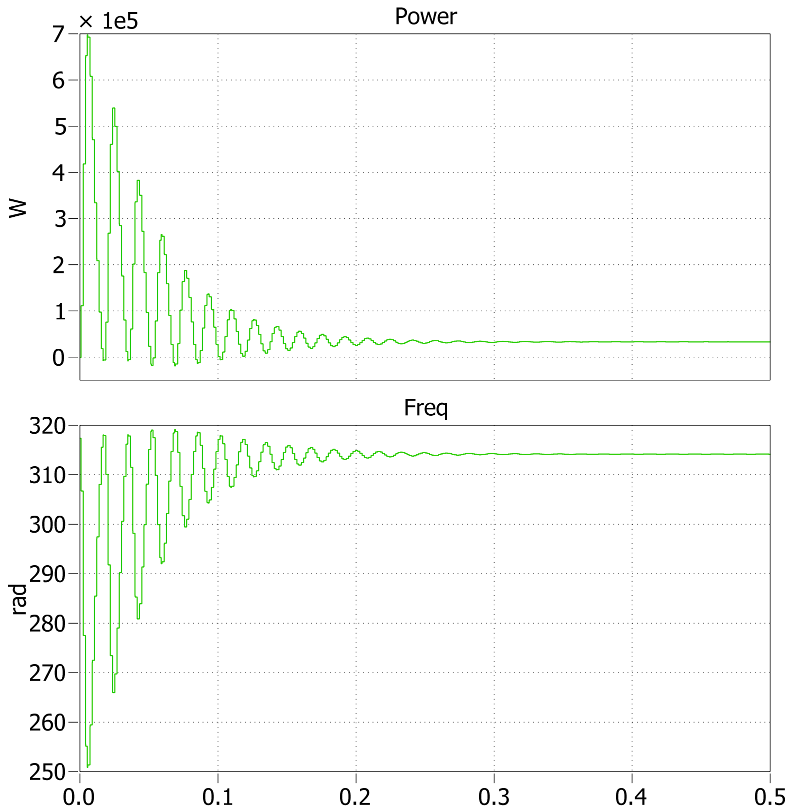

R_g = 0.05 Ω

PROSPECTS AND CHALLENGES

- SISO modeling and control
- Active stabilization techniques
- Interoperability of multi-vendor converters

SISO Modeling and Control

Symmetrical PLL for decoupled frequency response

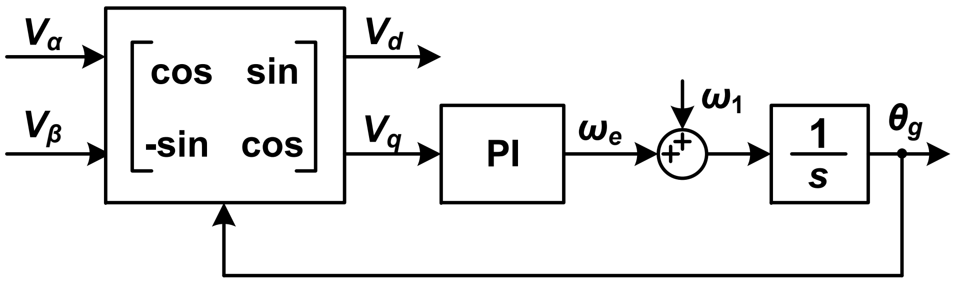

DQ-frame PLL

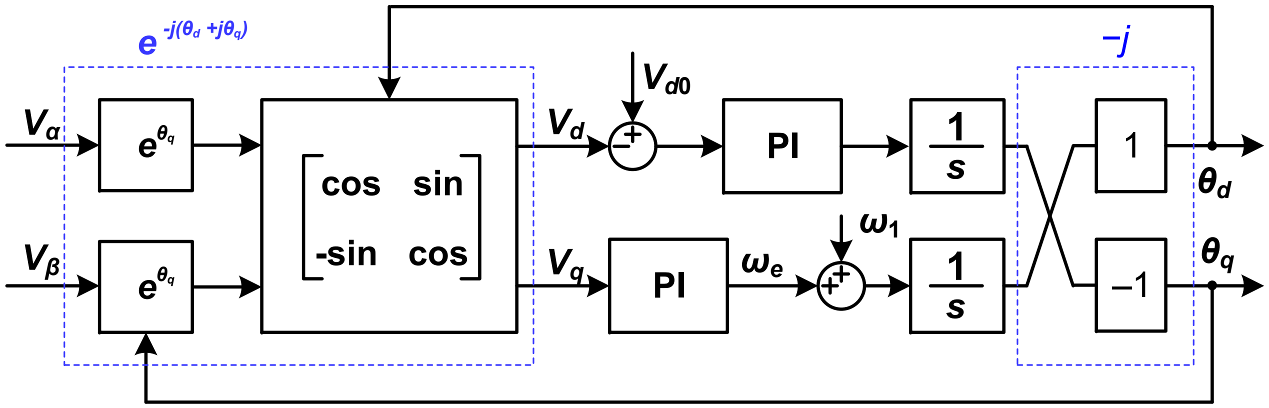

Symmetrical PLL[81]

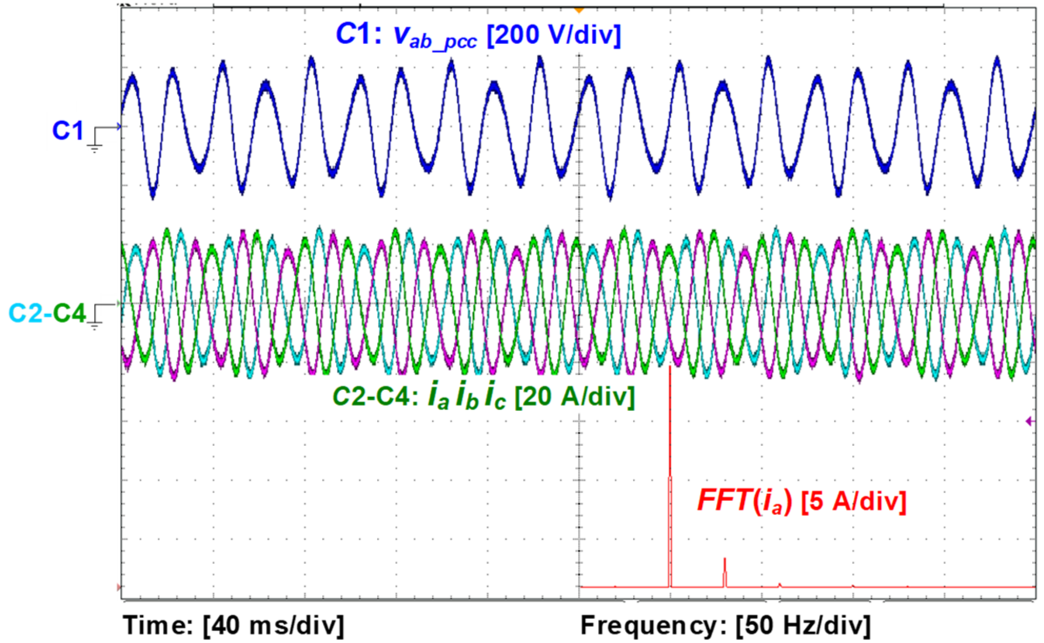

Frequency-decoupled response to 80 Hz disturbance

Active Stabilization - Virtual Impedance Control
A multi-loop control for impedance shaping

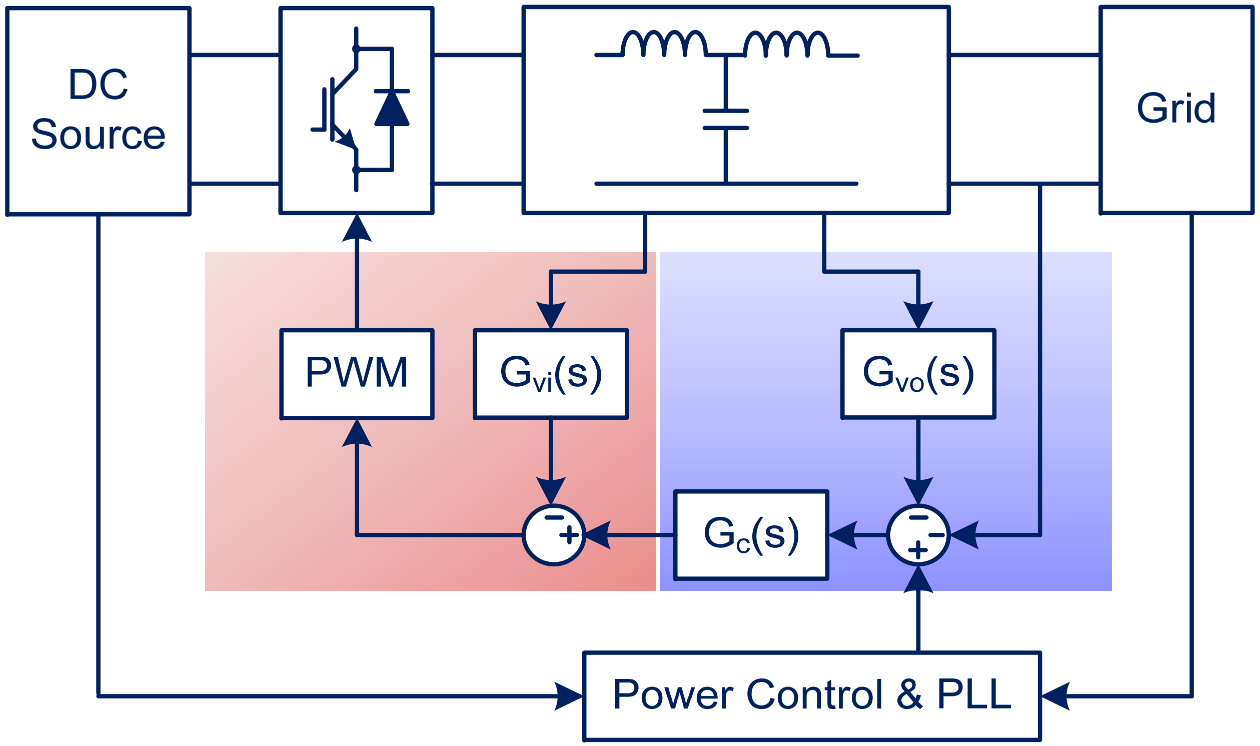

$G_{vo}(s)$:outer virtual impedance controller

$G_{vi}(s)$: inner virtual impedance controller

$G_c(s)$: current controller

- Modify the reference of modulator (duty cycle) with $G_{vi}(s)$
- Adjust the reference of controller reference with $G_{vo}(s)$

Active Stabilization - Active Damper
A power-electronic-based stabilizer for converter-based power systems

- **Reconfigure the poles (oscillation modes) and zeros of the power system**
- **No steady-state harmonic filtering, featuring low-power, high-frequency, high-bandwidth**

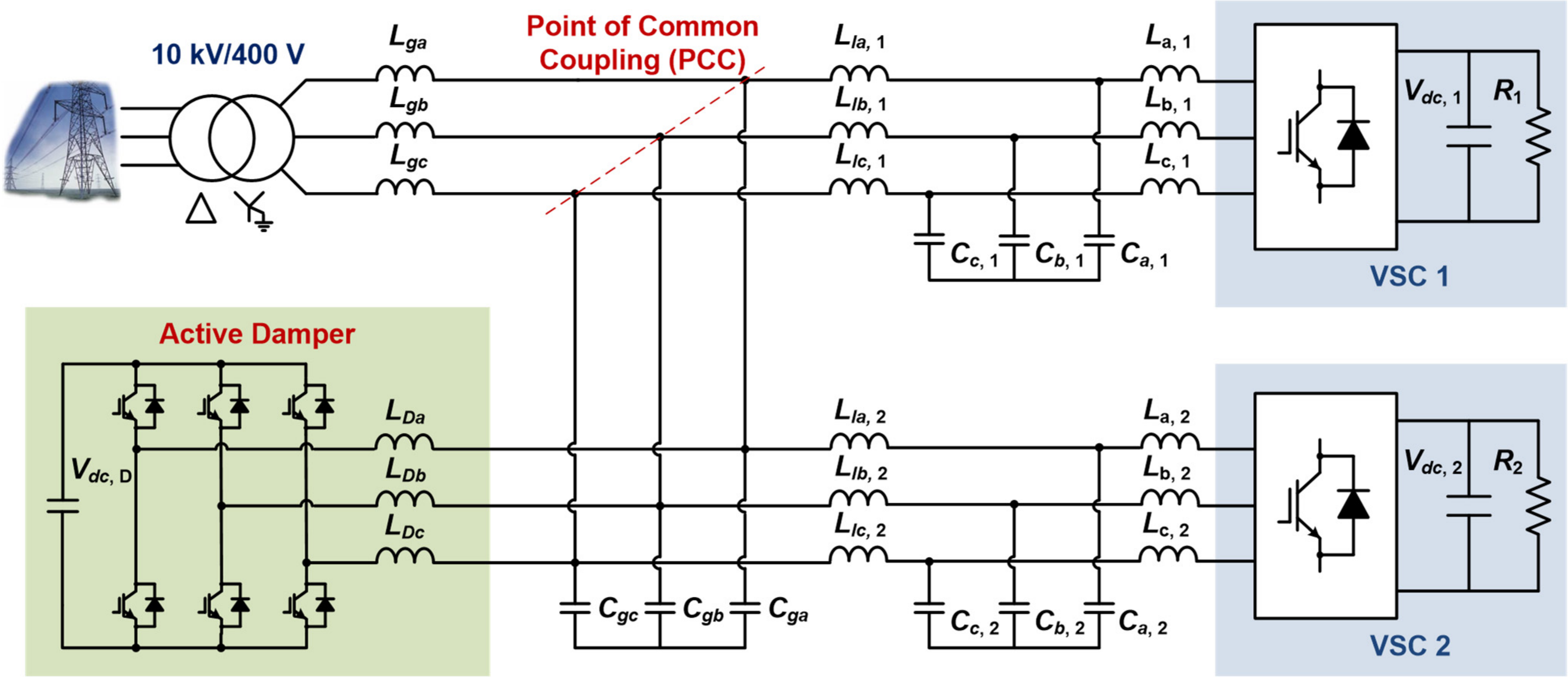

Interoperability of Multi-Vendor Power Electronic Converters
Standard EMT modeling, dynamic specification, design-oriented analysis

- New grid codes are demanded for self-disciplined stabilization, i.e. grid-neutral converters
- Grid-forming converters for actively regulating system voltage and frequency
- Design-oriented stability analysis is critical for utilizing the full controllability of power electronics
- Lack of unified models with physical insights (virtual impedance/machine)

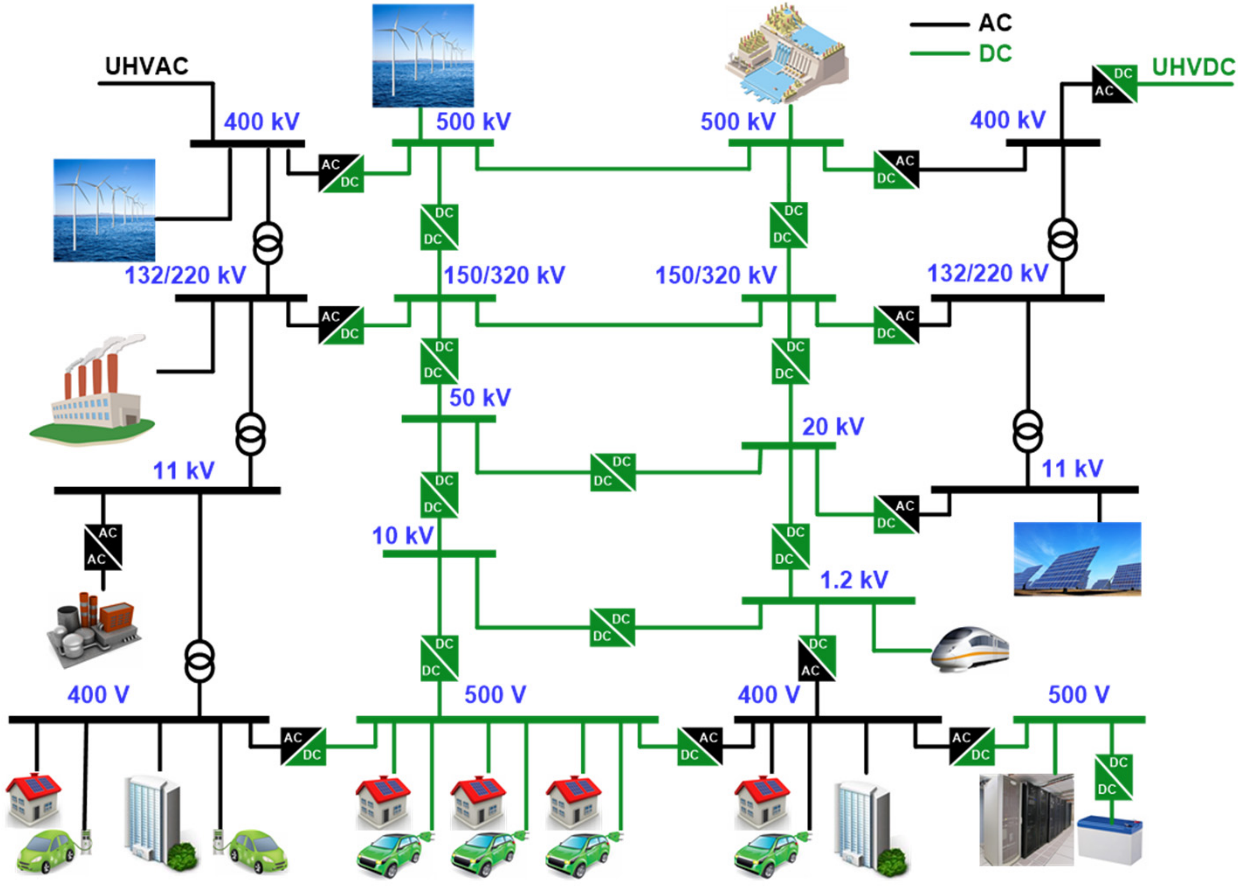

Power electronic based power systems

References

[1] X. Wang and F. Blaabjerg, “Harmonic stability in power electronic based power systems: concept, modeling, and analysis,” IEEE Trans. Smart Grid, vol. 10, pp. 2858-2870, May 2019.

[2] J. D. Ainsworth, “Harmonic instability between controlled static converters and a.c. networks,” Proc. Inst. Elect. Eng., vol. 114, pp.949-957, Jul. 1967.

[3] A. Wood and J. Arrillaga, “Composite resonance: a circuit approach to the waveform distortion dynamics of an HVDC converter,” IEEE Trans. Power Del., vol. 10, no. 4, pp. 173-192, Oct. 1995.

[4] A. E. Hammad, “Analysis of second harmonic instability for the Chateauguay HVDC/SVC scheme,” IEEE Trans. Power Del., vol. 7, no. 1, Jan. 1992.

[5] I. Pendharkar, “Resonance stability in electrical railway systems – a dissipativity approach,” European Control Conference (ECC), 2013, pp. 4574-4579.

[6] J. Arrillaga, *et al.*, *Power system harmonic analysis*, John Wiley & Sons, New York, Chapter 6, pp. 173-192

[7] E.V. Persson, “Calculation of transfer functions in grid controlled convertor systems,” IEE Proceedings, 117(5):989 to 997, May 1970.

[8] M. Sakui and H. Fujita, “Line harmonic current of three phase thyristor bridge rectifier with dc current ripple and overlap angle,” IEEJ vol. 105-B, no. 9, pp. 717 to 724, Sept. 1985.

[9] K. D. Ngo. “Low frequency characterization of PWM converters,” IEEE Trans. Power Electron., vol. PE-1, no. 4, pp. 223-230, Oct. 1986.

[10] E. V. Larson, D. H. Baker and J. C. McIver, “Low-order harmonic interaction on ac/dc systems,” IEEE Trans. Power Del., vol. 4, no. 1, pp. 493-501, Jan. 1989.

[11] P. Mattavelli, G. C. Verghese, A. M. Stankovic, “Phasor dynamics of thyristor-controlled series capacitor systems,” IEEE Trans. Power Syst., vol. 12, no. 3, pp. 1259-1267, Aug. 1997.

[12] E. Mollerstedt and B. Bernhardsson, “Out of control because of harmonics an analysis of the harmonic response of an inverter locomotive,” IEEE Control Systems Magazine, vol. 20, no. 4, pp. 70-81, Aug. 2000.

[13] J. J. Rico, M. Madrigal, and E. Acha, “Dynamic Harmonic Evolution Using the Extended Harmonic Domain,” IEEE Trans. Power Del., vol. 18, pp. 587–594, Apr. 2003.

[14] L. Harnefors, M. Bongiorno, and S. Lundberg, “Input-admittance calculation and shaping for controlled voltage-source converters,” IEEE Trans. Ind. Electron., vol. 54, no. 6, pp. 3323-3334, Dec. 2007.

[15] B. Wen, D. Boroyevich, R. Burgos, P. Mattavelli, and Z. Shen, “Analysis of D-Q small-signal impedance of grid-tied inverters,” IEEE Trans. Power Electron., vol. 31, pp. 675-687, Jan. 2016.

[16] M. Cespedes and J. Sun, “Impedance modeling and analysis of grid-connected voltage-source converters,” IEEE Trans. Power Electron., vol. 29, no. 3, pp. 1254-1261, Mar. 2014.

[17] X. Wang, L. Harnefors, and F. Blaabjerg, “Unified impedance model of grid-connected voltage-source converters," IEEE Trans. Power Electron., vol. 33, no. 2, pp. 1775-1787, Feb. 2018.

[18] X. Yue, X. Wang, and F. Blaabjerg, “Review of small-signal modeling methods including frequency-coupling dynamics of power converters," IEEE Trans. Power Electron., vol. 34, pp. 3313-3328, Apr. 2019.

References

[19] M. Lu, X. Wang, P. C. Loh, F. Blaabjerg, and T. Dragicevic, "Graphical evaluation of time-delay compensation techniques for digitally controlled converters," IEEE Trans. Power Electron., vol. 33, no. 3, pp. 2601-2614, Mar. 2018.

[20] S. Hiti, D. Boroyevich, et al. "Small-signal modeling and control of three-phase PWM converters," IEEE IAS 1994, pp. 1143-1150.

[21] R. D. Middlebrook, "Predicting modulator phase lag in pwm converter feedback loop," Powercon 1981, pp. 1-6.

[22] J. Kwon, X. Wang, F. Blaabjerg, C. L. Bak, A. R. Wood, and N. Watson, "Linearized modeling methods of ac-dc converters for an accurate frequency response," IEEE J. Emerg. Sel. Topics Power Electron., vol. 5, no. 4, pp. 1526-1541, Dec. 2017.

[23] A. Wood, D. J. Hume, and C. M. Osauskas, "Linear analysis of waveform distortion for HVDC and FACTs devices," in Proc. IEEE ICHQP 2000, pp. 1-7.

[24] S. R. Sanders, J. M. Noworolski, X. Liu, and G. C. Verghese, "Generalized averaging method for power conversion circuits," IEEE Trans. Power Electron., vol. 6, no. 2, pp. 251-259, Apr. 1991.

[25] C. Buchhagen, M. Greve, A. Menze, and J. Jung, "Harmonic stability – practical experience of a TSO," in Proc. Wind Integration Workshop, 2016, pp. 1-6.

[26] L. Harnefors, "Modeling of three-phase dynamic systems using complex transfer functions and transfer matrices," IEEE Trans. Ind. Electron. vol. 54, no. 4, pp. 2239-2248, Aug. 2007.

[27] S. Chung, "A phase tracking system for three phase utility interface inverters," IEEE Trans. Power Electron., vol. 15, no. 3, pp. 431-437, May 2000.

[28] D. Yang, X. Wang, and F. Blaabjerg, "Sideband-harmonic instability of paralleled inverters with asynchronous carriers," IEEE Trans. Power Electron., vol. 33, no. 6, pp. 4571-4577, Jun. 2018.

[29] J. Kwon, X. Wang, F. Blaabjerg, C. L. Bak, A. R. Wood and N. R. Watson, "Harmonic instability analysis of single-phase grid connected converter using harmonic state space (HSS) modeling method", IEEE Trans. Ind. Appl.,, Vol. 52, No. 5, pp. 4188 – 4200. Sept./Oct. 2016.

[30] J. Holtz, "The representation of ac machine dynamics by complex signal flow graphs," IEEE Trans. Ind. Electron., vol. 42, no. 3, pp. 263-271, Jun. 1995.

[31] L. Harnefors, X. Wang, A. G. Yepes, and F. Blaabjerg, "Passivity-based stability assessment of grid-connected VSCs – an overview," IEEE J. Emerg. Sel. Topics Power Electron., vol. 4, no. 1, pp. 116-125, Mar. 2016.

[32] X. Wang, F. Blaabjerg, and P. C. Loh, "Passivity-based stability analysis and damping injection for multiparalleled VSCs with LCL filters," IEEE Trans. Power Electron., vol. 32, no. 11, pp. 8922-8935, Nov. 2017.

[33] X. Wang, F. Blaabjerg, and W. Wu, "Modeling and analysis of harmonic stability in ac power-electronics-based power system," IEEE Trans. Power Electron., vol. 29, no. 12, pp. 6421-6432, Dec. 2014.

[34] N. M. Wereley, "Analysis and control of linear periodically time varying systems," Ph.D. dissertation, Dept. of Aeronautics and Astronautics, MIT, 1991.

References

[35] D. Maksimovic, A. M. Stankovic, V. J. Thottuvelil, and G. C. Verghese, "Modeling and simulation of power electronic converters," Proc. IEEE, vol. 89, pp. 898-912, Jun. 2001.

[36] M. K. Bakhshizadeh, X. Wang, F. Blaabjerg, J. Hjerrild, L. Kocewiak, C. L. Bak, and B. Hesselbaek, “Couplings in phase domain impedance moeling of grid-connected converters,” IEEE Trans. Power Electron. vol. 31, no. 10, pp. 6792-6796, Oct. 2016.

[37] J. M. Undrill and T. E. Kostyniak, “Subsynchronous oscillations Part I – comprehensive stability analysis,” IEEE Trans. Power App. Syst., vol. PAS-95, no. 4, pp. 1446-1455, Jul./Aug. 1976.

[38] B. Ferreira, "Understanding the Challenges of Converter Networks and Systems: Better opportunities in the future," IEEE Power Electronics Mag., vol. 3, no. 2, pp. 46-49, Jun. 2016.

[39] B. Kroposki, et al., “Achieving a 100% renewable grid: operating electric power systems with extremely high levels of variable renewable energy,” IEEE Power & Energy Mag. vol. 15, pp. 61-73, Mar./Apr. 2017.

[40] R. D. Middlebrook, “Input filter consideration in design and application of switching regulators,” in Proc. IEEE IAS 1976, 366-382.

[41] H. Zhang, L. Harnefors, X. Wang, H. Gong, J. Hasler, “Stability analysis of grid-connected voltage-source converters using SISO modeling,” IEEE Trans. Power Electron., vol. 34, pp. 8104-8117, Aug., 2019.

[42] C. Zhang, X. Wang, and F. Blaabjerg, “The influence of phase-locked loop on the stability of single-phase grid-connected inverter,” in Proc. IEEE ECCE 2015, pp. 4734-4744.

[43] H. Zhang, X. Wang, L. Harnefors, J. Hasler, and H. Nee, “SISO transfer functions for stability analysis of grid-connected voltage-source converters,” IEEE Trans. Ind. Appl., vol. 55, pp. 2931-2941, May-Jun., 2019.

[44] L. Harnefors, L. Zhang, and M. Bongiorno, “Frequency-domain passivity-based current controller design,” IET Power Electron., vol. 1, no. 4, pp. 455-465, Dec. 2008.

[45] X. Wang, Y. W. Li, F. Blaabjerg, and P. C. Loh, “Virtual-impedance-based control for voltage- and current-source converters,” IEEE Trans. Power Electron. vol. 30, pp. 7019-7037, Dec. 2015.

[46] D. Lu, X. Wang, and F. Blaabjerg, “Impedance-based analysis of dc-link voltage dynamics in voltage-source converters,” IEEE Trans. Power Electron. vol. 34, pp. 3973-3985, Apr. 2019.

[47] D. Yang, X. Wang, F. Liu, K. Xin, Y. Liu, and F. Blaabjerg， “Adaptive reactive power control of PV power plants for improved power transfer capability under ultra-weak grid conditions,“ IEEE Trans. Smart Grid, vol. 10, pp. 1269-1279, Mar. 2019.

[48] L. Zhang, L. Harnefors, and H.-P. Nee, “Power-synchronization control of grid-connected voltage-source converters,” IEEE Trans. Power Syst., vol. 25, no. 2, pp. 809–820, 2010.

[49] L. Zhang, H. Nee, and L. Harnefors, “Analysis of stability limitations of a VSC-HVDC link using power-synchronization control,” IEEE Trans. Power Syst., vol. 26, no. 3, pp. 1326–1337, 2011.

[50] D. Yang, X. Wang, and F. Blaabjerg, “Suppression of synchronous resonance for virtual synchronous generators,” in Proc. IET RPG, 2017.

[51] D. Yang, X. Wang, and F. Liu, K. Xin, Y. Liu, F. Blaabjerg, “A PLL-less vector current control of VSC-HVDC for ultra weak grid interconnection,” in Proc. IEEE ECCE, 2018.

THANKS FOR YOUR ATTENTION

QUESTIONS?

DEPARTMENT OF ENERGY TECHNOLOGY
AALBORG UNIVERSITY